TECHNICKÁ UNIVERZITA V LIBERCI
Fakulta textilní

Vysoce funkční materiály s obsahem aerogelu

Disertační práce

Studijní program: P3106 – Textile Engineering
Studijní obor: 3106V015 – Textile Technics and Materials Engineering

Autor práce: **Xiaoman Xiong, M.Eng.**
Vedoucí práce: doc. Rajesh Mishra, Ph.D.

Liberec 2018

TECHNICAL UNIVERSITY OF LIBEREC
Faculty of Textile Engineering

Aerogel Embedded High-performance Fibrous Materials

Dissertation

Study programme: P3106 – Textile Engineering
Study branch: 3106V015 – Textile Technics and Materials Engineering

Author: **Xiaoman Xiong, M.Eng.**
Supervisor: doc. Rajesh Mishra, Ph.D.

Liberec 2018

Prohlášení

Byla jsem seznámena s tím, že na mou disertační práci se plně vztahuje zákon č. 121/2000 Sb., o právu autorském, zejména § 60 – školní dílo.

Beru na vědomí, že Technická univerzita v Liberci (TUL) nezasahuje do mých autorských práv užitím mé disertační práce pro vnitřní potřebu TUL.

Užiji-li disertační práci nebo poskytnu-li licenci k jejímu využití, jsem si vědoma povinnosti informovat o této skutečnosti TUL; v tomto případě má TUL právo ode mne požadovat úhradu nákladů, které vynaložila na vytvoření díla, až do jejich skutečné výše.

Disertační práci jsem vypracovala samostatně s použitím uvedené literatury a na základě konzultací s vedoucím mé disertační práce a konzultantem.

Současně čestně prohlašuji, že tištěná verze práce se shoduje s elektronickou verzí, vloženou do IS STAG.

Datum:

Podpis:

Acknowledgement

This dissertation has been completed with the guidance and mentorship of many people. I would like to gratefully acknowledge their support of this thesis.

Firstly, I would like to express my sincere gratitude to my supervisor, Associate Professor Rajesh Mishra, who has guided me and encouraged me to carry on through these years and has contributed to this thesis with a major impact. Thank you for helping me, often with big doses of patience and immense knowledge, through the subtleties of research working and writing of this thesis. I am especially indebted to Professor Jiri Militky, who has been supportive of my scientific work and provided me extensive professional guidance to complete this work. In particular, I am grateful to Professor Hiroyuki Kanai at Shinshu University, for his altruistic guide and professional suggestions during my internship in Japan.

I am grateful to all of those with whom I have had the pleasure to work during my study in TUL. I would like to express my special gratitude to Professor Jakub Wiener for sharing his immense expertise. I would like to thank Dr. Mohanapriya Venkataraman for her great help on both scientific research and personal life throughout the past four years. I would like to thank Ing. Marie Kašparová and Darina Jašíková for their technical support on sample preparation and measurements of thermal properties. My sincere thanks also go to Professor Lubos Hes, Dr. Jana Salacova, Ms. Jana Stranska and Dr. Veronika Tunakova, for their support and allowing me to use their instruments.

My special thanks to the Dean of Faculty of Textile Engineering, Vice Dean Dr. Gabriela Krupincova and Vice Dean Dr. Pavla Tesinova for their continuous support. I also thank our HOD Dr. Blanka Tomkova, Secretary Katerina Struplova, Katerina Nohynkova, Hana Musilova, Bohumila Keilova for their seamless coordination and efficiency. My hearty thanks to management of Technical University of Liberec for the sustained support to pursue Ph.D degree in this esteemed institution.

Last but not the least, I would like to thank my parents and my supportive husband Tao Yang, whose love are with me in whatever I pursue.

I look forward to starting and successfully finishing more new chapters in life.

Synopsis

Fibrous materials are widely used as thermal insulators in various applications. Their thermal insulation ability is restricted when the material thickness is limited to few milli-meters. Nowadays, development of high-performance insulation materials to save energy consumption, increase comfort, decrease cost and complexity has drawn increasing attention. Silica aerogel, exhibiting superior thermal insulation performance with extremely low thermal conductivity, has been well acknowledged as one of the most attractive thermal insulating materials. The objective of this thesis was to develop aerogel embedded high-performance fibrous materials for thermal insulation application and investigate their performance.

Layered nanofibrous web/silica aerogel/ nonwoven materials were prepared via laminating method by using low melting powder as thermal binding material. The effect of aerogel and thermal adhesive on thermal insulation performance and air permeability was examined. A series model was considered for thermal resistance, the theoretical predicted and measured results were compared and analysed. Results revealed that novel techniques to combine silica aerogel with high porous textiles with less use of binding materials should be considered.

A novel aerogel-encapsulated fibrous material without using any binding material to bond aerogel particles was developed by using laser engraving technique and laminating method. Thermo Camera, Alambeta device and KES-FT-II Thermolabo were employed to measure thermal performance. Compression test was performed to examine the compression recovery which determines the sustainability of thermal insulation ability. Moreover, a laboratory-made dynamic heat transfer device was used to figure out convective thermal behaviour of these multi-layered materials as well as aerogel treated nonwovens under different airflow velocity and heating conditions. The real-time temperature curves of different materials were compared. The temperature difference and convective heat transfer coefficient under continuous heating condition were calculated and investigated. The findings could contribute to new developments in flexible aerogel-embedded high-performance textile materials for both industrial and clothing applications.

Flexible polyurethane and polyvinylidene fluoride nanoporous membranes embedded with silica aerogel were prepared by electrospinning technique. Thermal properties and air

permeability were evaluated and compared. It was concluded that nanofibers embedded with aerogel are good for thermal insulation in cold weather conditions. Thermal insulation battings incorporating nanofibers could possibly decrease the weight and bulk of current thermal protective clothing.

Statistical analysis software, Matlab_R2017a were used to conduct all the statistical results in this study. The findings are significant and can be used for further study in the areas of aerogel embedded high-performance fibrous materials for thermal insulation in building, industrial and protective textile fields.

Keywords: fibrous structure; silica aerogel; thermal measurement; compression recovery; nanofiber

Abstrakt

Vlákenné materiály jsou široce používány jako tepelné izolátory v různých aplikacích pro úsporu energie. Jejich tepelně izolační vlastnosti jsou omezeny, pokud je tloušťka materiálu omezena na několik milimetrů. V dnešní době je stále častěji kladen důraz na vývoj vysoce výkonných tepelně izolačních materiálů pro úsporu energie, zvýšení pohodlí, snížení nákladů a složitosti těchto systémů. Aerogel, který vykazuje vynikající tepelnou izolaci s extrémně nízkou tepelnou vodivostí, byl shledán jedním z nejatraktivnějších tepelně izolačních materiálů. Cílem této práce bylo vyvinout vysoce výkonný aerogel spojený s vlákennými materiály pro tepelnou izolaci a prověřit jeho výkon.

Vrstvená nanovlákenná síťovina /aerogel /netkané materiály byly připraveny použitím laminovací metody s práškem s nízkým bodem tání jako tepelně spojujícím materiálem. Byl zkoumán účinek aerogelu a tepelného lepidla na tepelnou izolaci a propustnost vzduchu. V úvahu byl vzat sériový model pro tepelný odpor, byly porovnány a analyzovány teoretické předpoklady a naměřené výsledky. Bylo navrženo, že by měly být vzaty v úvahu nové techniky kombinující aerogel s vysoce porézními textiliemi s menším využitím pojivových materiálů.

Nový aerogel obalený vlákenným materiálem bez použití jakéhokoliv pojivového materiálu, který spojuje částice aerogelu, byl vyvinut pomocí techniky laserového gravírování a laminovací metody. Pro měření tepelného výkonu byly použity termální kamera, zařízení Alambeta a KES-FT-II Thermolab. Byla provedena tlaková zkouška ke zkoumání kompresního zotavení, které určuje udržitelnost tepelné izolace. Dále bylo použito laboratorně vyráběné dynamické zařízení pro přenos tepla pro zjištění konvektivního tepelného chování těchto vícevrstvých materiálů, jakož i netkaných textilií obalených aerogelem, při různých rychlostech proudění vzduchu a zahřívání. Byly porovnány teplotní křivky v reálném čase z měření předehřátých podmínek. Byly vypočteny a posouzeny hodnoty teplotních rozdílů a konvektivního součinitele přestupu tepla za podmínek kontinuálního ohřevu. Zjištění by mohla přispět k novému vývoji pružných vysoce výkonných textilních materiálů se zabudovaným aerogelem pro průmyslové i oděvní aplikace.

Pružné polyuretanové a polyvinylidenfluoridové nanoporézní membrány kombinované s aerogelem na bázi oxidu křemičitého byly připraveny elektrostatickým zvlákňováním.

Tepelné vlastnosti a propustnost vzduchu byly hodnoceny a porovnávány. Byl učiněn závěr, že nanovlákna s aerogelem jsou vhodná pro tepelnou izolaci za chladného počasí. Tepelně izolační nosiče obsahující nanovlákna by mohly případně snížit hmotnost a objem tepelně ochranného oblečení.

Pro provedení a vyhodnocování všech statistických výsledků byl v této práci použit statistický a analytický software Matlab_R2017a. Dosažené výsledky jsou významné a mohou být použity pro další studium v oblasti tepelných vlastností vysoko pevnostních vlákenných materiálů s aerogelem, které mohou být využity například pro tepelnou izolaci budov či ochranné oděvy.

Klíčová slova: vlákenná struktura; aerogel; měření teploty; kompresní zotavení; nanovlákna

概要

纤维集合体材料广泛用作隔热材料于多种应用中以达到隔热储能的效果。这种材料的隔热性能与其厚度有关，当材料厚度只有几毫米时，隔热性能有限。现如今，开发具有高性能隔热保温材料以节约能量消耗，提升舒适性，降低材料成本及工艺复杂性，越来越获得科研学者的关注。硅气凝胶具有超低的导热系数和超强的隔热性能，是公认的最具吸引力的隔热材料之一。本论文的研究目的是开发气凝胶与纤维材料复合的高性能隔热保温材料并研究其性能。

以低熔点热熔粉作为热粘合剂，采用层压方式制备了多层复合的纳米纤维网/硅气凝胶/无纺布材料，研究了气凝胶及热熔粉对多层复合材料隔热性能及透气性的影响。采用串联模式模型对材料的热阻进行了理论预测，并对理论结果和实验数值进行了比较和分析。实验结果表明气凝胶与纤维材料的复合技术应尽可能少的使用粘合剂。

采用激光蚀刻和层压复合技术开发了一种新型的气凝胶封装式纤维材料，该材料不涉及气凝胶颗粒与粘合剂之间的粘合。热成像仪，Alambeta 设备和 KES-FT-II 热物性测试仪用来测试材料的热学性能，压缩实验用来评估材料的压缩回复性。此外，采用实验室自制的动态热传递测试装置研究了新型材料在不同风速和加热条件下的热对流传热行为，比较了多种材料在预加热实验条件下的实时温度曲线，研究了连续加热实验条件下采用不同结构的隔热材料时加热板与空气温度差及对流传热系数。

本论文还采用静电纺技术制备了柔性气凝胶/聚氨酯纳米膜复合材料和气凝胶/聚偏二氟乙烯纳米膜复合材料，测试并比较了复合材料的热学性能和透气性。实验结果表明气凝胶/纳米纤维复合材料具有超强的隔热保温性能，与传统隔热保温材料共同应用于热防护服，可降低成品的体积和重量。

数据统计分析软件 Matlab_R2017a 用于进行本研究中的所有统计分析。该研究结果具有重要意义，可用于气凝胶/纤维复合材料的高性能隔热保温领域的进一步研究和在建筑，工业及防护织物领域的应用。

关键词： 纤维状结构，硅气凝胶，热学性能，压缩回复，纳米纤维

Table of Contents

List of Figures

List of Tables

List of Symbols

Symbols		Description
D	[m]	Particle hard-shell diameter
f_V		Fiber volume fraction in the fibrous structure
h	[m]	Fabric thickness
h_0	[m]	Initial thickness of a fabric
h_1	[m]	Fabric thickness at maximum pressure
h_2	[m]	Recovered thickness after compression test
h_c	[W/m^2 · K]	Heat transfer coefficient
k_B	[J/K]	Boltzmann constant (1.38065×10^{-23})
K_n		Knudsen number
L_c	[m]	Characteristic length of fabric
l_s	[m]	Representative physical length scale
l	[m]	Mean free path of the gas molecules
p	[Pa]	Total pressure
q	[W/m^2]	Heat flux
Q_{inlet}	[W]	Heat flow inlet to heating rod
Q	[W]	Amount of heat release with fabric placed on the BT plate
Q_0	[W]	Amount of heat release without fabric on the BT plate
R	[m^2 ·K/W]	Thermal resistance
Re		Reynolds Number
R_{A0}	[m^2 ·K/W]	Thermal resistance of the layered fabric (sample A0)
R_M	[m^2 ·K/W]	Thermal resistance of the middle layer
R_N	[m^2 ·K/W]	Thermal resistance of the nanofiber web (sample N)
R_S	[m^2 ·K/W]	Thermal resistance of the nonwoven fabric (sample S)
R_t	[m^2 ·K/W]	Total thermal resistance of a multilayered fabric
ΔR	[m^2 ·K/W]	Reduction in thermal resistance due to thermal adhesive
S	[m^2]	The surface area of the fabric exposed to the airflow
T	[K]	Thermodynamic temperature
T_s	[K]	Solid surface temperature
T_∞	[K]	Fluid temperature
T_f	[K]	The temperature of fabric surface

T_{air}	[K]	The temperature of ambient air
ΔT	[K]	Difference of the temperatures
v	[m/s]	Velocity of the object relative to the fluid
W_C	[J]	The work done during compression
W_R	[J]	The work done during recovery process
ρ	[kg/m^3]	Density of the fluid /fibrous material
ρ_f	[kg/m^3]	Fiber density
ρ_s	[g/m^2]	Areal/surface density
ρ_V	[kg/m^3]	Bulk density of aerogel
λ	[W/ m· K]	Thermal conductivity
λ_0	[W/ m· K]	Thermal conductivity of stagnant air
λ_{aer}	[W/ m· K]	Thermal conductivity of aerogel granules
λ_g	[W/ m· K]	Thermal conductivity of the gas phase
λ_g^0	[W/ m· K]	Thermal conductivity of non-confined air
λ_s	[W/ m· K]	Thermal conductivity of the solid fibers
λ_{sg}	[W/ m· K]	The combined solid and gas thermal conductivity
μ	[kg/ (m · s)]	Dynamic viscosity of the fluid
β		A constant specific to the gas in the pores
ε		Porosity
α		Coefficient of heat retention ability
η	[m^2/s]	The kinematic viscosity of air at the film temperature
R^2		Coefficients of determination
Adj. R^2		Adjusted coefficients of determination

List of Abbreviations

Abbreviations	Description
DC	Direct Current
DMF	Dimethylformamide
DSC	Differential Scanning Calorimetry
GSM	Areal density/surface density
ISO	International Organization for Standardization
KES	Kawabata Evaluation System
PET	Polyethylene Terephthalate
PUR	Polyurethane
PVDF	Polyvinylidene Difluoride
RTV	Room Temperature Vulcanizing
SEM	Scanning Electron Microscope
TGA	Thermogravimetric Analysis

Chapter 1 Introduction

This chapter outlines the motivation and objectives of the work described in the thesis. The first section describes the motivation for performing the experimental and analytical work included, followed by the sub-objectives and approach of the study. Finally, an overall outline is given that summarizes the contents of the thesis followed by a section that discusses the potential contribution of this work to the field of development of nanoporous materials for thermal insulation.

1.1 Motivation

As conventional thermal insulators used in technical applications, nonwoven fabrics exhibit good thermal insulation ability. Their impact on thermal insulation performance is determined by the physical and structural parameters of fibrous structures. Especially, their thermal insulation ability strongly depends on the fabric thickness. Generally, the thermal insulating ability improves with the increase in fabric thickness. However, when this thickness is limited to a few milli-meters, the insulating performance is restricted. Thus, development of high-performance thermal insulation materials to save space and energy consumption, increase comfort, decrease cost and complexity has gain increasing attention.

Nowadays, silica aerogel has been well acknowledged as one of the most attractive thermal insulating materials for applications in protective clothing, automotive industry, building and construction products. Recently, the successful and cost-effective production of silica aerogels by the use of inexpensive precursors and the ambient pressure drying method has been achieved, this raises the possibility of continuous production with lower operating costs for industrial application. [1-3] Aerogel can be used as loose bulk material for thermal insulation, but for the majority of applications a bound form such as aerogel containing sheet is required. For this purpose, aerogels are usually incorporated into lightweight textile structure such as nonwoven fabric, with the assistance of binding material. Recently, combining nonwoven fabric with silica aerogel to enhance thermal insulation ability has gained increasing interest during the past several decades.

A lot of experimental studies confirmed that the aerogel present in textile structure would significantly improve the overall thermal performance, however, the application of aerogel granules has so far been limited to a few methods such as coating, padding and impregnation. In these obtained aerogel-embedded materials, aerogel granules are exposed

or filled into the void space of textile structure, the porous space of the loose textile structure is partly filled by additive agent, the thermal performance of the final product is thus reduced since the overall pore volume which is essential to entrap air pockets is decreased. Meanwhile, the nanopores of aerogel granules are filled or covered by binding materials, this would blunt their advantage in thermal insulation ability. Furthermore, the prepared materials may lack compression resilience, causing reduced recovery after exposure to external forces, which may influence the final use and the sustainability of thermal-insulating function. However, these problems were not considered in designing aerogel based fibrous materials. Moreover, existing works were mainly focused on pure fibrous materials in absolutely flat state with a simple airflow. There appears a gap in the study on the convective heat transfer through multi-component fibrous structure system or under more complicated condition. The materials could be used in building, piping and technical applications such as winter jacket, sleeping bag and glove in extreme weather, which are not always in absolutely flat state. However, there is sparse information available regarding natural and forced convection through aerogel-based nonwoven. Although numerical simulation has been applied to evaluate the heat flux, temperature distributions, and convective heat transfer coefficients of aerogel-embedded fibrous insulating materials, thermal performance of aerogel-based nonwoven under convection conditions is still not well understood.[4-5]

1.2 Objectives

The goal of the current study is to develop silica aerogel embedded fibrous materials for thermal insulation application and evaluate their performance. The major sub-objectives of this research are as follows:

1.2.1 To study the effect of silica aerogel and binding material on the transport properties of porous textiles

Researchers have stated that the application of aerogel in textile structure may cause adverse effect on the thermal insulation enhancement since the porosity of textile fabric is reduced by the adhesive, but this was not experimentally studied. In this research, layered nanofibrous web/silica aerogel/ nonwoven materials were prepared via a laminating method by using low melting powder as binding material to investigate the effect of aerogel and thermal adhesive on transport properties. Especially, their influence on thermal

insulation properties were analyzed and discussed. Moreover, a series model was used to predict the thermal resistance, the theoretical results were compared with measured data.

1.2.2 Development of aerogel-encapsulated fibrous structures by using laser engraving technique

From previous work, it was concluded that novel techniques to combine silica aerogel with high porous textiles with less use of binding materials should be considered. In this work, a new approach to apply silica aerogel into fibrous structure without using any binding material to bond aerogel particles was proposed. To take benefit of air trapping potential in porous materials, high porous nonwoven fabrics as well as sponge foam were selected as support layers to produce air pockets by laser engraving, aerogel granules could be applied into these pockets, together with laminating a thin fabric sheet onto both surfaces of the support layer. Since both sides of the support layer were covered by flexible fabric sheet to achieve a closed fibrous system and the adhesion of aerogel with this support structure was not involved, the resultant multi-layered materials could have light weight, excellent thermal insulation ability and good flexibility simultaneously.

1.2.3 Performance evaluation of novel multilayered fibrous materials in terms of thermal and compression properties

This work attempts to explore the potential of using laser engraving to develop aerogel-encapsulated fibrous materials for cold condition use. Thus, the thermal insulation function of these novel developed materials is the main point we have to concern. Thermal performance was studied in terms of infrared thermography, thermal conductivity, resistance and coefficient of heat retention ability. In addition, a laboratory-made dynamic heat transfer device was used to figure out convective thermal behavior of these multi-layered materials under different airflow velocities and heating conditions. The real-time temperature curves of different materials were compared. The temperature difference and convective heat transfer coefficient under continuous heating condition were calculated and investigated. Meanwhile, compression performance of the novel multi-layered fibrous materials as well as air permeability was examined. The findings could contribute to new developments in flexible aerogel-embedded high-performance textile materials for both industrial and clothing applications.

1.2.4 Electro-spun nanofibrous membranes with aerogel granules and their performance evaluation

Electrospun fibrous materials with interconnected pores have the potential for use as thermal insulation materials. In this research, electrospinning process was used to produce flexible polyurethane (PUR) and polyvinylidenefluoride (PVDF) nanoporous membranes embedded with silica aerogel. Presence of aerogel granules was confirmed through microscopic examination. The transport behavior of these samples was evaluated and the results were analyzed. Thermal properties such as thermal conductivity and thermal resistance were tested and compared. Thermal stability was investigated using thermogravimetric analysis and differential scanning calorimetry.

1.2.5 Comparative analysis of high-performance fibrous materials using different evaluation techniques

Several non-conventional techniques, such as KES-FT-II Thermolabo, thermal camera, and a laboratory-made new instrument, were adopted to evaluate the transmission behavior of aerogel-embedded fibrous materials. The results were evaluated statistically, the precision of evaluation techniques was analyzed and compared.

1.3 Dissertation outline

The content of this thesis is organized into five chapters.

- **Chapter 1** Introduction
  This chapter gives a general introduction of this research work such as motivation and detailed research objectives of this thesis.
- **Chapter 2** State of the Art in Literature
  A detailed study of published literature and understanding of studies conducted and limitations in past research are summarized.
- **Chapter 3** Experimental Materials and Methods
  This chapter describes experimental materials, production methods, measurement and data acquisition used for all experiments performed in this study. Explanation about methods and techniques used for characterization, thermal measurements, mechanical measurements and other experiments conducted are also elaborated.
- **Chapter 4** Results and Discussion

A detailed analysis of the results derived from various experiments is presented. The results were tabulated, suitable graphical representations were made and detailed statistical analysis was performed. Various interpretations were drawn from the analysis.

- **Chapter 5**

  This chapter contains the broad conclusions drawn from the result and analysis of the research. An additional section discussing future research and recommendation has been included. The outputs are in the form of scientific papers, book chapters and conference proceedings.

Chapter 2 State of the Art in Literature

2.1 Purpose

The purpose of this chapter is a detailed study of existing literature for the research conducted in this thesis and highlighting the gap in the scientific study of insulation materials. The first part starts with the basic physics of heat transfer in fibrous porous materials. The second part of this chapter details the different types of porous materials used as thermal insulators. The following part introduces the applications of fibrous thermal insulating materials. The later part of this literature review introduces details of fibrous materials and their performance such as thermal properties, air permeability and compressibility. Finally, the existing literature and the highlighted research gaps relevant to the various objectives of this research work have been summarized.

2.2 Physics of heat transfer in porous fibrous materials

Insulating materials are very basic and important requirement in various applications dealing with heat transfer problems. Insulating materials have in common is their low thermal conductivity, in order to reduce the total coefficient of heat transmission. Since dry stagnant air is one of the best insulating materials with the lowest thermal conductivity over a wide range of temperatures, fibrous insulators function by trapping a large amount of air in the pores within and between their fibers. Heat transfer through fibrous insulator involves combined modes of mechanisms: conduction, convection and electromagnetic radiation.

2.2.1 Conduction

Conduction is the transfer of heat by physical contact of two surfaces with temperature differences. The conduction process occurs at the molecular level and involves the transfer of energy from the more energetic molecules to those with a lower energy level.

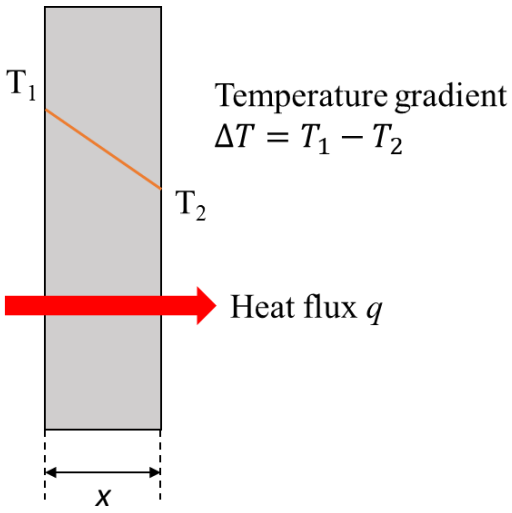

Figure 2. 1 Heat transfer by conduction

Under steady state conditions, heat transfer through a fibrous material in the direction of fabric thickness h [m], as shown in Figure 2.1, can be expressed as a one-dimensional form of the Fourier's heat conduction equation:

$$q = \lambda\left(\frac{\Delta T}{h}\right) \tag{2.1}$$

where q is the heat transfer rate in the thickness direction per unit area [W/m^2], λ is a transport property known as the thermal conductivity [W/ m · K] and is a characteristic of the material.

Fibrous insulator possesses a large amount of void space and usually more than 95% of their volume is occupied by air, the overall heat conduction in fibrous material is therefore the sum of contributions from the solid fiber and the trapped air in the inter-fiber spaces. For high-porosity fibrous materials, gas conduction is one of the most dominant modes of heat transfer while solid conduction is the least significant component of heat transfer since the thermal conductivity of air is a dozen times less than that of fibers. Hager and Steere found that fiber conduction accounted for only 0.3% of the total heat transfer.[6] Strong reported that solid conduction could account for 6-7% of the total in highly compressed glass fiber systems due to a large degree of fiber-fiber contact.[7] The contribution of gas conduction increases with an increase in temperature and static pressure, being negligible in vacuum conditions.[8] The combined solid and gas thermal conductivity λ_{sg} in high-porosity fibrous materials can be calculated by the empirical equation as given[9]

$$\lambda_{sg} = f_V\,\lambda_s + (1 - f_V)\,\lambda_g \tag{2.2}$$

where λ_s is the thermal conductivity of the solid fibers [W/m·K], λ_g is the thermal conductivity of the gas phase [W/m·K], f_V is the fiber volume fraction in the fibrous structure.

2.2.2 Convection

Convection is heat transfer by a fluid or gas caused by molecular motion. Air in contact with a warm surface absorbs heat and becomes less dense. The difference in density produced by the temperature differences forces warmed air to rise and natural convection occurs. Wind can strongly affect convection and speed up heat exchange by forced convection. The essential components of heat transfer by convection mechanisms are given in Newton's law of cooling

$$q = h_c(T_s - T_\infty) \tag{2.3}$$

where T_s is the solid surface temperature [K], T_∞ is the fluid temperature [K], h_c is the convection heat transfer coefficient [W/m^2 · K] which depends on conditions in the boundary layer and is influenced by the surface geometry, the nature of the fluid motion, and an assortment of fluid thermodynamic and transport properties.

The Reynolds Number *Re* characterizes the flow properties (laminar or turbulent):

$$Re = \frac{\rho L_c v}{\mu} \tag{2.4}$$

where ρ is the density of the fluid [kg/m^3], L_c is the characteristic length of fabric [m], v is the velocity of the object relative to the fluid [m/s], μ is the dynamic viscosity of the fluid [kg/(m · s)].

As a highly porous structure, fibrous material is inherently air-permeable. Air intrusion which occurs through the void space is usually observed in this porous material. This bulk movement of gas molecules within a porous fibrous structure may include both the natural and forced convection. Natural convection refers to temperature driven air movements as the driving forces are generated in the vertical direction in response to gravity and air density. In contrast, forced convection corresponds to air movement governed by wind or mechanical ventilation. Unlike the vertical transport of density dependent airflows, forced convection can generate highly turbulent, multi-directional flows as a function of venting

characteristics, insulation geometries, and wind speed.[10] The forced convective heat transfer through fibrous insulators is greatly influenced by wind speed.[11]

2.2.3 Radiation

Heat transfer by radiation is caused by the electro-magnetic waves which are transported from an object with higher temperature to the one with lower temperature. In fibrous structures the radiation exchange occurs only among neighboring volume elements, with the environment at the surface as well as internally among the fibers due to the very large extinction coefficient of the fibers. The radiation component is determined by the temperature of the fibers, fiber size, solidity and emissivity of the fibers and the bounding surfaces.[12] It is confirmed that radiation heat transfer through nonwoven insulations is the dominant mode of heat transfer at temperatures higher than 400K-500K.[13]

2.3 Knudsen effect in porous medium

In a porous medium the heat transfer through the gaseous phase is dictated by the Knudsen effect which expresses the gaseous conduction as a function of the air pressure and the effective pore dimension.[14] The corresponding equation is as follows:

$$\lambda_g = \frac{\lambda_g^0(T)}{1+2\beta K_n} \tag{2.5}$$

where K_n, the Knudsen number is

$$K_n = \frac{l}{l_s} \tag{2.6}$$

where l, the mean free path of the gas molecules [m] is

$$l = \frac{k_B T}{\sqrt{2}\pi d^2 p} \tag{2.7}$$

where λ_g^0 is the thermal conductivity of non-confined air [W/m· K]; β is a constant specific to the gas in the pores; l_s is a representative physical length scale [m], relates to a gap length over which thermal transport occurs through a gas phase; k_B is the Boltzmann constant (1.38065×10^{-23} [J/K]); T is the thermodynamic temperature [K]; d is the particle hard-shell diameter [m]; p is the total pressure [Pa].

Thus, the gaseous thermal conductivity in nanoporous material is directly proportional to

the pressure and pore sizes and indirectly proportional to the density. The decrease of the pore size or the gas pressure are thus two ways to decrease the gaseous heat transfer, as illustrated in Figure 2. 2.[15] The combination of very low pressure and very low pore dimension can reduce the gas heat transfer to almost zero.

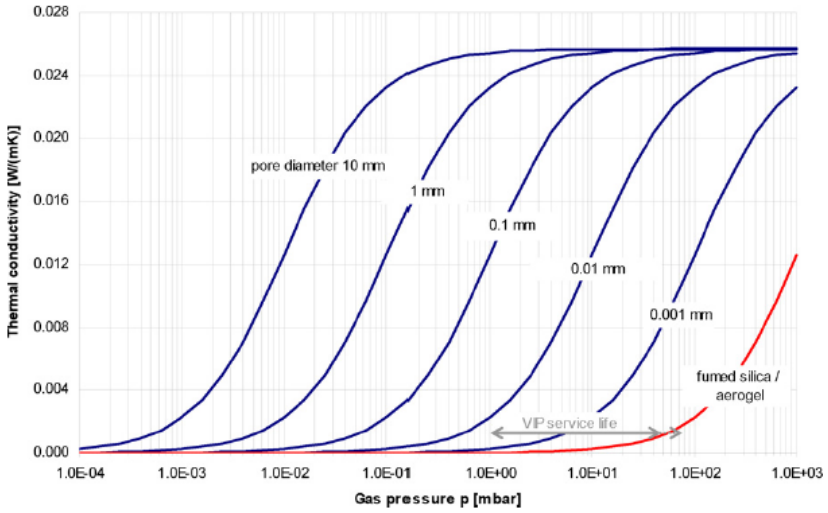

Figure 2. 2 Thermal conductivity as a function of pore size and gas pressure[15]

The effective conductivity of several porous media as a function of the gaseous pressure has been reported in Figure 2. 3.[15] For mesopores and inter-granular voids that have characteristic sizes of respectively 50 nm and 0.3 mm, Knudsen effect occurs respectively around 1 bar for mesopores and between 0.1 and 1 mbar for inter-granular voids.

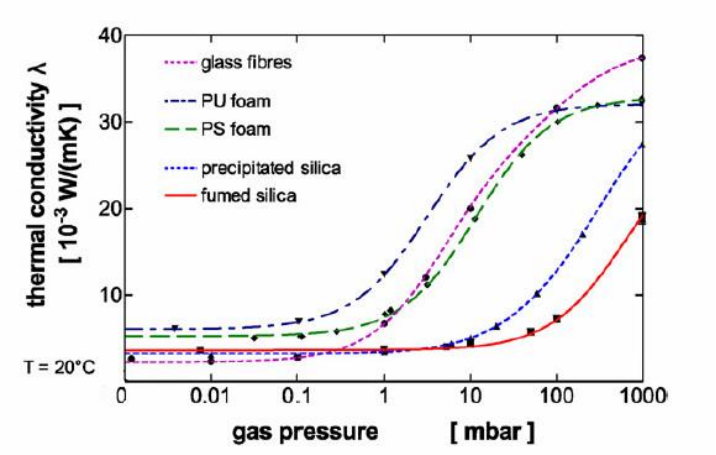

Figure 2. 3 Thermal conductivity of several porous materials as a function of gaseous pressure[15]

2.4 Porous materials in thermal insulation

2.4.1 Most commonly used categorization of insulating materials

Thermal insulation materials are materials or mixtures of materials which lowers the energy losses by retarding the amount of heat loss or gain. Insulation materials can be classified into three major categories: fibrous, cellular, and granular insulations as shown in Figure 2. 4.[16]

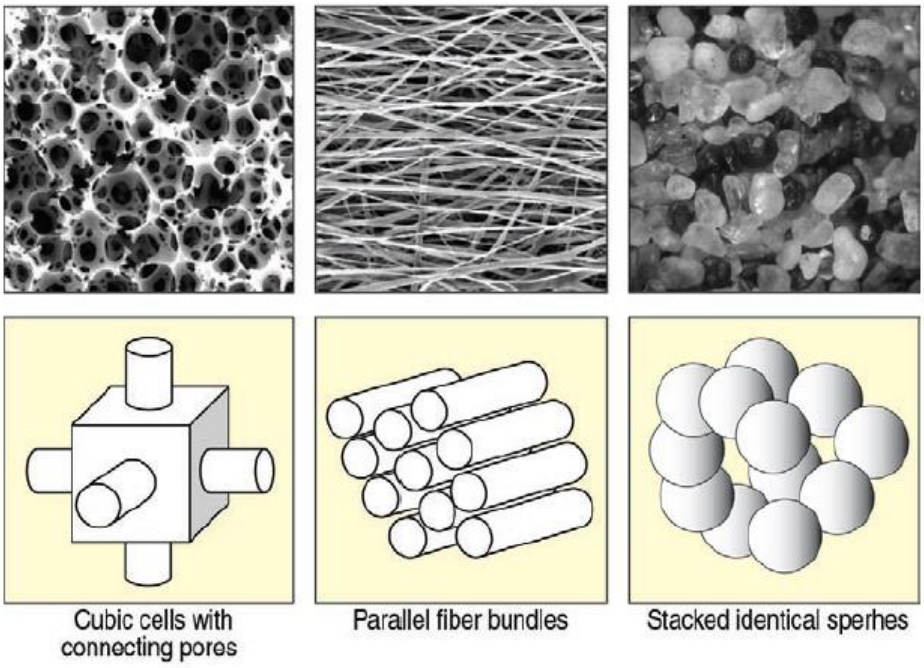

Figure 2. 4 Most commonly used categorization of porous insulating materials[16]

Fibrous insulations are made from natural or synthetic fibers with small diameters, consisting of a series of tunnel-like openings that are formed by interstices in material structures. Cellular insulation is composed of small individual cells of glass or formed plastic which are either interconnected or sealed from each other, to form a cellular structure. Materials made from open-celled polyurethane and foams are examples of cellular materials. Granular insulation materials, in the form of rigid boards, consist of relatively rigid, macroscopic bodies whose dimensions exceed those of the internal voids by many orders of magnitude, or loosely packed assemblages of individual particles. Among these materials, fibrous materials have a unique structure of complex geometry that belongs to a typical kind of porous material, exhibiting other features that make their use advantageous as insulation materials, for example, allowing cost-effective manufacture

and great flexibility of the processes and products.

2.4.2 Fibrous materials

Nonwovens are manufactured sheets or web structures bonded together by entangling fibers or filaments, by various mechanical, thermal, and/or chemical processes.[17] Nonwoven fabrics are mainly in a flat form (two dimensional) or three-dimensional structure when their thickness becomes significant. Due to the unique structure, nonwoven fabrics possess plenty of functional properties such as high bulkiness and resilience, great compressional resistance, good filling properties and excellent thermal-insulating properties.[18] Cost-effective nonwoven fabrics act as an excellent thermal insulator by lowering conductive and convective heat energy transfer through fabrics. Thermal properties of nonwoven assemblies can be engineered by changing the type of fiber, porosity and the amount of air inside the structure.

2.4.3 Nanofibrous materials

Electrospinning is a low-cost technique using electrostatic forces to produce nano or micro scale fibers from polymer solutions.[19-21] Nanofibers are usually collected in the form of nanofibrous web or membrane. An electrospun nanofibrous web possesses several amazing characteristics such as high density of pores, high surface area to volume ratio, high permeability, low basis weight and small fiber diameter.[22] A typical microstructure is shown in Figure 2. 5.

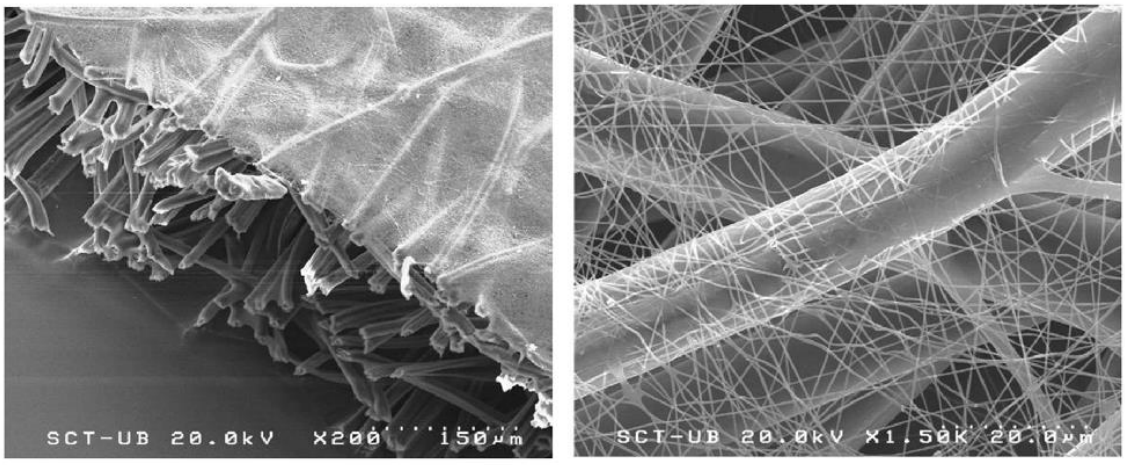

Figure 2. 5 Nanofibrous layer on nonwoven fabric[23]

Electrospun fibrous materials with interconnected pores have the potential for use as a

thermal insulation material. In fact, insulation property of the electrospun membrane is poor at low bulk density although it improves at higher density, and thinner nanofibers exhibit greater thermal insulation characteristics.[24-25] When the nanofiber diameter is less than 261 nm with bulk density more than 176 kg/m^3, thermal conductivity drops below 0.02 W/m · K.[26] This has been attributed to greater surface area to volume ratio which increases radiation absorption and scatter. Reducing fiber diameter also has the effect of reducing membrane pore size. This also reduces radiation due to less photon passing through open spaces between nanofibers.

2.4.4 Silica aerogel

Silica aerogel can be defined as a coherent, rigid three-dimensional network of contiguous particles of colloidal silica, which can be prepared by the polymerization of silicic acid or by the aggregation of particles of colloidal silica.[27-28] Silica aerogel possesses a special microstructure with very high porosity, the pore volume represents more than 90% of its overall volume and their characteristic size range from 2 and 50 nm. Figure 2.6 shows the 3D network of porous silica, which is constructed by primary and secondary silica particles.[29]

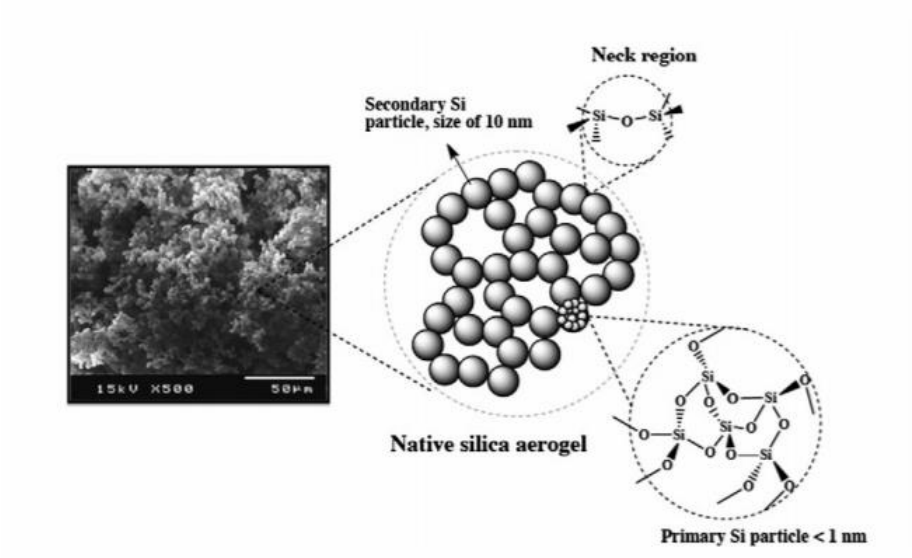

Figure 2. 6 Typical SEM image of silica aerogels with schematic representation of primary and secondary silica particles[29]

Silica aerogel demonstrates superior thermal insulation performance with extremely low thermal conductivity (0.015 W/m·K), low bulk density (0.1 g/cm^3) and high specific

surface area (1000 m^2/g).[30-32] However, since the silica aerogels comprise highly open structures in which the secondary particles of silica are connected to each other with only few siloxane bonds, the silica aerogels generally have poor mechanical stability, such as low strength and high brittleness. The flexural strength of the pure silica aerogel with the density of 0.1 g/cm^3 was approximately 0.02 MPa and the collapse strength under compression of the silica aerogel with the density of 0.21 g/cm^3 was approximately 2.5 MPa.[33-34] The low flexural and collapse strength of the aerogels greatly limited their applications for thermal insulation.

2.4.5 Combination

2.4.5.1 Aerogel-embedded fibrous materials

Aerogel-embedded fibrous materials are mainly made of fibers, aerogel and air. The effective thermal conductivity of these materials essentially depends upon the volume fraction of fiber, aerogel and air inside the composites.[35-36] Mostly polypropylene, polyester and glass nonwoven fibrous structures are used for aerogel-embedded fibrous composites.

Two general strategies were usually used to prepare silica aerogel-embedded fibrous materials. The first technique involves immersing the nonwoven fabric into the sol-gel solution or impregnating a fiber network by such a mixture and followed by supercritical drying to produce silica aerogel-fiber composites in the form of blankets.[37-40] Most commercially available aerogel blankets are produced by this method.[41] A two-step process via the ambient drying process was successfully used to produce mineral wool-aerogel blanket, the cost and production time of this proposed process can be significantly decreased. As aerogel is mixed with mineral wool, the measured thermal conductivity of mineral wool-aerogel composite can be reduced to 0.055 W/m· K.[42] The thermal resistance and mechanical deformation of aerogel blankets have been evaluated under compressive mechanical loading.[43] Results indicated that aerogel blankets remain remarkably effective thermal insulation materials under compression.

The second one is the incorporation of existing aerogel beads into a nonwoven fibrous web before bonding of the low melting point fibers or by using additive binding materials to prepare silica aerogel-polyester nonwoven composite. This method is widely used due to lower production costs of aerogel granules.[44] Silica aerogel nanoparticles have been

incorporated in wool-Aramid blended fabrics by coating, results showed that the coating of aerogel nanoparticle could increase thermal resistance by up to 68.64%.[45] A study of coating silica aerogel on cotton woven fabrics indicated that the thermal properties of coated high-density cotton fabric were strongly influenced by finishing agent concentration.[46] The fibrous structure density and the aerogel present in the fibrous nonwovens with silica aerogel impregnation have significant effect on thermal properties of the overall structures.[47] Meanwhile, thermal insulation of aerogel-embedded nonwoven was observed to strongly dependent on the weight and compressional properties of the fabric.[48] The modeling and simulation of heat transfer for aerogel-embedded nonwoven fabric has confirmed the improvement of thermal behavior when treated with aerogel.[49]

However, the fine dust particles of silica aerogels could result in an unpleasant feeling when using silica aerogel-embedded products. In this case, the aerogel-embedded nonwovens could be sandwiched between two layers of fabrics to avoid the direct contact of these fabrics with human skin. In addition, the probable infiltration of the binding materials into the pores of the aerogel definitely eliminates the attractive properties of the aerogels.[50]

2.4.5.2 Aerogel-filled hydrospace fabric

Hydrospace, made from a carded and cross-laid web, involves the formation of molded voids within the cross-section of hydroentangled fabrics using hydroentanglement technique. The voids within the material have a predefined shape and size, which can be filled with solids, liquids, waxes or gels. The fabric surfaces can be tailored to control the rate of delivery of the cavity contents in a specific direction.[51] These voids filled with loose aerogel particles composed of amorphous silica are shown in Figure 2.7.[52] It is evident that the aerogel-filled voids give rise to a lower radiated temperature as compared to the air-filled voids (Figure 2. 8).

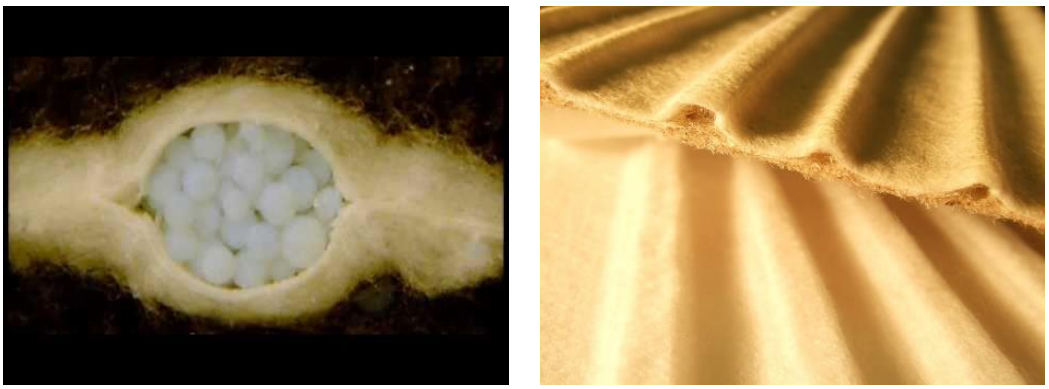

Figure 2. 7 Image of hydrospace fabric filled with loose aerogel particles[52]

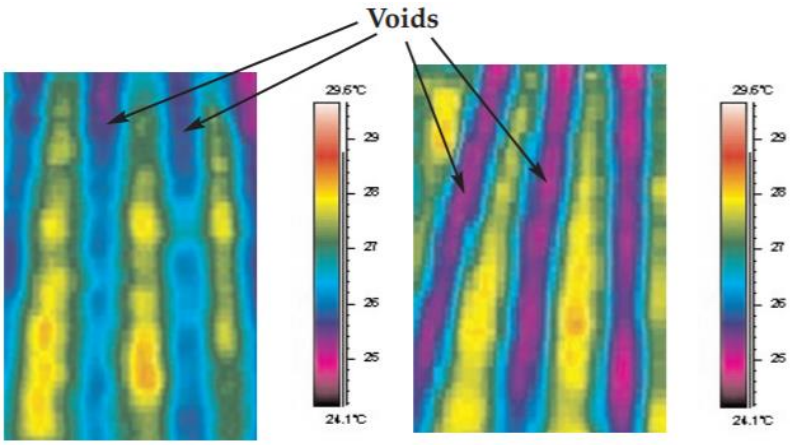

Figure 2. 8 Infrared image of a hydrospace fabric (Left with air, right with aerogels)[52]

2.4.5.3 Nanofiber-reinforced aerogel composites

Electrospun PVDF nanofiber supported SiO_2 aerogel composites that had a low thermal conductivity of 0.027 W/m·K were successfully synthesized via electrospinning and sol-gel processing.[53] In addition, the compressive strength and the flexibility of the aerogel composites were significantly improved via the reinforcement of the electrospun PVDF fibers. It opens a controllable way to improve and engineer the mechanical properties of the aerogel composites with low thermal conductivity via combining the aerogels by using electrospun nanofibers. Yin song Si[54] prepared silica nanofibrous membranes with ultra-softness and enhanced tensile strength via an electrospinning technique with a sol-gel solution containing NaCl. The as-prepared silica nanofibrous membranes with ultra-softness and relatively high tensile strength exhibit an ultra-low thermal conductivity of 0.0058 W/ m·K as seen in Figure 2. 9.

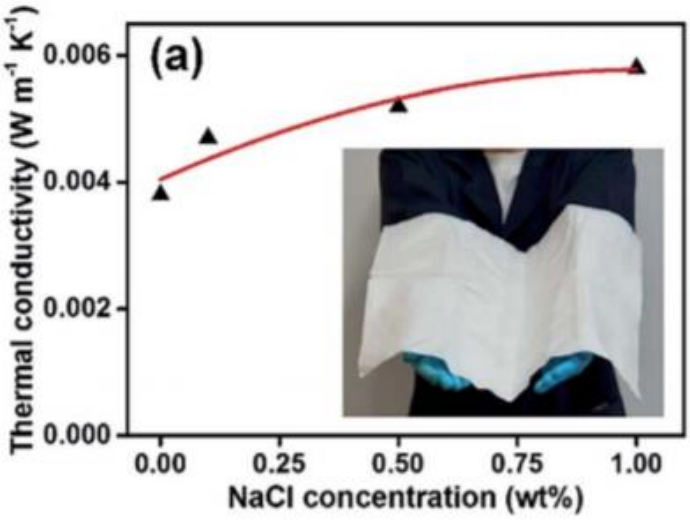

Figure 2. 9 Thermal conductivity of the silica nanofibrous membranes[54]

2.5 Applications of fibrous insulators

Fibrous materials, are very basic and important requirement in applications dealing with heat transfer problems for building, industrial facilities and protective textiles. Fibrous insulation material can be installed on the building structure, roof, walls and attic spaces, as well as domestic hot water plumbing lines, chilled water supply and return lines and air distribution ducts to improve energy efficiency and to protect the building constructional elements against thermal impact. These thermal insulators could be a major contributor for achieving energy efficiency especially in buildings located in sites with harsh climatic conditions.[55] For industrial facilities thermal insulation is installed on process equipment, piping, steam and condensate distribution systems, boilers, smoke stacks, bag houses, furnaces, kilns and storage tanks, et for process control, energy efficiency and safety.[56] In addition, flexible fibrous materials with high insulating ability have been utilized as garment components within clothing systems.[57] Especially, high-performance fibrous materials are necessary to be used in extremely cold weather conditions to protect human body against climatic influence. Examples include winter jacket, sleeping bags, blanket, gloves or embedded thermal protective clothing.

2.6 Characteristics of fibrous thermal-insulating materials

This section literately presents thermal properties of fibrous thermal-insulating materials especially the effect of various physical and structural parameters of fibrous thermal-insulating materials on thermal behavior. Air permeability and compressibility

which are related to thermal performance and the sustainability of thermal insulating function are also investigated.

2.6.1 Thermal properties of fibrous materials

Thermal properties of a fibrous material are affected by the physical parameters of the fiber component as well as structural parameters of the fibrous structure. This part groups the thermal properties of fibrous materials into several determining factors such as fiber properties, fabric structure, environmental factors and so on.

2.6.1.1 Fiber properties

Fiber is the key component of fabrics. Fibers in the fabric structure serve two main functions in providing thermal insulation. Firstly, they develop air spaces and prevent air movement. Secondly, the fibers provide a shield to heat loss from radiation. The thermal properties depend on fiber type, physical structure of the fibers, such as fiber fineness, length, cross-section shape and fiber crimp. The thermal conductivity of various fibers is shown in Figure 2. 10.

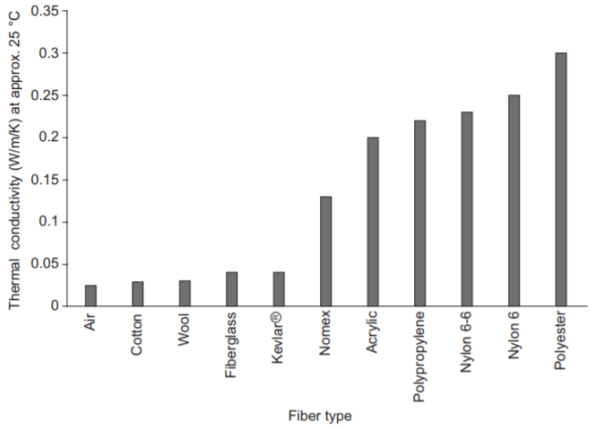

Figure 2. 10 Thermal conductivity of various fibers[58]

For a given material density or packing fraction, the finer the fiber, the higher the surface-to-volume ratio.[59] As a result, smaller spaces for still air between fibers can be formed, achieving a higher thermal insulation because the heat transfer by conduction and convection through the still air is limited. In addition, the increased absorption surface area for radiation could be another reason for the low thermal conductivity of nonwovens containing fine fibers.[59-61] In recent years using fine microfibers which possess larger

surface area and twice the bulk of the normal fibers in garments particularly in sportswear, sleeping bags and tents to achieve high thermal insulation is a good example.

Thermal conductivity of fibrous material increases with the fiber length and approaches a stable value when the fiber length is sufficiently long as seen in Figure 2. 11.[62] However, the length of fiber was observed to have no direct effect on radiative thermal conductivity.[63]

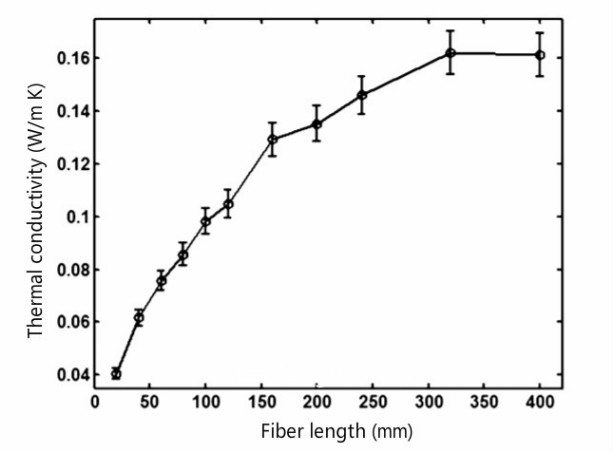

Figure 2. 11 Effect of fiber length on thermal conductivity[62]

Fiber crimp develops more trapped air by creating interstices in the structure that effectively increase the fabric thermal insulation and also resist its movement. Man-made fibers can be produced with a degree of crimp or surface irregularity that increases thermal resistance. Wool fibers possess natural crimp and maintain a high volume of still air, explaining their traditional use in cold weather clothing.

A study of heat transfer in three con-figurations of fibers, hollow, solid and a mixture of the two by Kong et al.[64] found that fiber porosity has a significant effect on heat transfer. Fabrics made from hollow fibers can provide better thermal insulation values due to the larger trapped air volume provided. Hollow fibers developed with different cross-sectional shapes and even some voids on the fiber surface, or more convolutions created along the fiber result in additional thermal insulation as well as reduction in fiber weight.

2.6.1.2 Fabric structural parameters

A fibrous material is inherently a porous material which is defined as a material characterized by the presence of a solid matrix, and a void phase that is presented by its porosity. Porosity describes the fraction of void space in the total material volume.

Porosity of fibrous structures ε is usually calculated by using experimentally evaluated fiber density ρ_f[kg/m^3] and the density of corresponding fibrous materials ρ [kg/m^3]

$$\varepsilon = 1 - \frac{\rho}{\rho_f} \tag{2.8}$$

The areal density (GSM) ρ_s [g/m^2] can be calculated according to the following equation:

$$\rho_s = \rho_f \cdot h \tag{2.9}$$

where h is the thickness of a fibrous material [m].

Porosity has been reported to be an important factor in determining the thermal insulating performance of a fibrous insulator.[65-67] Thermal conductivity increases with the porosity of material (in the porosity range of 70–90%) at a near-linear rate as shown in Figure 2. 12.[68] The same result was found by Wang[62] in the study of a numerical simulation for predicting the effective thermal conductivity of natural fibrous materials. In addition, thermal properties are influenced by pore features as well. When materials have the same porosity, the one with small and close pores has a smaller thermal conductivity then the one with big and open pores, due to the weakening of the heat-convection in the air.[69]

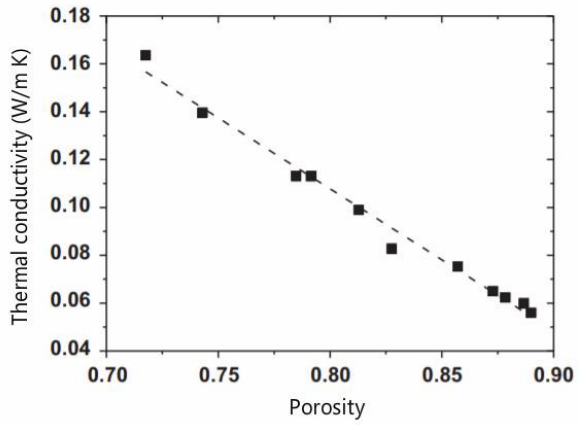

Figure 2. 12 Thermal conductivity as a function of porosity[68]

A number of studies indicate that fabric thickness is the single most important variable in determining thermal insulation. A thicker fabric provides more air space and, therefore, more entrapped air in the fabric. Thermal insulation increases with fabric thickness, whereas if fabric thickness is maintained constant then thermal insulation decreases with increase in weight as quantity of enclosed air is reduced.[70-72] In some case fabric thermal insulation exhibits a linear relation with fabric thickness as shown in Figure 2. 13.[73-74] Multiple fabric layers add to the overall thickness which contributes to the total insulation

provided by the layered system.

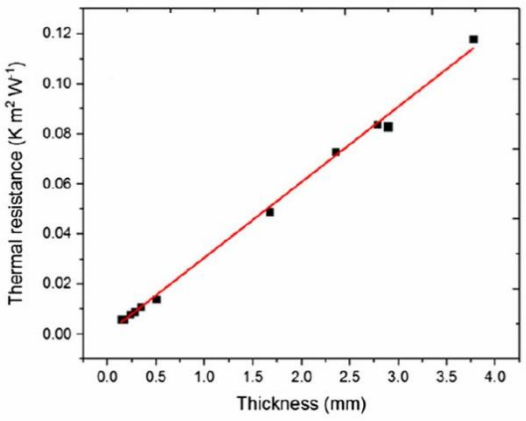

Figure 2. 13 Thermal resistance of nonwovens as a function of fabric thickness[74]

Fabric density is a significant factor influencing the radiation component of effective thermal conductivity and the radiative thermal conductivity decreases with the increase in fabric density.[63] Mao[75] also stated that the increase in bulk density causes drastic reduction in radiative heat transfer and if fiber orientation and heat flux flow are parallel then radiative heat component increases because of less reflection of incident radiations. Meanwhile, increasing the through-thickness orientation of the fibers increases the thermal conductivity of the solid structure as shown in Figure 2. 14.[76] This is because increasing fibers' through-thickness orientation increases the probability that heat flows along the length of the fibers and through the narrow fiber-to-fiber contact areas.

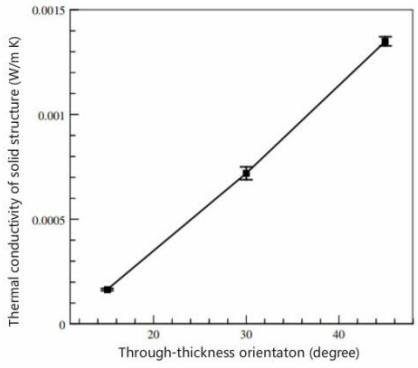

Figure 2. 14 Effect of through-thickness fiber orientation on thermal conductivity[76]

2.6.1.3 Other factors

Caps et al[77] reported that wind speed affects the thermal insulation of a nonwoven because it causes forced convection of heat through trapped air and if the heat flow is parallel to

fiber orientation then the conductivity increases. Besides, thermal conductivity of fibrous materials increases with increasing environmental temperature because the contribution of radiation, convection, and conduction to the thermal conductivity of a fabric increases significantly with increases in the temperature.[78] Paul et al[79] concluded that elimination of bonding material while making multilayered fabrics reduces heat transfer through fabric.

2.6.2 Air permeability of fibrous materials

Air permeability is known as one of the important performance characteristics of fibrous porous materials. Base on Darcy's law, air permeability is directly proportional to the pressure gradient between the two sides of a measuring fabric.[80-81] The physical characteristics of the fibers and their aggregate pattern directly influence the air permeability of nonwoven structures.[82] The air permeability of nonwoven fabrics decreases with the increase in fabric thickness and fabric density while increases with the increase in porosity.[83-85] Air permeability has been reported to increase with the increase in pore size and the ratio of pore area to total area of fabric, which are more significant than fabric porosity.[86] Moreover, it was stated that the thermal behavior of fibrous materials under convection is strongly related to air permeability.[86] Banks-Lee et al.[87] compared the thermal conductivity of composite nonwovens with air permeability and obtained a very high degree of correlation.

2.6.3 Compression performance of fibrous materials

Due to high degree of flexibility and compressibility, fibrous assemblies readily undergo structural deformation when exposed to a compressive stress. In many cases, a product is designed, manufactured, and even tested and rated, in the absence of any compressive stress. However, in practice, and often, the material is subjected to compression.[88]

Fiber bending, slippage, and compression of fiber at contact points between fibers are main processes occurring under the compression forces.[89] The compression hysteresis as shown in Figure 2. 15 (a) gives a strong indicator about the material capacity to absorb energy and/or relief pressure.[90] The area under the loading curve is the total mechanical energy input, the area under the return curve is considered as the return of stored energy, and the area between the two curves is the energy which cannot be returned but rather dissipated and converted to heat.

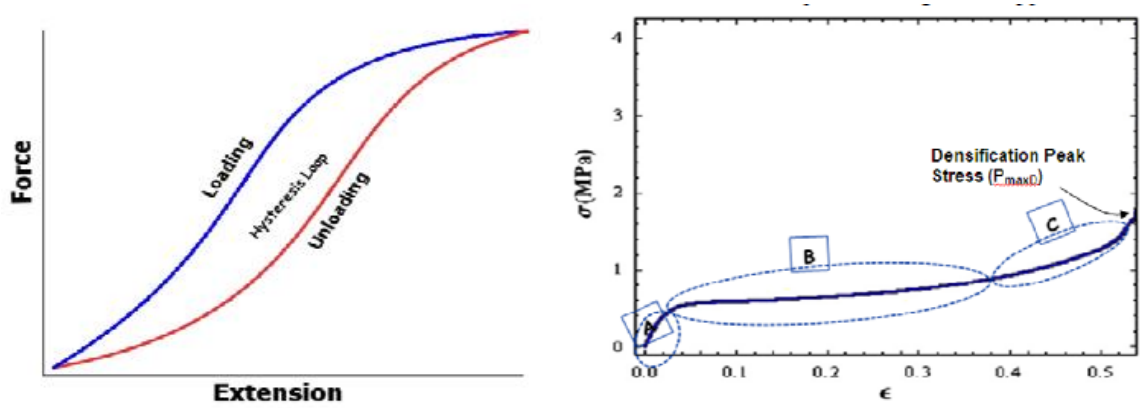

Figure 2. 15 (a) Hysteresis loop for a typical viscoelastic material and (b) Stress-strain curve under compression testing. A: linear elastic region, B: plateau region, C: densification region[90]

Generally, the deformation of typical viscoelastic material shows three main regions as seen in Figure. 2. 15 (b). These regions can be divided into an initial linear elastic region where strain energy is stored in the reversible bending of the struts, a plateau region where struts begin to impinge upon each other and finally the third region which is the densification area. During the final stage, the material essentially becomes a solid composed of the solid material. This densification occurs when foam cells crush each other causing the internal compression strength to increase rapidly.[91]

Compressional resistance of perpendicularly-laid and cross-laid nonwovens have been compared by Parikh et al.[92-93]. Results showed that perpendicularly-laid nonwovens have higher compressional resistance and better recovery properties than cross-laid nonwovens. S. Jaganathan et al.[94] have investigated different compression levels on the pore characteristics of polyester fibrous structure. They stated that the pore size distribution has become markedly narrower under the compression and the tail of the distribution is dramatically reduced as seen in Figure 2.16. Meanwhile, after compression the nonwovens tended to have a gradient density distribution in the thickness direction (Figure 2.17). Since the pore characteristics and fabric thickness are very important factors in determining thermal properties of fibrous materials, the compressibility was reported to have a linear relationship with thermal conductivity.[95]

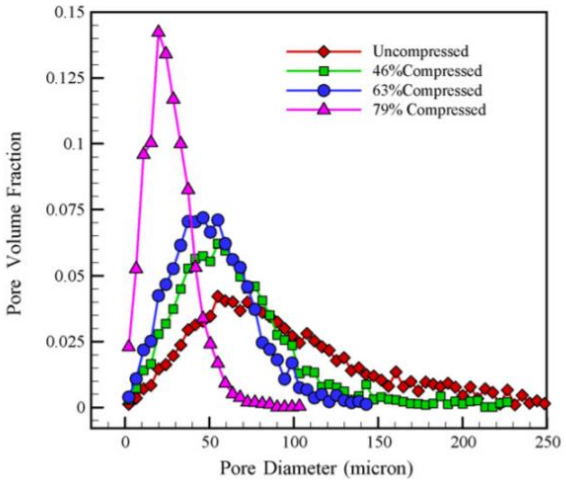

Figure 2. 16 Effect of compression on the geometric pore size distribution of the fibrous structures[94]

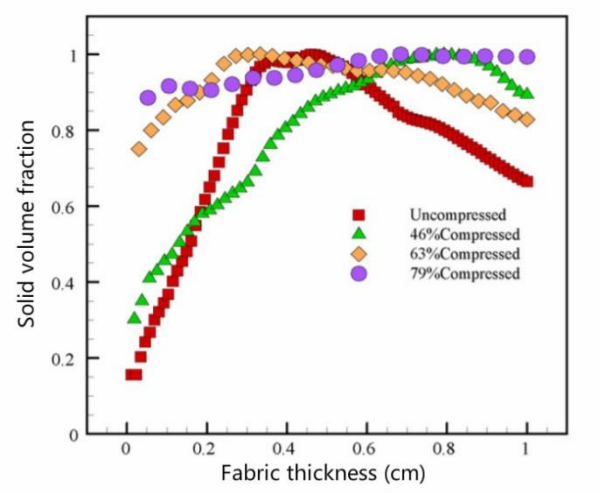

Figure 2. 17 Change of the solid volume fraction in the thickness direction due to compression[94]

Chapter 3 Experimental Part

3.1 Materials

In this study, six types of layered nanofibrous web/silica aerogel/ nonwoven samples with different aerogel content (sample A0, A1, A2, A3, A4 and A5) were used to examine thermal performance as well as air permeability. These samples were prepared via laminating technique by using low melting powder as thermal binding material. The top layer was polyacrylonitrile nanofiber web, the bottom layer was polyester nonwoven substrate, the thin middle layer was the mixture of thermal adhesive powder and silica aerogel particles. Hydrophobic amorphous silica aerogel particles which are most suitable for applications in textile material to provide super insulating properties in a flexible form were used. The effect of aerogel content and thermal adhesive on thermal insulation properties was investigated and analyzed.

Twelve multi-layered samples with novel structures were developed. The samples were designed with three layers: a middle layer with novel structure, and thin fabric layers laminated on both sides. These samples are prepared on the basis of three highly porous Struto nonwoven fabrics and one polyurethane foam which were selected as middle layers to produce air pockets by laser engraving. Aerogel granules can be injected into these air pockets and sealed in the structure by laminating a fabric layer on both surfaces. Details of the samples are presented in Table 3.1. Sample codes P, Q and X refer to three types of Struto nonwovens with different fabric thickness and density, the details were given in the section of sample preparation. These Struto nonwovens are perpendicularly laid nonwoven textiles where the fibrous layers show considerably increased resistances to compression and deformation and a high level of recovery after loading. Elastic recovery in the case is higher than standard textiles with horizontally laid fibers. Based on each Struto nonwoven, three structures including regular structure, air pockets structure and aerogel-encapsulated structure were prepared for comparison. For example, sample P1, P2 and P3 correspond to multilayered materials with different middle layer structures, respectively regular Struto nonwoven P, Struto nonwoven P with air pockets and aerogel-encapsulated Struto nonwoven P. Sample Q1, Q2, Q3 and sample X1, X2, X3 follow the same configurations. Sample Y1, Y2 and Y3 are multi-layered materials with the three different structures of polyurethane foam as middle layers.

Sample B1, B2 and B3 are 50:50 ratio compositions of polyester/polyethylene nonwoven fabrics treated with aerogel. The aerogel particles were added during the thermal bonding of the nonwoven web. The samples were chosen in three different thickness. Thermal performance under convective heat transfer were measured to compare with newly developed aerogel-encapsulated materials.

Table 3. 1 Description of samples

Sample No.	Aerogel content g/m^2	Fabric thickness mm	95% confidence interval	Areal density g/m^2	95% confidence interval	Fabric density kg/m^3	95% confidence interval
A0	0	1.25	1.25±0.01	62.01	62.01±2.12	49.61	49.61±1.57
A1	1.25	1.30	1.30±0.06	63.75	63.75±1.97	49.41	49.41±1.52
A2	2.50	1.37	1.37±0.05	67.28	67.28±2.44	49.11	47.72±1.73
A3	3.75	1.42	1.42±0.09	69.97	69.97±1.85	49.27	49.27±1.30
A4	5.00	1.48	1.48±0.11	71.77	71.77±1.46	48.49	48.49±0.97
A5	6.25	1.53	1.53±0.04	73.21	73.21±1.23	47.85	47.85±0.83
B1	1.38	3.50	3.5±0.02	278.6	278.6±1.02	79.6	79.6±0.51
B2	9.31	6.60	6.6±0.07	440.2	440.2±1.05	66.7	66.7±0.32
B3	13.48	6.20	6.2±0.01	498.5	498.5±1.10	80.4	80.4±0.62
P1	0	12.80	12.80±0.13	420.32	420.32±7.30	32.83	32.83±0.57
P2	0	12.92	12.92±0.22	386.58	386.58±9.40	29.92	29.92±0.73
P3	26.76	12.88	12.88±0.19	415.25	415.25±10.4	32.24	32.24±0.81
Q1	0	9.88	9.88±0.09	363.41	363.41±9.50	36.78	36.78±0.96
Q2	0	10.11	10.11±0.11	344.75	344.75±8.90	34.10	34.10±0.79
Q3	38.42	10.18	10.18±0.17	381.36	381.36±7.72	37.42	37.42±0.78
X1	0	12.50	12.50±0.23	279.57	279.57±5.79	22.37	22.37±0.46
X2	0	12.64	12.64±0.17	262.38	262.38±7.48	20.76	20.76±0.59
X3	29.33	12.64	12.64±0.15	293.65	293.65±7.72	23.23	23.23±0.61
Y1	0	7.09	7.09±0.03	287.81	287.81±3.64	40.59	40.59±0.52
Y2	0	7.15	7.15±0.05	272.15	272.15±3.28	38.06	38.06±0.46
Y3	14.98	7.13	7.13±0.05	292.08	292.08±4.95	40.96	40.96±0.69

3.2 Sample preparation

3.2.1 Production of layered nanofibrous web/silica aerogel/ nonwoven

Polyacrylonitrile nanofiber web with areal density of 1.17 g/m^2 from CXI lab (nanocenter, TUL, Czech Republic) was selected as top layer, a nonwoven substrate made by 100% polyester was used as bottom layer. The nonwoven was light-weight and highly porous needle-punched. The thickness of nonwoven substrate was 1.21 mm, weight 52.02 g/m^2. Silica aerogel granules purchased from Cabot aerogel Corp. were incorporated with the layered systems, specifications of the aerogel granule are shown in Table 3. 2.

Table 3. 2 Specifications of aerogel particles

Properties	Value range
Particle size (mm)	0.1-0.7
Pore diameter (nm)	~ 20
Particle density (kg/m^3)	About 120
Thermal conductivity (W/m·K)	0.012 (at 25°C)

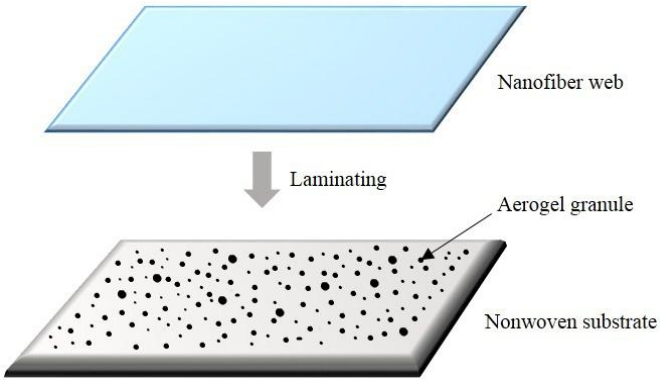

Figure 3. 1 Structure of layered nanofibrous web/silica aerogel/ nonwoven

The layered nanofibrous web/silica aerogel/ nonwoven materials were prepared via laminating technique, using low melting powder as thermal binding material. Aerogel granules as well as low melting powder were uniformly applied to the nonwoven substrate, followed by the placement of nanofiber web at the top (Figure 3. 1). The low melting powder used was 10 g/m^2, which was determined by previous studies. The layered system was subsequently held together on a heated plate at 110°C at a given pressure, and the layered fabric was obtained as it cooled down. In order to investigate the effect of aerogel content on thermal properties, layered fabrics containing varying content of aerogel were

developed. A layered fabric without aerogel granules was also prepared as control sample.

3.2.2 Fabrication of silica aerogel-encapsulated nonwovens

Three types of nonwoven fabrics prepared at Technical University of Liberec, Czech Republic, by using a vibrating perpendicular lapper, as well as one PU foam were selected as support layer to encapsulate silica aerogels. The nonwoven samples were made by 70 % polyethylene terephthalate (PET) and 30 % bi-component PET fibers, the fiber specifications are listed in Table 3. 3. The sheath part of bi-component fibers is low-melting polyethylene terephthalate with melting temperature around 120℃, and the core part is polyethylene terephthalate with melting temperature 160-180℃. The thermal conductivity values of PET and Bi-component PET are between 0.15 W/m K and 0.24 W/m K.

Table 3. 3 Specifications of polyester fibers used to fabricate nonwovens

Fiber type	Diameter μm	95% confidence interval for diameter	Fiber length mm	Ratio of core and sheath
PET	26.91	26.91 ± 0.439	57.00	-
Biocomponent PET	14.58	14.58 ± 0.198	38.00	3:1

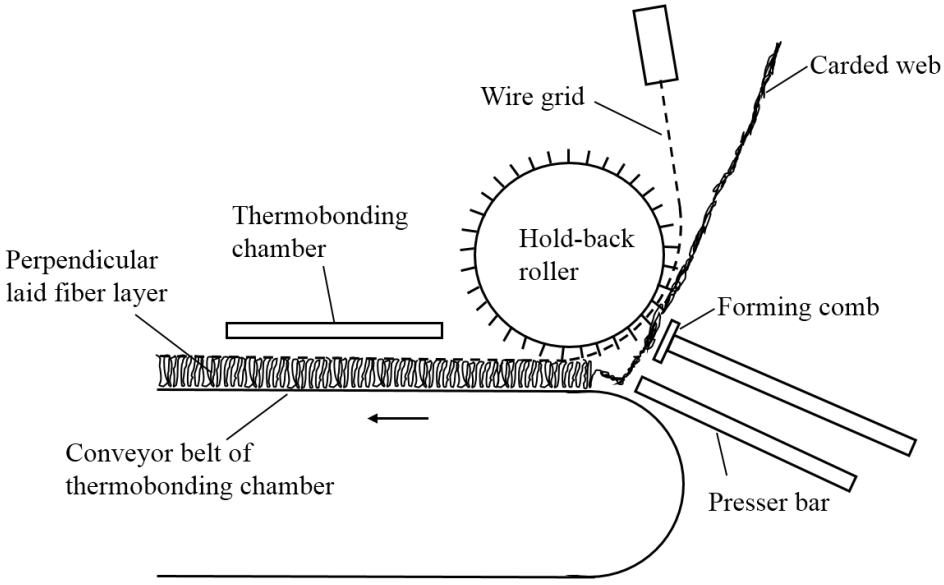

Figure 3. 2 Vibrating perpendicular lapper used to fabricate Struto nonwovens

The vibrating perpendicular lapper used to fabricate Struto nonwovens is illustrated in

Figure 3. 2. The carded web is fed onto the conveyor belt and a reciprocating forming comb pulls the carded web toward the hold back roller to form a fold. The fold is pulled off the comb by a system of needles placed on a reciprocating compressing bar and pushed to the fiber layer, which is created and moved between the conveyor belt and a wire grid.[96] The fiber layer is bonded by melting bonding fibers present in the fiber blend when it passes through the thermo-bonding chamber. The characteristics of the obtained nonwoven specimens are listed in Table 3. 4.

Table 3. 4 Structural parameters of materials used as support layers

Sample codes	Structure	Porosity %	Bulk density kg/m^3	Thickness mm	Areal density g/m^2
P	Struto nonwoven	96.69	25.56	12.42	317.51
Q	Struto nonwoven	97.93	26.79	9.68	259.28
X	Struto nonwoven	99.19	16.48	12.05	198.64
Y	PU sponge	92.72	29.54	6.67	197.01

A spun-melt PET nonwoven fabric with thickness 0.25 mm and GSM 25 g/m^2 was used as cover layer (M) to laminate onto both sides of the support layers. In order to bond the cover fabric (M) with support layer and maintain the flexibility of the multilayer materials, an extra soft textile adhesive film with thickness 0.10 mm, was used for laminating process. This adhesive film is made by applying acrylic adhesives to polyethylene nonwoven sheet.

Figure 3. 3 Image of laser system GFK Marcatex FLEXI-150

In order to produce air pockets on the nonwoven fabrics to encapsulate silica aerogels, the support layers (P, Q, X and Y) were treated by a commercial pulsed CO_2 laser system GFK Marcatex FLEXI-150 (as shown in Figure 3. 3) to remove certain materials as the laser beam vaporizes the surface.[97]

This CO_2 laser machine consists of CO_2 laser, computer laser treatment software, automatic control and laser mechanics. The laser treatment can make design on fabrics by scanning the design by line with the laser, according to the resolution dot of designed graphic images. The laser head moves back and forth to engrave a series of dots in one line at a time. While it moves line by line, the dot pattern will form the designed image by laser engraving on fabrics.[98] Before the laser treatment, the dot pattern file was designed in grey scale by Photoshop CS4 graphic design software as shown in Figure 3. 4 (a).

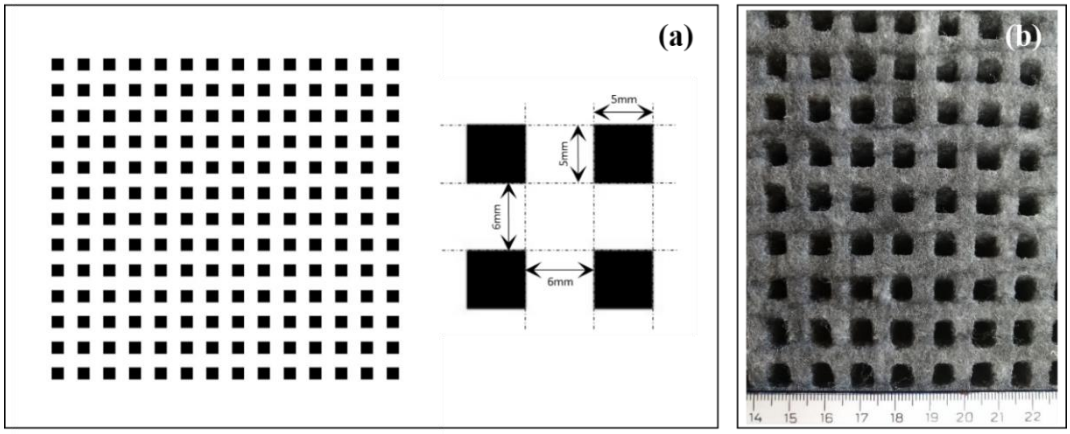

Figure 3. 4 Dot pattern used for laser engraving: (a) Designed dot pattern and (b) Typical image of laser engraved sample

The generated wavelength of laser beam was set at 10.6 μm and the input voltage was 100V. Nonwoven samples were placed in the laser treatment cabinet for testing with different parameters such as duty circle, pixel time and resolution, followed by the laser engraving on nonwovens with optimized parameters. The duty cycle is synonymous with the power applied and represents the ratio of the laser time on (pulse width) and laser time off. Its maximum value is 50% for the equipment used. The pixel time is the time in microseconds used to mark each pixel of the image.[99] Therefore, by adjusting duty cycle and pixel time it is possible to search out the best experimental conditions with this specific equipment. The specifications of optimized parameters are listed in Table 3. 5. P', Q', X' and Y' refer to laser-engraved support layers, corresponding to nonwoven materials P, Q, X and PU foam Y respectively.

Table 3. 5 Specifications of parameters for laser treatment

Parameter	P'	Q'	X'	Y'
Duty circle %	50	50	45	45
Pixel time μs	100	50	50	80
Resolution dpi	96	96	96	96

Since the obtained dot dimension is strongly dependent on the structural parameters and physical properties of the support layers, in order to achieve the designed air pocket size for different support layers, the duty circle and pixel time required for laser treatment varies with the fabric thickness and GSM. Typical image of laser engraved nonwoven fabric is shown in Figure 3. 4 (b).

Conventionally, laminating can be used to combine two fabrics by applying adhesive or using heat and pressure. A laminated technical textile normally consists of two or more textile layers, bonded closely together by means of an added adhesive or the adhesive properties of the component layers.[100] In this work, the covering fabric was laminated onto the Struto nonwovens by using an adhesive film. A piece of adhesive film was inserted between the covering fabric and a laser-treated support layer, proper pressure was applied to bring sufficient adhesive effect between the support layer and covering fabric. The obtained fabrics was then turned over, aerogel granules were injected into these air pockets. Another covering fabric was subsequently combined with the composites to form a closed fabric system. The fabrication process was illustrated in Figure 3. 5.

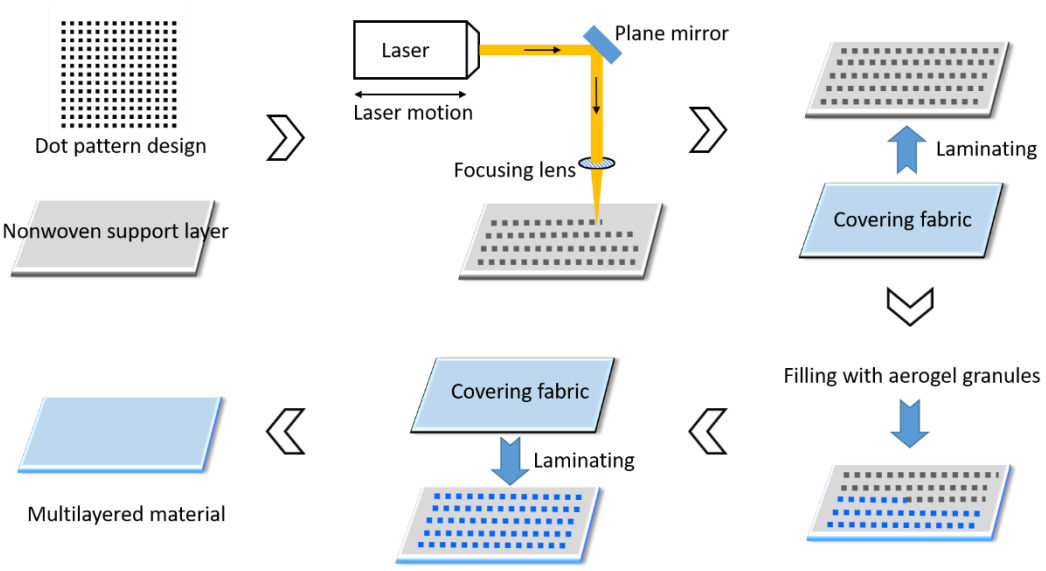

Figure 3. 5 Fabrication process of aerogel-encapsulated materials

The resultant materials were multi-layered structures, with aerogel-encapsulated nonwovens as middle layers. Different cases of middle layers including untreated nonwovens and nonwoven with air pockets were prepared as control samples.

3.2.3 Polyester/polyethylene nonwoven fabrics treated with aerogel

Three types of 50:50 ratio compositions of polyester/polyethylene nonwoven fabrics treated with aerogel were selected to measure thermal performance under convection heat transfer with air. The aerogel used was hydrophobic amorphous silica aerogel, which is mesoporous and has nearly 98% of air and 2% solid. Due to the interconnected nanoporous characteristic, aerogel can hold air within its structure and does not allow free flow of air, which enables it to be a superior thermal insulation material. The aerogel particles were added during the thermal bonding of the nonwoven web.

3.2.4 Electrospinning of nanofibrous membranes embedded with aerogel

In order to investigate the mechanisms of heat transfer through fibrous insulation where the fiber diameter less than 1 micrometer, flexible electrospun nanofibrous membranes embedded with silica aerogel was produced via electrospinning process. The electrospun PUR and PVDF nanofibrous microstructures were fabricated and then used to reinforce the SiO_2 aerogel.

PUR resin (Larithane AL286, Novotex Italiana S.p.A., molecular weight 2000 g mol^{-1}) and PVDF (Solef 1015, molecular weight 573 X 103 g mol^{-1}) was used as received from the CXI lab (Nanocenter, TUL, Czech Republic). Dimethylformamide (DMF) was selected as solvent. Hydrophobic amorphous silica aerogel in powder and granular form were purchased from Cabot Aerogel Corporation. The PUR and PVDF were separately dissolved in DMF at a concentration of 18 wt. %. The solutions were stirred in a magnetic stirrer for 2 hours at room temperature. Subsequently, silica aerogel particles were added into the solution. These mixtures were stirred again for 3 hours at room temperature prior to electrospinning. The solution viscosity was tuned by adjusting the solution concentration and was then electrospun.

Electrospinning was carried out using Nanospider technology, which is a modified electrospinning method based on the possibility of creating Taylor Cones and the subsequent flow of material not only from the tip of a capillary, but also from a thin film of a polymer

solution.[101-102] Nanospider consists of rotating roller which serves as a polymer solution reservoir as well as a nanofiber generator. The roller is partially immersed in the tank with the polymer solution, the applied high voltage generator unit is connected to the roller. A grounded collector electrode is positioned on the top and perpendicular to the rotation of the roller. A nonwoven substrate material moves along the collector electrode, thereby facilitating the production of electrospun nanofibers as a continuous free streamlined process.[103]

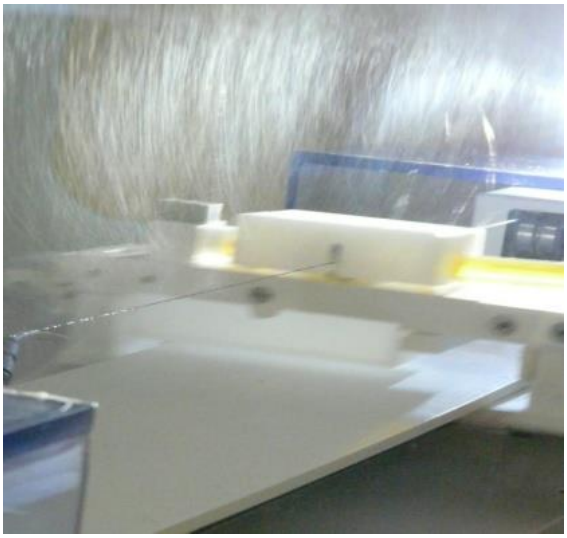

Figure 3. 6 Image of single wire electrode

The single wire electrode was selected to spin the nanofibers as shown in Figure 3. 6. The solution was delivered under the conditions given in the Table 3. 6.

Table 3. 6 Equipment setup for production of nanofibrous layer embedded with aerogel

Parameters	Specifications
Distance of electrode	175mm
Wire speed	0.2mm/s
Substrate speed	15 mm/min
Carriage speed	380-430mm/s on 500mm distance
Substrate	Spunbond PP
Voltage	-10/60kV
Size of the girder	ø 0.7 mm
Air flow	90/100m³h
Humidity	With dry box

The nanofibers were collected on a spunbond polypropylene fabric substrate. The substrate was chosen to provide mechanical properties. The electrospun nanofibrous membranes were then dried for two hours before using for the tests. Eleven different PUR and PVDF nanofibrous membranes embedded with aerogel were prepared. The details of electrospun nanofibrous layers embedded with silica aerogel were presented in Table 3. 7.

Table 3. 7 Details of electrospun nanofibrous layer embedded with silica aerogel

Type	Samples	Description	Areal density g/m^2	95% confidence interval	Thickness mm	95% confidence interval
PUR based nanofibrous layer	PUR1	only PUR	6.01	6.01± 0.19	0.083	0.083± 0.003
	PUR2	PUR + aerogel (Powder)	5.11	5.11± 0.16	0.089	0.089± 0.003
	PUR3	PUR + aerogel (Granular)	7.28	7.28± 0.02	0.112	0.112 ± 0.004
	PUR4	PUR + aerogel (Powder)	7.29	7.29± 0.04	0.206	0.206± 0.006
	PUR5	PUR + aerogel (Granular)	10.58	10.58± 0.13	0.248	0.248± 0.007
PVDF based nanofibrous layer	PVDF1	only PVDF	6.80	6.80± 0.21	0.11	0.11± 0.003
	PVDF2	only PVDF	10.62	10.62± 0.27	0.20	0.20± 0.007
	PVDF3	PVDF + aerogel (Powder)	6.58	6.58± 0.08	0.17	0.17± 0.004
	PVDF4	PVDF + aerogel (Powder)	16.00	16.00± 0.14	0.05	0.05± 0.002
	PVDF5	PVDF + aerogel (Granular)	9.18	9.18± 0.37	0.19	0.19± 0.02
	PVDF6	PVDF + aerogel (Granular)	11.89	11.89± 0.34	0.23	0.23 ± 0.009

3.3 Measurement methods

3.3.1 Measurement of scanning electron microscope

The morphology and microstructure of aerogel treated nonwoven, electrospun PUR and PVDF nanofibrous layer embedded with silica aerogel were studied using a SEM (VEGA TESCAN Inc. USA) at 30 kV. To avoid a repulsive reaction of electron beam, the sample surface is coated with a thin layer of gold. SEM allows high depth of sharpness providing information about structures at various distances from the scanning level, it is very useful to evaluate the basic characteristics of nanofibrous structure.

3.3.2 Measurement of cross-sectional morphology

Cross sectional morphology of the layered nanofibrous web/silica aerogel/ nonwoven sample was examined using a Dino-lite digital microscope. The Dino-lite digital microscope is a handheld digital microscope which connects directly to a computer

through a USB port. Dino Capture 2.0 software was used to capture images.

3.3.3 Measurement of thermogravimetric and differential scanning calorimetry

Thermogravimetric and differential scanning calorimetry analysis were conducted on electrospun nanofibrous layers embedded with silica aerogel. Netzch STA 409 equipment, as seen in Figure 3.7, was used for Thermogravimetric Analysis (TGA). Analysis was performed within a temperature range of 25 to 450 ºC at a heating rate of 10 ºC/min and N_2 atmosphere. Differential Scanning Calorimetry (DSC) analysis was conducted using TA Instruments MDSC 2920 equipment (Figure 3.8) within a temperature range of 0 to 400 ºC at a heating rate of 10 ºC/min in N_2 atmosphere. ASTM D882-95a specification was followed for strip-cutting samples from a thin sheet.

Figure 3. 7 Image of Netzch STA 409 equipment

Figure 3. 8 Image of MDSC 2920 equipment

3.3.4 Measurement of thermal properties by Alambeta

The measurements of thermal insulation parameters were performed with the use of ALAMBETA device constructed in Czech Republic (Figure 3. 9). Alambeta device was used for fast evaluation of transient and steady state thermo-physiological properties. The instrument consists of two measuring heads between which the test specimen was placed. Both measuring heads are equipped with thermocouples and heat flow sensors. The lower measuring head was adjusted to the ambient temperature, the upper heated measuring head was adjusted to a controlled constant differential temperature. When upper measuring head was lowered on the measuring specimen, the heat flow at the upper surface and the underside of the test specimen can be measured.

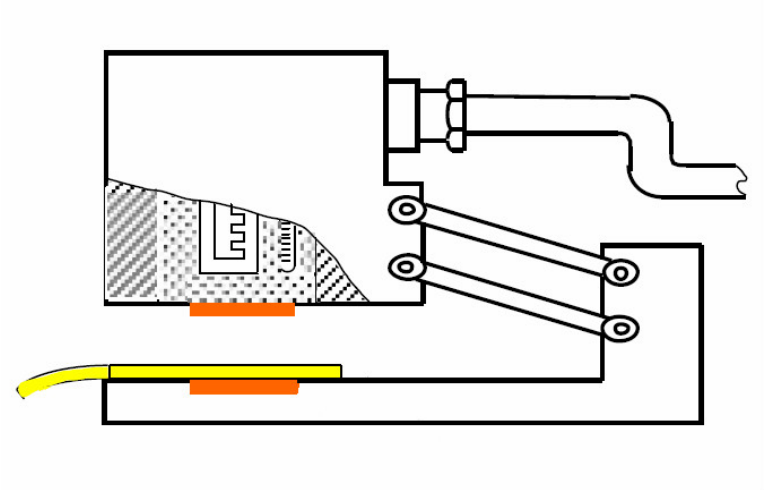

Figure 3. 9 Schematic of Alambeta device

3.3.5 Measurement of infrared thermography

Infrared thermography is actually visual displays of the amount of infrared energy emitted, transmitted, and reflected by an object. The amount of radiation emitted by the heat plate through the fabric was detected, therefore the thermography allows to see temperature variations.

The thermography measurement was conducted using FLIR ThermaCAM TVS300 thermal camera as shown in Figure 3. 10. Tests were carried out in a test chamber with an opening on its upper surface, the dimension of the chamber was 45 cm × 32 cm × 12 cm. A guard hot plate with constant temperature 33˚C was located in the chamber to provide uniform thermal radiation, the thermal camera was placed in the air space with a distance

of 40 cm from the hot plate, facing to the opening of the chamber as well as the hot plate. When the specimen was placed on the hot plate, pictures were taken every 5 seconds up to when the heat transfer reaches steady state. The room temperature was kept at 23± 2°C. The specimen size used for measurements was 20 cm × 20 cm. The temperature of the surface was calculated using Avio Thermography Studio 2007 software in which each pixel of the picture was allocated to one temperature value. The average was subsequently created on the basis of all the values.

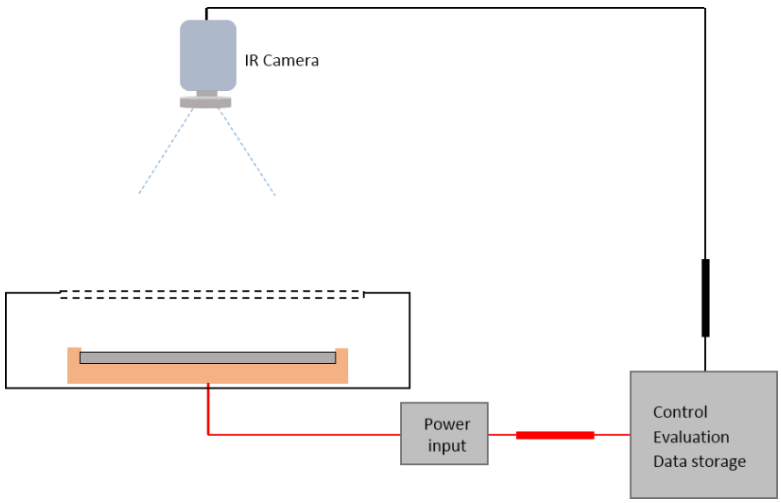

Figure 3. 10 Setup of thermography measurement

3.3.6 Measurement of thermal properties by KES-FT-II Thermolabo Tester

Examination of heat retention ability and thermal conductivity is performed with KES-FT-II Thermolabo device. All the tests were carried out in the standard atmospheric condition of 65 ± 4% and 23 ± 2°C. All the samples were conditioned under the standard condition for 24 h before testing.

This device used for analyzing thermal properties is composed by several components (Figure 3. 11): Measuring body T, used for measuring warm or cold feeling; Measuring body BT, used for measuring constant thermal conductivity; Larger measuring body BT, used to measure heat loss and thus to determine the ability to retain heat; Water box, used to maintain a constant temperature while measuring warm or cold feeling and the coefficient of thermal conductivity; Wind column, used to supply a selected constant air flow rate at a constant air temperature for the determination of heat retention ability.[104]

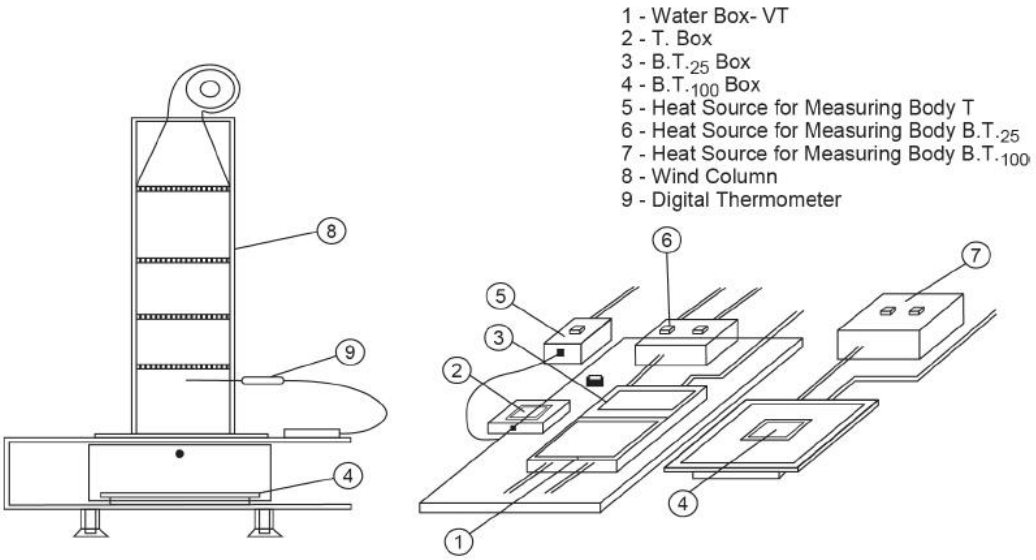

Figure 3. 11 Components of measuring device KES-FT-II Thermolabo Tester[104]

Thermal conductivity is measured by steady heat flow method using the BT box and water box. The heat source plate-BT box is set at a constant temperature 33°C to simulate a human skin temperature. The water box is kept at 23°C, the fabric specimen is placed on the surface of the water box. The heat source plate is shifted onto the top of the specimen, thus the direction of heat flow agrees with the direction of the acceleration of gravity. The temperature difference between BT box and water box is 10°C. The heat lost from the hot plate is then indicated directly on the display. According to the thickness of the specimen, heat loss, temperature difference between BT box and water box, the thermal conductivity can be calculated.

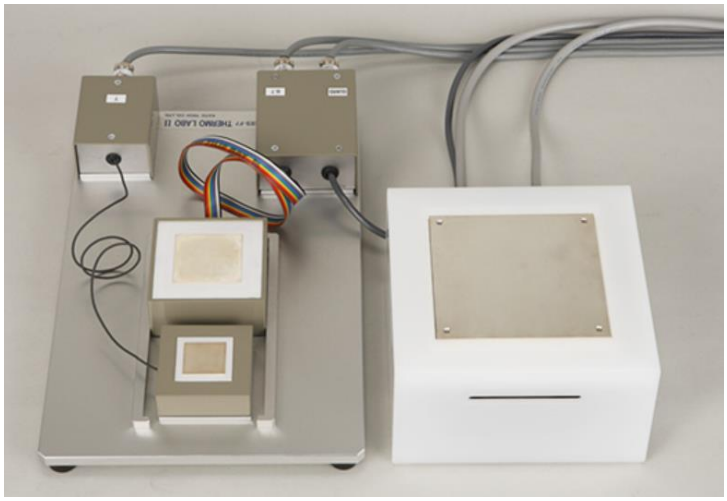

Figure 3. 12 Image of BT box, T box and water box

Coefficient of heat retention ability is determined with the help of the wind column. The BT plate is heated to 33˚C and the heat loss is measured. A constant air flow rate of 0.3 ms^{-1} is present in wind column, with a constant air temperature of 23 ˚C ± 2 ˚C. Loss of heat flow in both conditions, without fabric on BT plate and with fabric on BT plate, is measured. From the obtained values of the heat flow loss, the coefficient of heat retention ability α can be calculated according to the formula:

$$\alpha = \frac{Q_0 - Q}{Q_0} \times 100 \tag{3.1}$$

where Q is the amount of heat release [W] with a fabric placed on the BT plate, Q_0 is the amount of heat release [W] without fabric on the BT plate.

3.3.7 Measurement of dynamic convective heat transfer behavior

A dynamic heat transfer device was made in our laboratory to evaluate thermal performance of multilayered samples and aerogel treated nonwovens under different airflow velocities. Real-time temperature values of the heating rod and nonwoven fabric were collected to analyze how the fabrics prevent against heat loss in natural and forced convection.

3.3.7.1 Experimental setup

The tests were carried out in a laboratory made device, the schematic diagram of the device is presented in Figure 3. 13. The main part of the measuring section consists of a subsonic wind tunnel with a square cross section of 20cm×20cm, an electric heating rod with a diameter of 2cm and length 20cm placed perpendicular to the airflow direction in the wind tunnel, and a fan ventilator connected in the right corner of the lower duct. The heating rod, composed by a Ni-Cr 80-20 heating wire with a stainless-steel shell, having a rated wattage 500 W and voltage 230 V, was connected to a control unit and powered by a Sefram DC power supply. The input power was adjusted by control unit. For mounting the heating rod in the testing section, two holes were drilled on the duct wall, the heating rod was able to be inserted into the testing section. The fan ventilator, acting as a suction fan, inlets airflow velocities at room temperature. Different airflow velocities can be achieved by switching the fan speed.

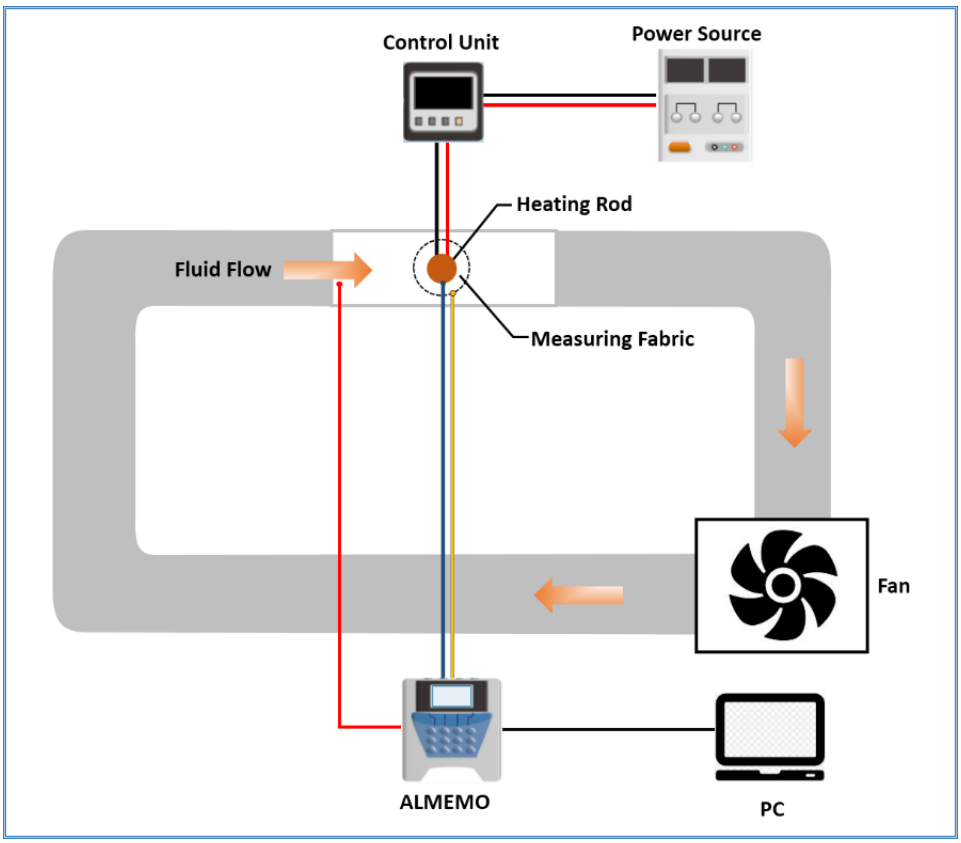

Figure 3. 13 Schematic diagram of the measurement device

The experiments involve measurements of real-time temperatures of the heating rod as well as the fabric insulator, wind velocity, wind pressure and the temperature of airflow before entering the testing section. Temperatures of the heating rod and fabric were measured by using T-type copper constantan thermocouples. Two thermocouples were respectively attached on the heating rod surface and fabric surface with the help of high temperature RTV silicon. A thermoanemometrické sensor FVAD35TH4 was mounted in the upstream to monitor the velocity, pressure and temperature of the free stream. The uncertainty in the measurement of airflow velocity was ±0.04 m/s. All these thermocouples and sensor were connected through ALMEMO 2590-2A - 2 datalogger to a PC device.

3.3.7.2 Experimental procedures

A fabric specimen with a size of 20 cm ×8 cm was wrapped on the heating rod by using insulating rubber tape to seal the lateral gap as seen in Figure 3.14. Any gaps between the fabric and the heating rod were eliminated. Heat energy conducted from the heating rod to the fabric will dissipate by convection.

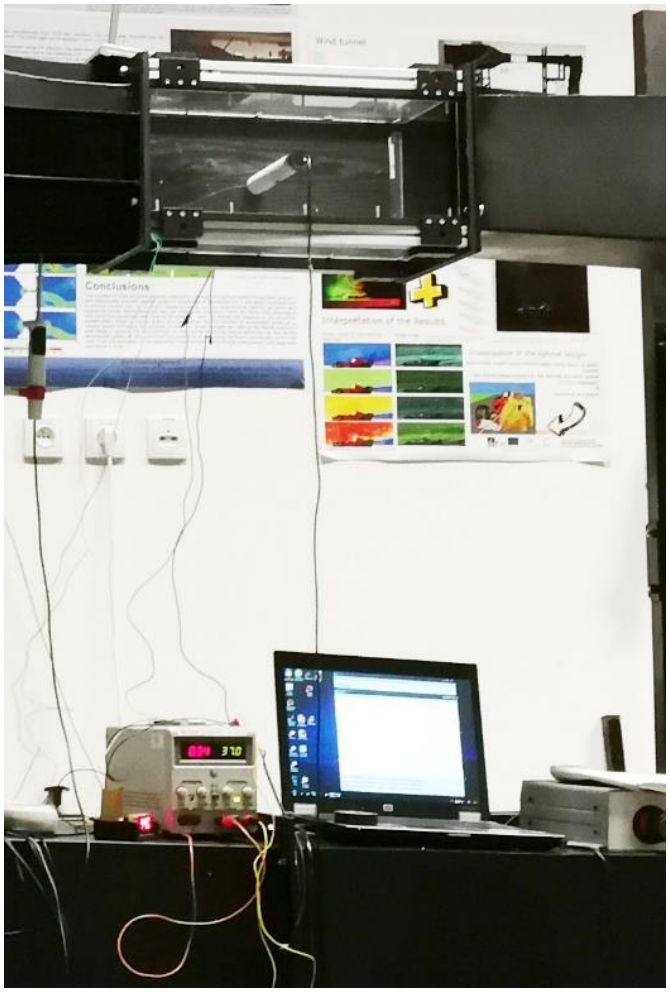

Figure 3. 14 Image of the main testing section

The tests were carried out at different values of air velocity under two different heating conditions, preheated and continuous heating conditions, to investigate how the fabric help prevent heat loss from the heating rod. The preheated condition refers to preheat the heating rod to a specific temperature value and switch off the heating power to let the system cools down with a selected air velocity. The continuous heating condition involves non-stop heating during the whole measuring process. The voltage and current supplied from DC power for heating were 37 V, 0.33 A for each measurement. Five airflow velocity levels, 0, 1, 5, 10 and 15 m/s were used to study the effect of airflow velocity on the heat loss rate of different fabrics by convection.

In this study, the preheated temperature was chosen to be around 60℃, the ambient temperature was kept at 23±2℃. At the beginning of a preheated condition measurement,

the heating rod was heated to 60℃, the power supply was cut off and the fan ventilator was switched on to inlet airflow with a selected velocity. The sensed data of temperature values, airflow pressure and velocity were collected at an interval of 3.2 second. During the continuous heating measurement, the heating rod was kept being powered and the airflow was allowed to be delivered when the temperature of the heating rod reached 60℃. Data were taken as soon as the inlet air reached a selected velocity. The experimental work includes two parts: the first dealt with the flow around a heating rod without fabric, and the second with the flow around the porous fabric wrapped on the heating rod. For each part, measurements were performed under both preheated and continuous heating conditions at different air velocity levels.

3.3.7.3 Fluid flow around the heating rod

For the circular heating rod in cross flow, as the airflow approaches the front side of the rod, the fluid pressure rises and the free stream fluid is brought to rest at the forward stagnation point as shown in Figure 3. 15.[105] The high pressure forces the fluid to move along the surface and boundary layers develop on both sides. The free stream velocity depends on the angle from the stagnation point. The pressure force is counteracted by viscous forces and the fluid separates from both sides of the rod and form two shear layers. The innermost parts of the shear layers are in contact with the rod surface and moves slower than the outermost part. As a result, a highly irregular wake is formed in the downstream region.

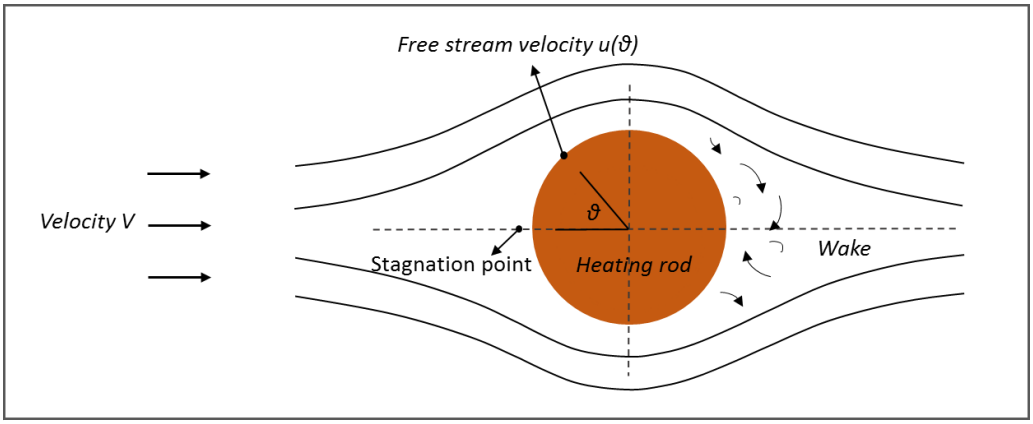

Figure 3. 15 Fluid flow around a circular rod

3.3.8 Measurement of air permeability

Air permeability is described as the rate of air flow passing perpendicularly through a known

area, under a prescribed air pressure differential between the two surfaces of a material. Tests were performed according to standard ISO 9237 using a FX-3300 air permeability tester. The fabric sample is fixed as an obstacle in a flow of air by the clamping holder. A pressure difference between both sides of the fabric sample develops as a consequence of hydraulic losses. The pressure difference is recorded by using of the manometer. The measured value is a speed of air in meter per second or a volume rate of the flow in liter per hour. Two air pressure differentials 100 Pa and 200 Pa between the two surfaces of the material were used.

3.3.9 Measurement of compression properties

ORIENTEC STA-1225 universal testing device (as seen in Figure 3. 16) was used for compression testing. This device is multi-purpose tester with the ability to test a wide range of materials and operating conditions by changing measuring heads. In this work, the circular pressure pads with foot area 36.3 cm^2 and diameter 68 mm were used for compression testing. The maximum pressure was set at 560 gf/cm^2. The sample size used in compression test was 20 cm × 20 cm, the loading speed was set at 2 mm/min.

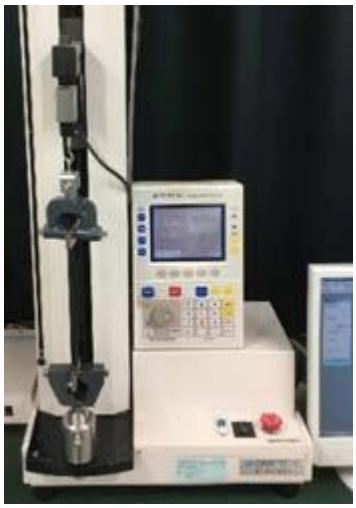

Figure 3. 16 Image of ORIENTEC STA-1225 universal testing device

The obtained compression behavior of a fabric is described by the relationship between the applied force per unit area and the resulting fabric thickness, in the form of compression load-displacement curve. From compression hysteresis curves, compression resistance, compression resilience and thickness loss can be calculated according to the following Equations:

$$Compression\ resistance\ (\%) = \frac{h_0 - h_1}{h_0} \times 100 \quad (3.2)$$

$$Compression\ resilience(\%) = \frac{W_R}{W_C} \times 100 \quad (3.3)$$

$$Thickness\ loss(\%) = \frac{h_0 - h_2}{h_0} \times 100 \quad (3.4)$$

where h_0 is the initial thickness [mm], h_1 is the fabric thickness at maximum pressure [mm], h_2 is the recovered fabric thickness [mm], W_C is the work done during compression [J] and W_R is the work done during recovery process [J].

Chapter 4 Results and Discussion

4.1 Microscopy images

4.1.1 Cross sectional images of layered nanofibrous web/silica aerogel/ nonwoven

Cross sectional images of the layered fabrics were taken with identical magnification using a Dino-lite digital microscope. The magnification was chosen to be 50. The images are shown in Figure 4. 1. It was observed that the nanofiber webs were well laminated with the nonwoven substrates without obvious air gap layers. Aerogel granules were deposited on the nonwoven substrates under the nanofiber webs. Remarkably, significant increase in fabric thickness was observed for sample A4 and A5.

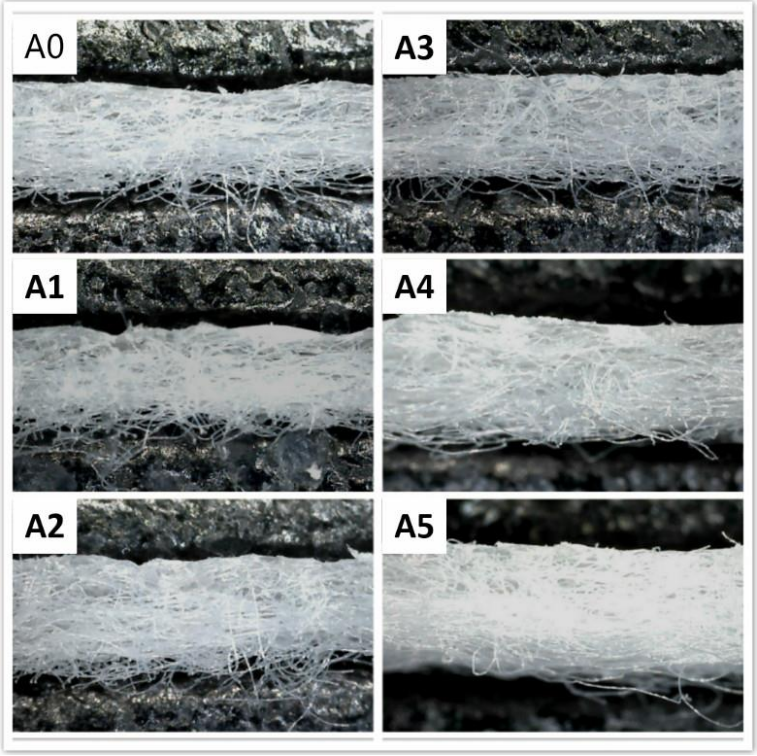

Figure 4. 1 Cross sectional images of layered nanofibrous web/silica aerogel/ nonwoven

4.1.2 Morphology of aerogel treated nonwoven fabrics

High resolution images for the aerogel/polymer nonwoven fabrics are shown in Figure 4. 2. It is clear that aerogel particles are dispersed between the fibers in the three-dimensional fibrous structure, which covers the void spaces between fibers. The aerogel particles are attached to the fibers by the thermal bonding of low-melting point fiber components. Fabric B1, with less aerogel content in the structure, demonstrated considerable fiber cross

nodules. Fabric B2 and B3, having more aerogel particles, showed more compact structure with less fiber cross nodules. Meanwhile, the size distribution of aerogel particles is quite large, most of the particles have smaller magnitude with fiber diameter. During actual use the fine particles easily get away from the fibrous structure when suffering various external forces.

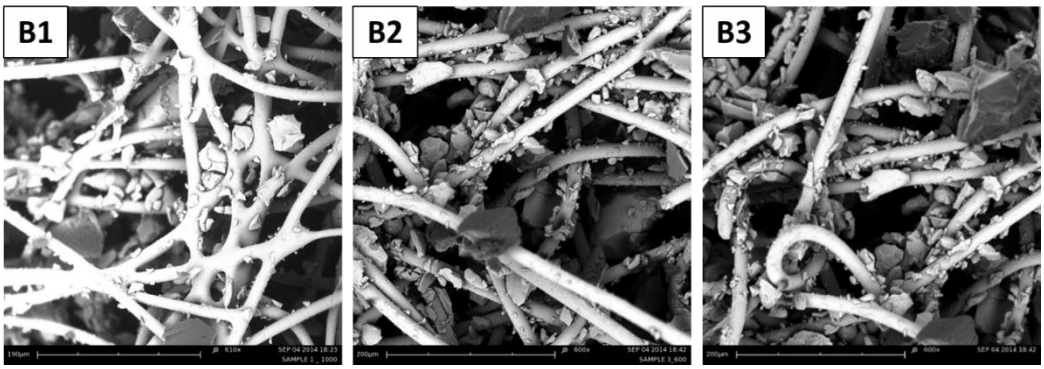

Figure 4. 2 Scanning electron microscope images of aerogel/polymer nonwovens

4.1.3 Microstructures of nanofibrous membranes

Figure 4. 3 and 4. 4 present the morphologies and microstructures of electrospun PUR and PVDF nanofibrous membranes with and without aerogel particles. The electrospun nanofibrous membranes consisted of fibers in the sub-micrometer range arranged in a three-dimensional network structure with high porosity and fully interconnected pores. The intact morphology of the nanofibrous membranes embedded with aerogel implied that the optimized polymer solution concentration could improve the strength and the flexibility of the aerogels. As the aerogels were electrospun with PUR and PVDF nanofibers, the aerogels were separated into large quantity of small areas.

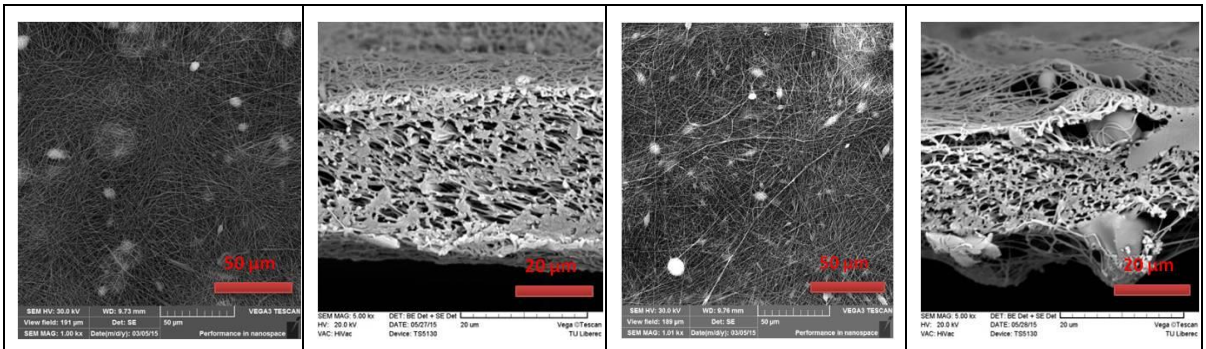

PUR 1	PUR 1 (cross section)	PUR 2	PUR 2 (cross section)

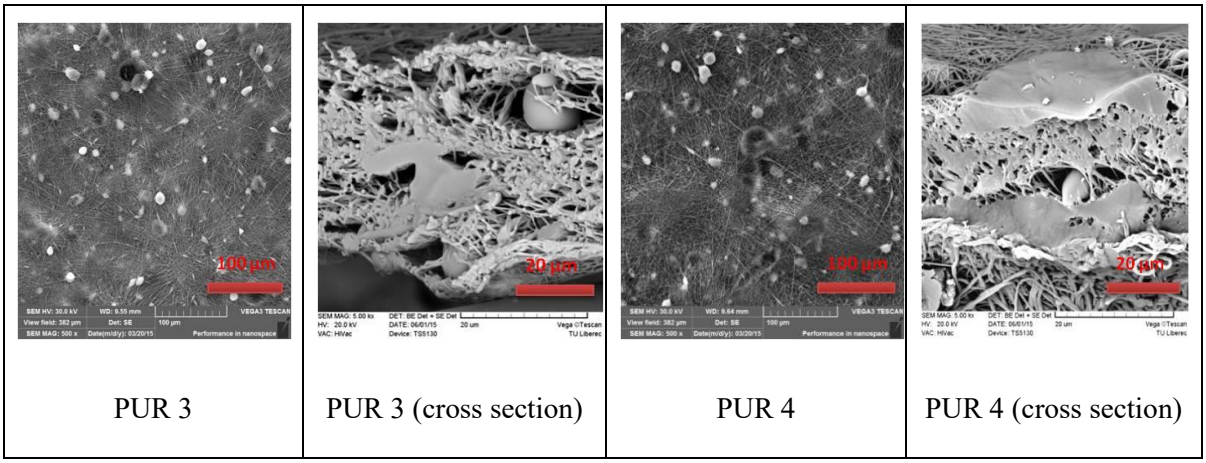

Figure 4. 3 Morphology and microstructure of PUR nanofibrous membranes embedded with SiO_2 aerogel

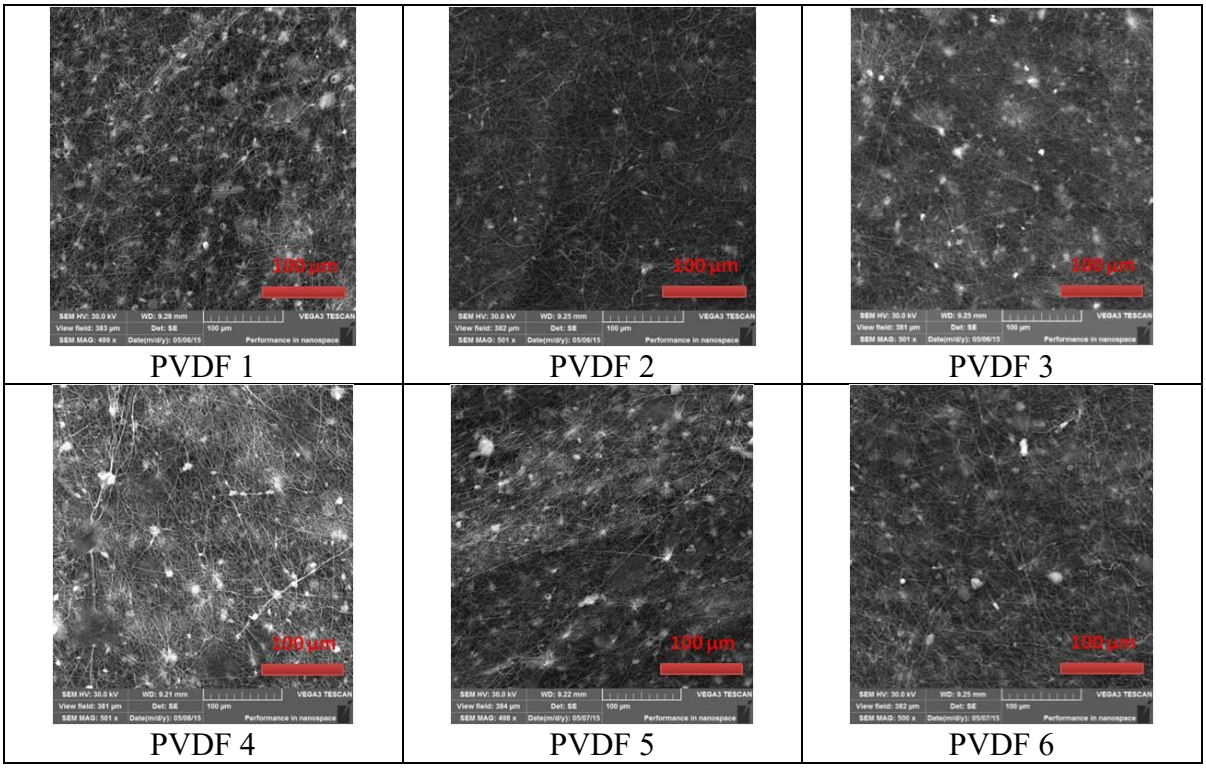

Figure 4. 4 Morphology and microstructure of PVDF nanofibrous membranes embedded with SiO_2 aerogel

4.2 Thermal properties of layered nanofibrous web/silica aerogel/ nonwoven

4.2.1 Thermal conductivity and thermal resistance

Thermal conductivity, λ [W/m·K], measures the rate at which heat is transferred through unit area of the fabric across unit thickness under a specified temperature gradient.

Thermal resistance, R [m^2 ·K/W], expresses the ability of a material to prevent heat flow through the thickness over unit surface area. Thermal resistance is related to thermal conductivity and fabric thickness h [m]:

$$R = \frac{h}{\lambda} \tag{4.1}$$

Amount of stagnant air within the fabric and fabric density are the most important factors governing thermal insulation of textiles. The higher the thermal resistance, the lower the heat loss.

The measured thermal properties of nonwoven substrate, nanofiber web and the integrated fabric of these two materials are given in Table 4. 1. An obvious difference was observed in thermal resistance of sample A0 and S, this is attributed to the thermal adhesive which may block the open pores throughout the nonwoven substrate and reduce the trapped air in this layered fabric. Since the thermal performance of high porous textile is determined by the stagnant air present in textile structure, more heat flowed through the layered fabric A0 due to its decreased air volume fraction.

Table 4. 1 Thermal performance of samples without aerogel

Samples	Thermal conductivity 10^{-3} W/m·K	95% Confidence Interval	Thermal resistance 10^{-3} m^2· K/W	95% Confidence Interval
Nanofiber web (N)	0.044	0.044±0.006	0.90	0.90±0.025
Nonwoven substrate (S)	34.63	34.63±0.20	35.40	35.40±0.10
Layered fabric (A0)	36.98	36.98±0.60	31.94	31.94±0.50

For multilayered fabric systems, the layers are considered to set as a series of thermal resistance, according to electrical analogy with conduction heat transfer, the total thermal resistance R_t is the sum of thermal resistance of each layer.[106] However, the use of thermal binding powder in this layered structure will improve thermal conductivity as mentioned above, this will cause some reduction in total thermal resistance since the fabric thickness is not proportionally decreased. This reduction in thermal resistance, ΔR [m^2 ·K/W], can be obtained by

$$\Delta R = R_S + R_N - R_{A0} \tag{4.2}$$

where R_S is thermal resistance of the nonwoven fabric (sample S) [m^2 ·K/W], R_N is thermal resistance of the nanofiber web (sample N) [m^2 ·K/W], R_{A0} is thermal resistance of the

layered fabric A0 [m^2 ·K/W].

In this study, the reduction in thermal resistance ΔR is 4.36×10^{-3} m^2 ·K/W, which accounts for 13.65% of the total thermal resistance. This indicated that the use of adhesive in textile structure has significant effect on the final thermal insulation performance, which is noteworthy for the fabrication of textile composites as thermal insulators.

Table 4. 2 Thermal conductivity and thermal resistance of layered nanofibrous web/silica aerogel/ nonwoven

Sample No.	Thermal conductivity 10^{-3} W/m· K	95% Confidence Interval	Thermal resistance 10^{-3} m^2· K/W	95% Confidence Interval
A1	35.27	35.27±0.35	39.97	39.97±0.38
A2	35.00	35.00±0.45	40.33	40.33±0.42
A3	34.64	34.64±0.27	41.07	41.07±0.31
A4	34.37	34.37±0.39	43.26	43.26±0.25
A5	34.28	34.28±0.18	44.58	44.58±0.34

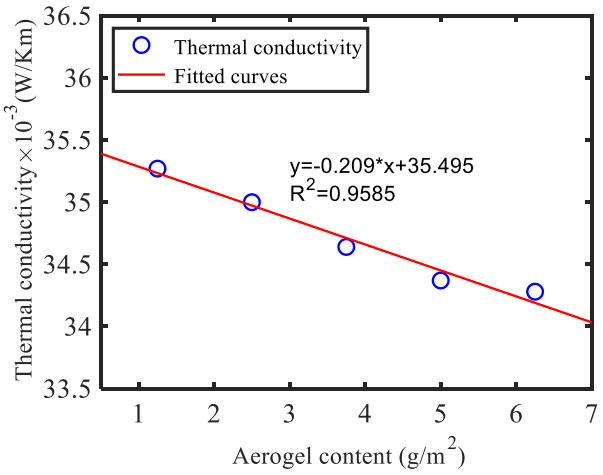

Equation y = a + b*x	**Value**	**t-test Significance "Yes" or "No"**	**Adj. R-Square**	**F-test Significance "Yes" or "No"**
Intercept	35.495	Yes	0.9585	Yes
Slope	-0.209	Yes		

Figure 4. 5 Effect of aerogel content on thermal conductivity

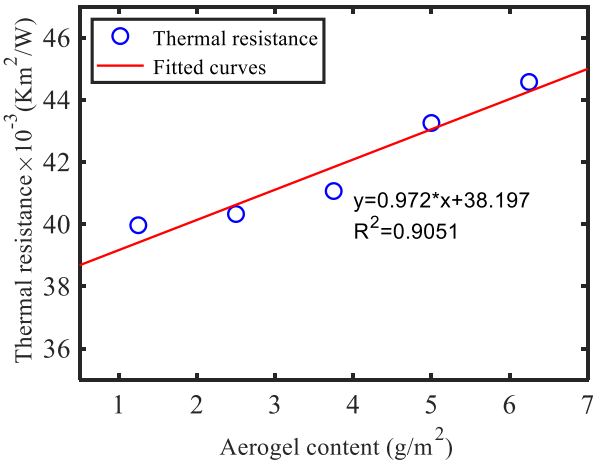

Equation y = a + b*x	Value	t-test Significance "Yes" or "No"	Adj. R-Square	F-test Significance "Yes" or "No"
Intercept	38.197	Yes	0.9051	Yes
Slope	0.972	Yes		

Figure 4. 6 Effect of aerogel content on thermal resistance

Thermal conductivity and thermal resistance of layered nanofibrous web/silica aerogel/ nonwovens are listed in Table 4. 2. The aerogel-embedded fabrics showed lower thermal conductivity and much higher thermal resistance in comparison with sample A0, indicating that the aerogel content present in the fabrics plays a major role and gives better thermal insulation performance. The effect of aerogel content on thermal conductivity and thermal resistance are presented in Figure 4. 5 and Figure 4. 6. It was observed that the thermal conductivity and thermal resistance of layered fabrics were directly proportional to the areal density of aerogel, with adjusted coefficients of determination above 0.90. This is because the increment of trapped air in the layered fabric is determined by the amount of aerogel.

The linear correlation between thermal conductivity and fabric density is illustrated in Figure 4. 7. Fabric density represents the volume proportion of fibers in a fibrous material, it is related to the volume fraction of air trapped in the fabric which is referred as fabric porosity. Results showed that the thermal conductivity of layered nanofibrous web/silica aerogel/ nonwoven increases with the increase in fabric density, this is attributed to the less porosity in higher density fabrics. Especially, the thermal resistance is directly proportional to fabric thickness with adjusted coefficients of determination 0.9096 (as seen in Figure 4.

8), indicating fabric thickness is the primary factor contributing to the thermal insulating ability of a fibrous material.

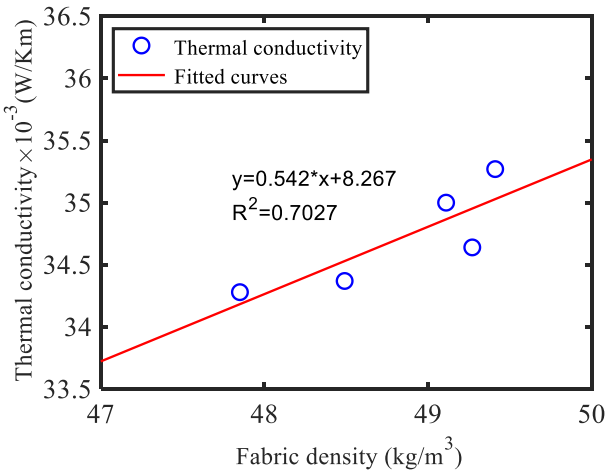

Equation y = a + b*x	Value	t-test Significance "Yes" or "No"	Adj. R-Square	F-test Significance "Yes" or "No"
Intercept	8.267	Yes	0.7027	Yes
Slope	0.542	Yes		

Figure 4. 7 Effect of fabric density on thermal conductivity

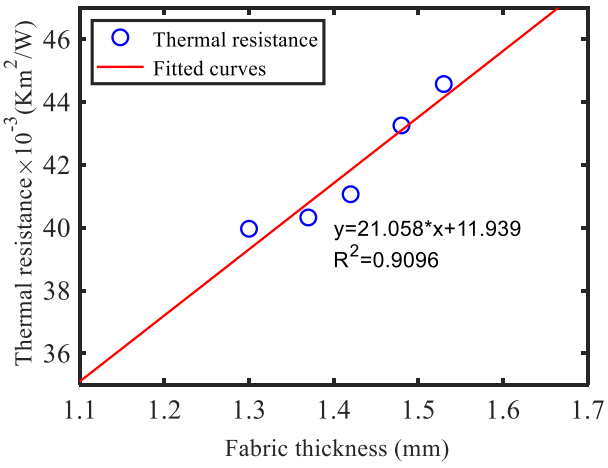

Equation y = a + b*x	Value	t-test Significance "Yes" or "No"	Adj. R-Square	F-test Significance "Yes" or "No"
Intercept	11.939	Yes	0.9096	Yes
Slope	21.058	Yes		

Figure 4. 8 Effect of fabric thickness on thermal resistance

4.2.2 Series model for thermal resistance

The decrease of thermal resistance induced by adhesive strongly depends on the amount of thermal binding powder and its distribution. In this study, the amount of thermal binding powder in each layered fabric is totally identical, if the thermal binding powder is assumed to uniformly spread only in the middle layer consisted by aerogel granules and air, then the reduction in thermal resistance in each layered system can be approximately considered to be the same. Therefore, the total thermal resistance of a layered fabric with aerogel can be calculated by

$$R_t \approx R_S + R_M + R_N - \Delta R \tag{4.3}$$

where R_M is thermal resistance of the middle layer [m^2 ·K/W].

The thermal performance of this middle layer is determined by aerogel granules and the air space in the structure. Assuming it is a homogeneous layer without aerogel loss from this layer, then the thermal conductivity of this layer λ [W/ m·K] can be obtained by using

$$\lambda = \lambda_0(1 - f_V) + \lambda_{aer} f_V \tag{4.4}$$

where f_V, the volume fraction of aerogel granules, is

$$f_V = \frac{\rho_s}{\rho_V \cdot h} \tag{4.5}$$

where λ_0 is the thermal conductivity of stagnant air (0.024 W/K·m at 25℃), λ_{aer} is the thermal conductivity of aerogel granules [W/K· m], ρ_s is the areal density of aerogel in layered fabric [g/m^2], ρ_V is the bulk density of aerogel [kg/m^3] and h is the thickness of the middle layer [mm].

Thus, the total thermal resistance of a layered fabric R_t can be expressed as

$$R_t = R_S + R_N + \frac{\rho_V \cdot h^2}{\lambda_0 \cdot (\rho_V \cdot h - \rho_S) + \lambda_{aer} \cdot \rho_S} - \Delta R \tag{4.6}$$

Thermal resistance values obtained from experiment and series model are shown in Table 4. 3 and Figure 4. 9. Results showed a good agreement between thermal resistance from experiment and those from series model. Average error was about 2.07 %. The error showed a decreasing trend with the increasing of aerogel content, this could be explained by the assumption that the thin middle layer between nanofiber web and nonwoven substrate is a uniformly continuous layer, if the aerogel particles are too less to form a

continuous layer, the thermal resistance will be underestimated by theoretical model since the thickness of the middle layer is decreased.

Table 4. 3 Comparison of theoretical and experimental values of thermal resistance

Samples code	From experiment (R) 10^{-3} m^2·K/W	From series model (R')10^{-3} m^2·K/W	Error (%) $\frac{\lvert R-R'\rvert}{R}\times 100$
A1	39.97	38.00	4.93
A2	40.33	39.07	3.12
A3	41.07	39.74	3.23
A4	43.26	42.48	1.80
A5	44.58	44.80	0.50

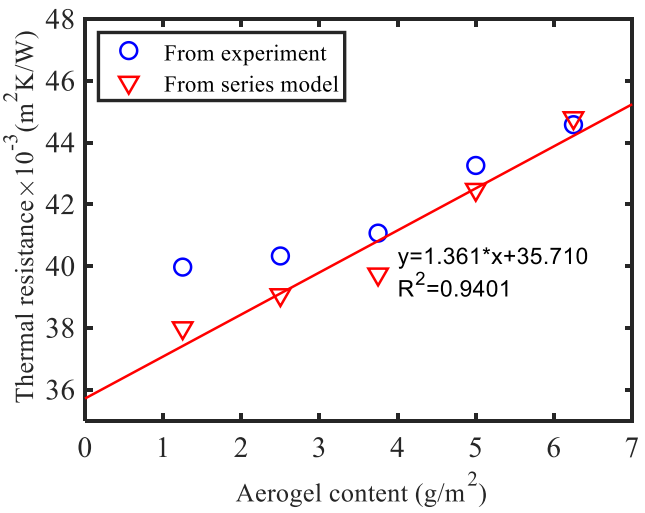

Equation y = a + b*x	Value	t-test Significance "Yes" or "No"	Adj. R-Square	F-test Significance "Yes" or "No"
Intercept	35.710	Yes	0.9401	Yes
Slope	1.361	Yes		

Figure 4. 9 Theoretical and experimental values of thermal resistance

4.3 Thermal properties of novel multilayered fibrous materials

4.3.1 Thermal properties from Alambeta

Thermal conductivity and thermal resistance of the novel multilayered fibrous materials are shown in Figure 4. 10 and Figure 4.11. It is apparent that in each sample group, air

pockets (sample P2, Q2, X2 and Y2) give slightly decrease to thermal conductivity value and small rise to thermal resistance as compared to regular materials (P1, Q1, X1 and Y1). This is because the large voids formed by laser treatment will enlarge the amount of still air in the structure, causing less heat transfer through the fabrics by conduction. Heat transfer by free convection in nonwoven materials is negligible because the fibers subdivide the gas into sufficiently small pores and the tortuous nature of air channels present prevent any heat transfer by convection.[107] Thus, the regular samples can be assumed to be free of convection. The samples gained lots of huge air-filled voids after laser treatment, which may allow air flows through and cause heat transfer by convection. However, the covering fabrics laminated on the surfaces could behave as barriers to prevent against natural convection.

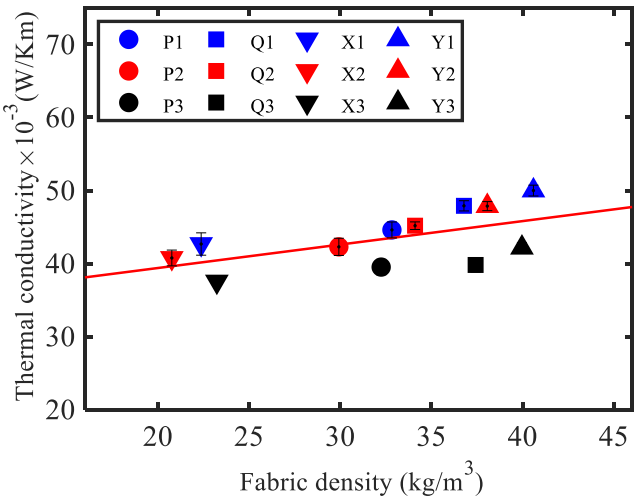

Equation y = a + b*x	Value	t-test Significance "Yes" or "No"	Adj. R-Square	F-test Significance "Yes" or "No"
Intercept	32.96	Yes	0.4398	Yes
Slope	0.3212	Yes		

Figure 4. 10 Thermal conductivity of multilayered fibrous materials

Aerogel-encapsulated structure (sample P3, Q3, X3 and Y3) give decrease to thermal conductivity while the thermal resistance significantly increases. For the aerogel-encapsulated materials, the large open voids are filled by nanoporous structural aerogel, this will further prevent the convection current transfer through the structure. Furthermore, since the pore size in the aerogel granules is lower than the mean free path of

air molecules, according to Knudsen effect these extremely small pore size will cause a very low gaseous thermal conductivity, resulting in less heat transfer through the structure and significant improvement of thermal insulation performance.

Usually, with the increase in fabric density, fabric porosity decreases, this will lead to an increase in thermal conductivity. However, silica aerogel has higher density and lower thermal conductivity than stagnant air, the multi-layered material becomes denser with the addition of aerogel particles while its thermal conductivity decreases. Sample P3, Q3, X3 and Y3, possessing higher fabric densities due to the addition of aerogel particles, showed the lowest thermal conductivities in comparison to regular samples and air-pockets samples. Thermal conductivity values of aerogel-encapsulated samples were all scattered below the linear fitting line, this further proved the above statement.

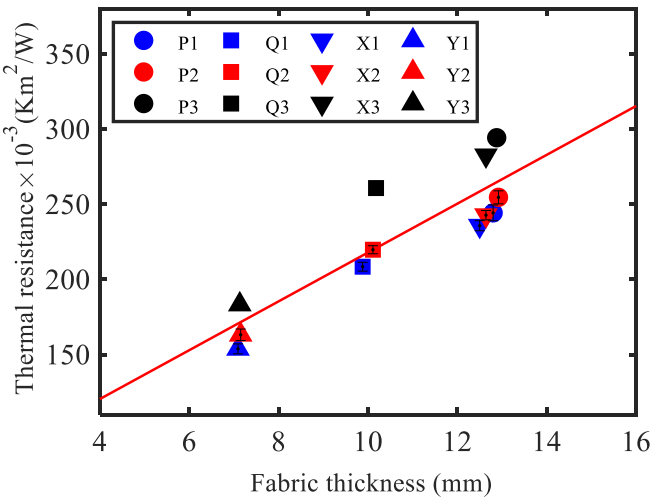

Equation y = a + b*x	Value	t-test Significance "Yes" or "No"	Adj. R-Square	F-test Significance "Yes" or "No"
Intercept	55.47	Yes	0.7792	Yes
Slope	16.25	Yes		

Figure 4. 11 Thermal resistance of multilayered fibrous materials

Figure 4. 11 illustrates the correlation of thermal resistance and fabric thickness of the multilayered fibrous materials. Thermal resistance is a function of fabric thickness and thermal conductivity. Samples with higher thickness showed better thermal resistance. But in each sample group, for example sample P1, P2 and P3, they have very close fabric thickness but considerable variance in thermal resistance values, this is attributed to the

different middle layer structures.

Analysis of variance was performed for each group using *t*- test method to determine whether there are any significant differences in thermal insulating properties. Results showed that for nonwoven based multilayered fibrous materials the variance of thermal conductivity values within groups are all significant (*p-value* < 0.05), the differences between air pockets and aerogel-encapsulated structure are found to be very significant (*p-value* < 0.01). For foam-based materials the thermal conductivity difference between regular sample and laser-engraved one is observed to be highly significant (*p-value* < 0.00001), however, the values between air pockets and aerogel-encapsulated structure shows insignificant difference. This may be attributed to the least content of silica aerogel in sample Y3. With respect to thermal resistance, in each group all the values from different structures show very significant difference (*p-value* < 0.01). Variance analysis indicates that the aerogel-encapsulated structure has significant effect on thermal insulation enhancement while the air pockets can improve thermal insulating properties to some degree.

4.3.2 Thermal properties from KES-FT-II Thermolabo

The heat retention coefficient of multilayered fibrous materials is illustrated in Figure 4. 12. It is apparent that the materials with air pockets had better ability to retain heat compared to regular samples. The highest heat retention ability was observed from materials with aerogel-encapsulated structure. The heat transfer in aerogel is affected through its solid-state component, the air occupying the pores is a bad heat conductor. Moreover, as a result of the micro-porous structure, the gas conductivity in silica aerogel becomes substantially lower than that for a free gas.[108]

From Figure 4. 12, It also can be observed that with the increase in fabric thickness, the heat retention ability of the multi-layered fabric increases in the same way as thermal resistance. Similar to thermal resistance, the coefficient of heat retention ability was linear related to the thickness of a multilayered fibrous material, with adjusted coefficients of determination 0.7156. This reveals that the fabric thickness is an important factor in determining heat retention ability of a multilayered fibrous material.

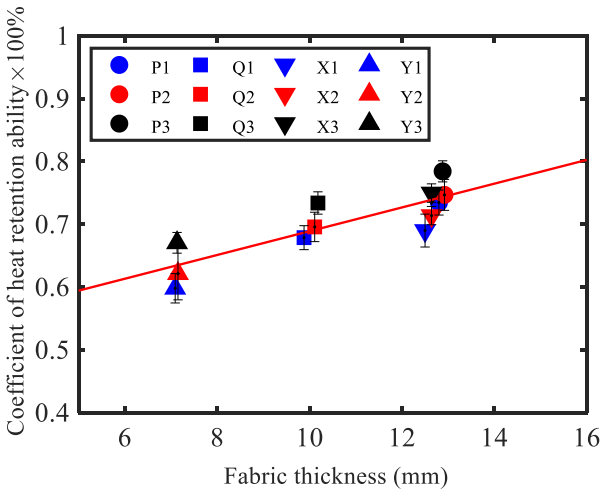

Equation y = a + b*x	Value	t-test Significance "Yes" or "No"	Adj. R-Square	F-test Significance "Yes" or "No"
Intercept	0.4995	Yes	0.7156	Yes
Slope	0.01892	Yes		

Figure 4. 12 Heat retention coefficient of multilayered fibrous materials

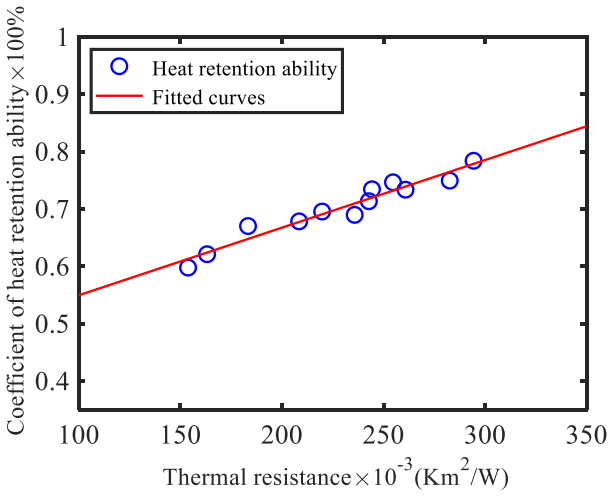

Equation y = a + b*x	Value	t-test Significance "Yes" or "No"	Adj. R-Square	F-test Significance "Yes" or "No"
Intercept	0.4317	Yes	0.915	Yes
Slope	0.001179	Yes		

Figure 4. 13 Correlation of heat retention coefficient and thermal resistance

Since thermal resistance and coefficient of heat retention are both related to fabric thickness, the correlation of thermal resistance and heat retention ability is illustrated in

Figure 4. 13. The two parameters correlate well with adjusted coefficients of determination 0.915. The correlation validates the accuracy of the measured results and proves that the two instruments are both suitable for measuring thermal properties of multi-layered fibrous materials.

Figure 4. 14 shows the thermal conductivity of multi-layered fabrics from KES-FT-II Thermolabo. Similar to the results from Alambeta, the lowest values were observed from materials with aerogel-encapsulated structures, revealing less heat transferred by conduction. Samples with air pockets, demonstrated lower thermal conductivity in comparison to regular samples, which is due to the existence of more trapped air in the structures. As the fabric density increases, the measured thermal conductivity increases as well. Aerogel content present in the fabrics plays a major role and gives lower thermal conductivity. This agrees well with the results from Alambeta device.

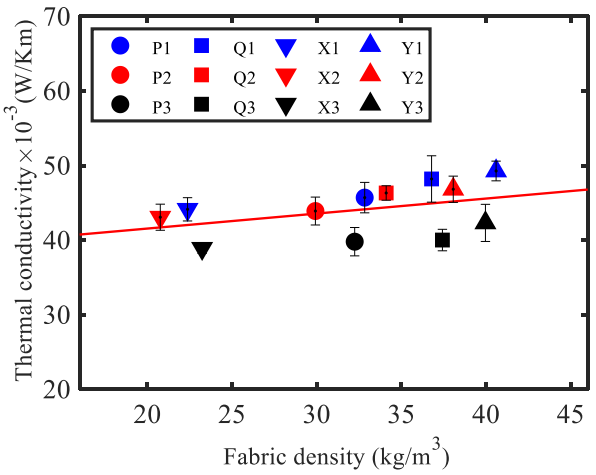

Equation y = a + b*x	Value	t-test Significance "Yes" or "No"	Adj. R-Square	F-test Significance "Yes" or "No"
Intercept	37.53	Yes	0.3715	Yes
Slope	0.2011	Yes		

Figure 4. 14 Thermal conductivity from KES-FT-II Thermolabo

Generally, thermal conductivity value from KES-FT-II Thermolabo was higher than that from Alambeta device. As seen in Figure 4. 15, thermal conductivity of the multilayered fibrous materials from both instruments were found to be well correlated with adjusted coefficients of determination 0.9353.

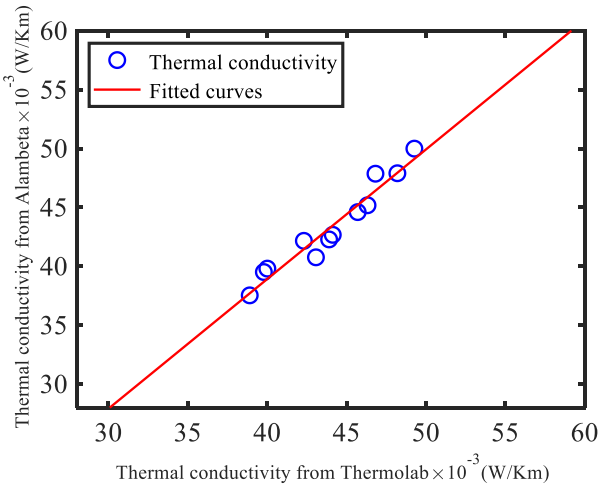

Equation y = a + b*x	Value	t-test Significance "Yes" or "No"	Adj. R-Square	F-test Significance "Yes" or "No"
Intercept	-5.125	Yes	0.9353	Yes
Slope	1.101	Yes		

Figure 4. 15 Correlation of thermal conductivity from KES-FT-II Thermolabo and Alambeta

4.3.3 Infrared thermography

Infrared radiation emitted by a material is detected in a non-contact way by an infrared detector, the temperature of the material is obtained. The dependence of material temperature on time was illustrated in Figure 4.16.

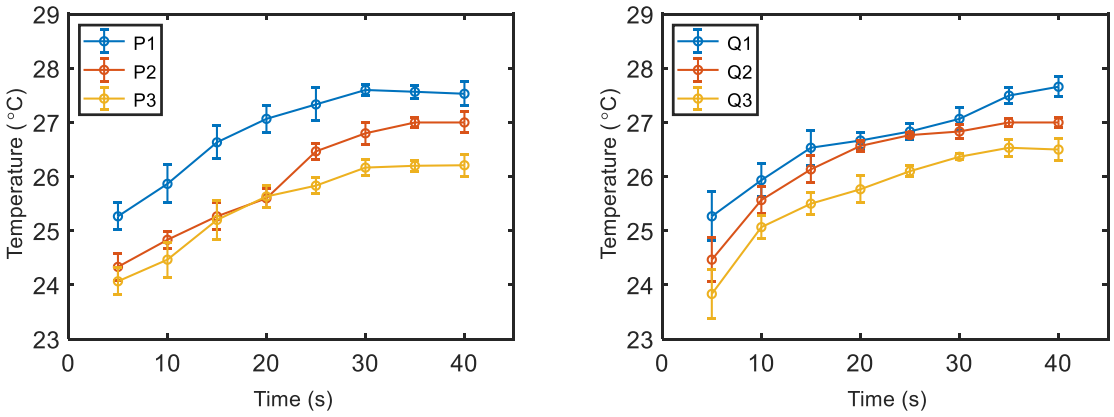

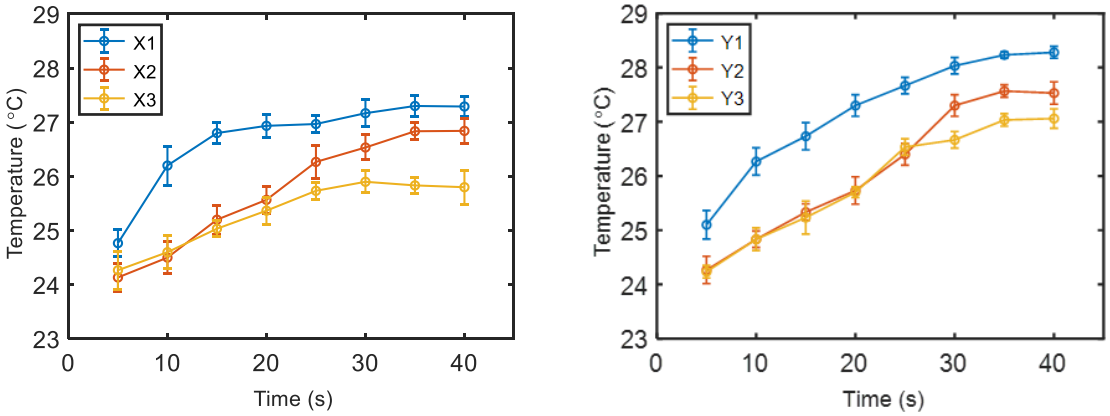

Figure 4. 16 Dependence of detected temperature on time

As the placement of a multilayered material, the initial temperatures from aerogel-encapsulated samples and air pockets samples are much lower than regular samples. Meanwhile, the temperature of all the samples demonstrate an increasing trend with the time. However, for regular samples, the temperature values sharply increase with the time, but this increase is slower for aerogel-encapsulated samples and materials with air pockets.

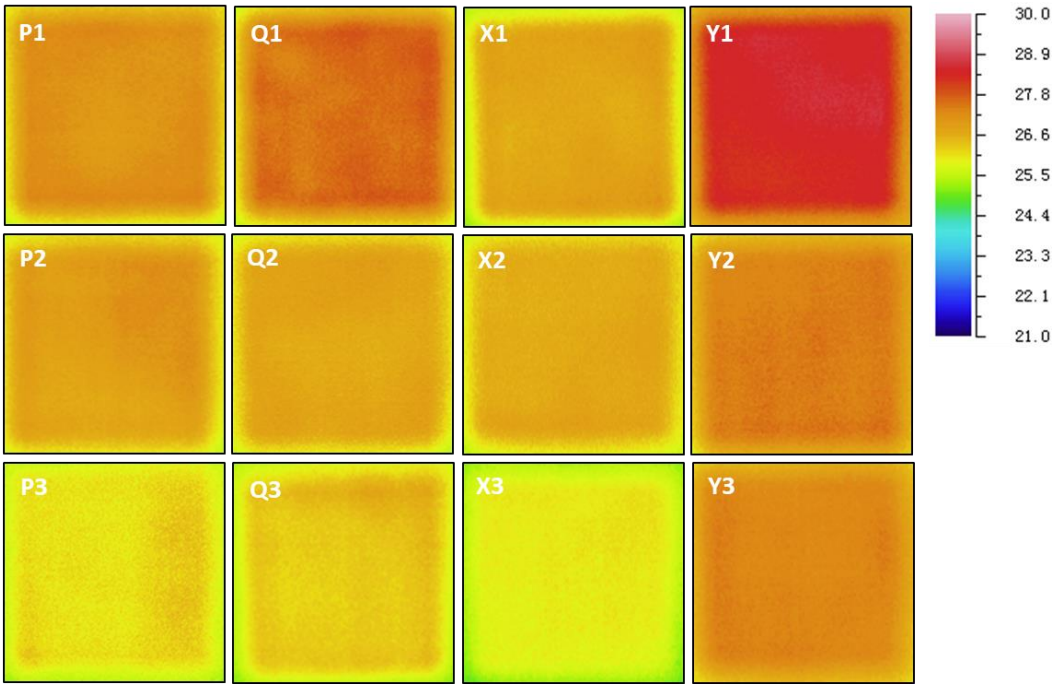

Figure 4. 17 Infrared thermography images under steady state

Figure 4. 17 illustrates the actual infrared thermography images under steady state. It is clear that for each group, temperatures for samples with air pockets are lower than that from regular samples, and the lowest values are observed from aerogel-encapsulated

materials, indicating that the aerogel-encapsulated structure provides good thermal performance under infrared radiation. Results also reveals that the Struto nonwoven based materials have better thermal performance in comparison with PU foam-based samples, this could be attributed to the higher fabric density and lower fabric thickness of the PU foam-based materials. Still, the aerogel particles and air pockets present in the porous PU foam could contribute to the improving of thermal performance.

The obtained temperature values from Avio Thermography Studio 2007 software are presented in Table 4. 4. The quantitative analysis of infrared thermography data enables accurate determination of the temperature of a material. Generally, under infrared radiation the aerogel-encapsulated materials demonstrated lowest temperature values, with 1- 1.5°C lower than regular multilayered samples when the temperature difference between hot plate and environment is 10 °C. Normally, this temperature gap will be enlarged under greater temperature gradient condition.

Table 4. 4 Temperature of different multilayer fabrics under steady state

Sample No.	Max. temperature °C	Min. temperature °C	Mean temperature °C	95% Confidence Interval
P1	27.7	27.2	27.5	27.5±0.299
P2	27.2	26.9	27.0	27.0±0.200
P3	26.5	26.0	26.2	26.2±0.299
Q1	27.8	27.5	27.7	27.7±0.196
Q2	27.3	26.7	27.0	27.0±0.340
Q3	26.6	26.3	26.5	26.5±0.195
X1	27.5	27.1	27.3	27.3±0.226
X2	27.0	26.7	26.8	26.8±0.196
X3	26.0	25.5	25.8	25.8±0.299
Y1	28.5	27.9	28.3	28.3±0.392
Y2	27.7	27.2	27.5	27.5±0.297
Y3	27.3	26.9	27.1	27.1±0.226

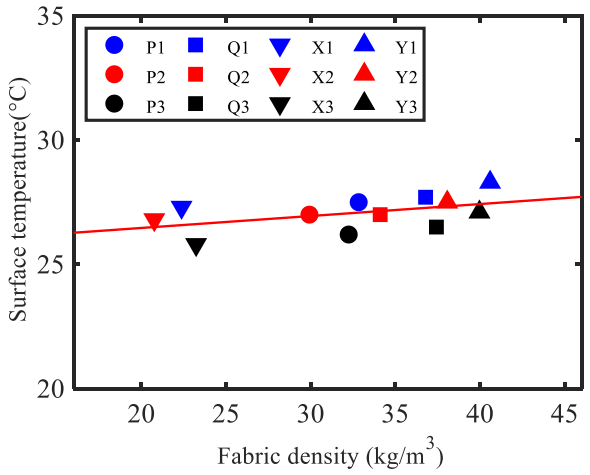

Equation y = a + b*x	Value	t-test Significance "Yes" or "No"	Adj. R-Square	F-test Significance "Yes" or "No"
Intercept	25.5	Yes	0.4399	Yes
Slope	0.04808	Yes		

Figure 4. 18 Correlation of material temperature and fabric density

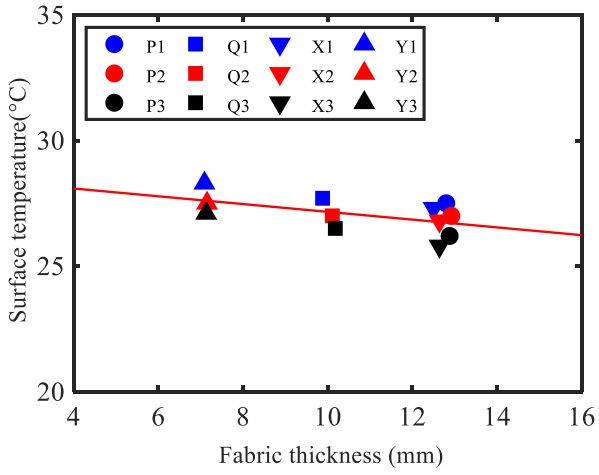

Equation y = a + b*x	Value	t-test Significance "Yes" or "No"	Adj. R-Square	F-test Significance "Yes" or "No"
Intercept	28.71	Yes	0.3023	Yes
Slope	-0.5147	Yes		

Figure 4. 19 Correlation of material temperature and fabric thickness

Figure 4.18 illustrates the correlation of material temperature and fabric density. With the increase in fabric density, the fabric temperature showed a slowly rising trend. This is

attributed to the more fiber fraction which is more conductive and less air fraction in the mutilayered materials. Figure 4.19 shows the correlation of material temperature and fabric thickness. The temperature of multilayered fibrous material decreases as the fabric density increases. Thicker fabrics gives better insulation ability, and thus demonstrates lower temperature when the hot plate temperature is kept constant.

4.3.4 Thermal behavior under convection

4.3.4.1 Thermal behavior of the heating rod without fibrous insulator

The flow pattern is dependent on the Reynolds number *Re* which was given by

$$Re = \frac{v \cdot L_c}{\eta} \tag{4.7}$$

where v is the air velocity [m/s], L_c is the characteristic length [m], η is the kinematic viscosity of air at the film temperature [m^2/s].

The Reynolds number range for this heating rod was 1259-18880. The temperature change of the heating rod is presented in Figure 4.20 and Figure 4.21. Apparently, under preheated condition a rapid temperature drop is observed at the beginning of the cooling process, indicating a high heat loss rate. This rate subsequently slows down until the heating rod cools to ambient temperature. The overall heat loss rate is determined by airflow velocity. At air velocity 0m/s the rod temperature slowly decreases by natural convection. As the airflow velocity increases, this temperature dramatically drops and the overall heat loss rate significantly increases. Under preheated conditions the rod temperature is found to have an exponential relation with the cooling time.

As for the continuous heating condition, the same trend is observed. Remarkably, under continuous supply of heat flow the heating rod quickly reaches a stable temperature at airflow velocity 1m/s. This could be explained by that a steady state in which the heat flow inlet to the heating rod is equal to the heat loss is achieved. After that, an increasing of airflow velocity causes a dramatic rise in heat transfer rate and thus a rapid dropping of the heating rod temperature. Under continuous heating conditions the rod temperature is exponentially related to the cooling time as well.

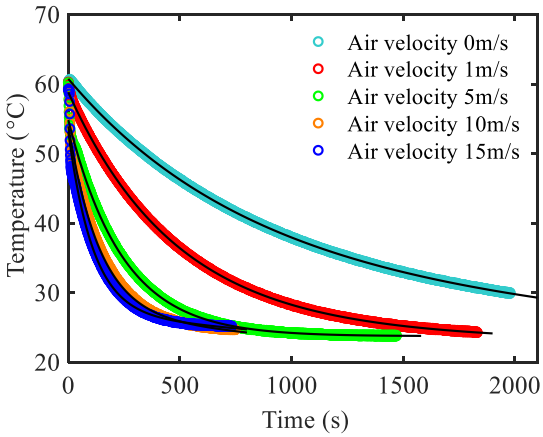

Exponential model Exp2: f(x) = a*exp(b*x) + c*exp(d*x)		
Air velocity m/s	Goodness of fit:	Coefficients (with 95% confidence bounds):
0	SSE: 6.982 R-square: 1 Adj. R-square: 1 RMSE: 0.04972	a = 28.39 (28.22, 28.56) b = -0.001251 (-0.001257, -0.001244) c = 32.36 (32.19, 32.53) d = -8.185e-05 (-8.381e-05, -7.988e-05)
1	SSE: 17.7 R-square: 0.9999 Adj. R-square: 0.9999 RMSE: 0.0823	a = 34.34 (34.26, 34.42) b = -0.002072 (-0.002079, -0.002066) c = 24.48 (24.39, 24.57) d = -2.185e-05 (-2.374e-05, -1.997e-05)
5	SSE: 114.1 R-square: 0.999 Adj. R-square: 0.999 RMSE: 0.2333	a = 31.17 (31.08, 31.26) b = -0.00412 (-0.004146, -0.004094) c = 23.66 (23.56, 23.77) d = 2.38e-06 (-1.2e-06, 5.96e-06)
10	SSE: 410.3 R-square: 0.9927 Adj. R-square: 0.9927 RMSE: 0.6207	a = 27.22 (26.74, 27.69) b = -0.007114 (-0.007337, -0.006891) c = 26.72 (26.18, 27.26) d = -0.0001242 (-0.0001545, -9.383e-05)
15	SSE: 576.7 R-square: 0.9872 Adj. R-square: 0.9872 RMSE: 0.7439	a = 26.1 (25.7, 26.5) b = -0.009019 (-0.009315, -0.008724) c = 27.02 (26.58, 27.46) d = -0.0001116 (-0.0001388, -8.441e-05)

Figure 4. 20 Real-time temperature curves of the heating rod under preheated condition

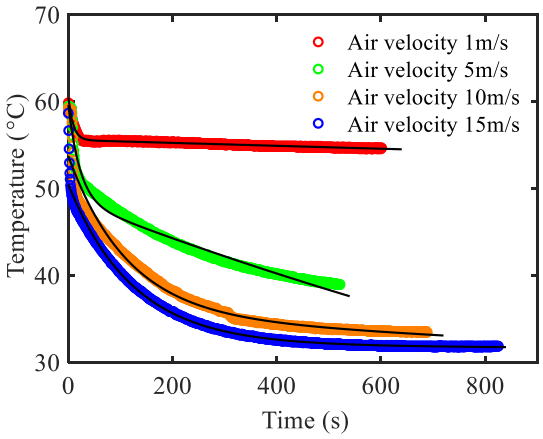

Exponential model Exp2: f(x) = a*exp(b*x) + c*exp(d*x)		
Air velocity m/s	Goodness of fit:	Coefficients (with 95% confidence bounds):
1	SSE: 5.114 R-square: 0.9833 Adj. R-square: 0.9832 RMSE: 0.07729	a = 4.867 (4.789, 4.945) b = -0.1093 (-0.1121, -0.1066) c = 55.62 (55.61, 55.64) d = -3.058e-05 (-3.117e-05, -2.999e-05)
5	SSE: 268.7 R-square: 0.9791 Adj. R-square: 0.979 RMSE: 0.6017	a = 10.87 (10.46, 11.27) b = -0.04482 (-0.0478, -0.04183) c = 48.78 (48.64, 48.92) d =-0.0004796 (-0.0004886, -0.0004706)
10	SSE: 609.1 R-square: 0.9746 Adj. R-square: 0.9745 RMSE: 0.788	a = 18.32 (17.84, 18.81) b = -0.008832 (-0.009308, -0.008356) c = 35.45 (34.91, 35.99) d = -9.539e-05 (-0.0001218, -6.895e-05)
15	SSE: 163.5 R-square: 0.9926 Adj. R-square: 0.9926 RMSE: 0.3728	a = 18.46 (18.28, 18.63) b = -0.008019 (-0.00819, -0.007848) c = 32.05 (31.85, 32.24) d = -1.042e-05 (-1.943e-05, -1.406e-06)

Figure 4. 21 Real-time temperature curves of the heating rod under continuous heating

4.3.4.2 Thermal behavior under preheated condition

In preheated condition, the heating rod has an initial temperature around 60℃. It will lose heat by conduction due to the temperature difference between the heating rod and the fibrous insulator, the fabric gains heat. Some of this heat energy is turned into heat capacity, the rest is transferred to the fabric outer surface and lost by convection when the inlet airflow flows over. The net heat loss from the system leads to temperature drops of

the heating rod and the fabric insulator. Typical real-time temperature curves of the system under different airflow velocities are illustrated in Figure 4. 22.

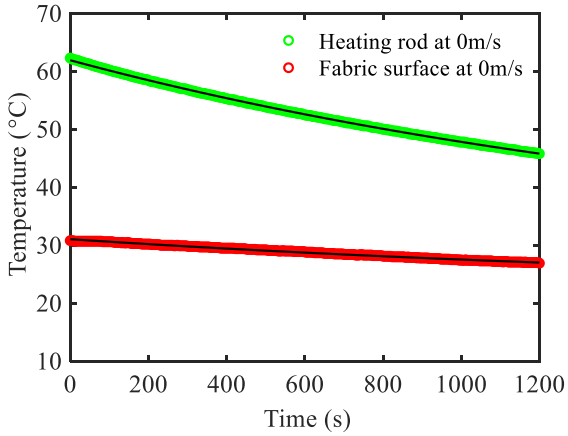

Exponential model Exp2: f(x) = a*exp(b*x) + c*exp(d*x)		
Airflow velocity 0m/s	Goodness of fit:	Coefficients (with 95% confidence bounds):
Heating rod	SSE: 5.561 R-square: 1 Adjusted R-square: 1 RMSE: 0.05721	a = 31.02 (30.88, 31.15) b = -0.0005621 (-0.0005646, -0.0005596) c = 26.9 (26.76, 27.05) d = -2.831e-05 (-2.914e-05, -2.748e-05)
Fabric	SSE: 4.659 R-square: 0.9995 Adj. R-square: 0.9995 RMSE: 0.05237	a = 8.046 (7.921, 8.171) b = -0.0005313 (-0.00054, -0.0005227) c = 23 (22.87, 23.13) d = -8.624e-06 (-9.496e-06, -7.752e-06)

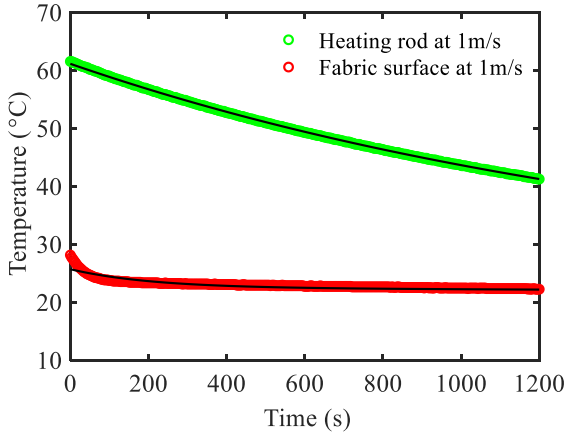

Exponential model Exp2: f(x) = a*exp(b*x) + c*exp(d*x)		
Airflow velocity 1m/s	Goodness of fit:	Coefficients (with 95% confidence bounds):
Heating rod	SSE: 8.105 R-square: 1	a = 36.52 (36.4, 36.65) b = -0.0006264 (-0.0006289, -0.000624)

	Adjusted R-square: 1 RMSE: 0.06981	c = 24.67 (24.53, 24.8) d = -1.979e-05 (-2.071e-05, -1.887e-05)
Fabric	SSE: 78.61 R-square: 0.9092 Adj. R-square: 0.909 RMSE: 0.2174	a = 3.237 (3.132, 3.342) b = -0.00486 (-0.005128, -0.004592) c = 22.52 (22.49, 22.55) d = -1.089e-05 (-1.129e-05, -1.049e-05)
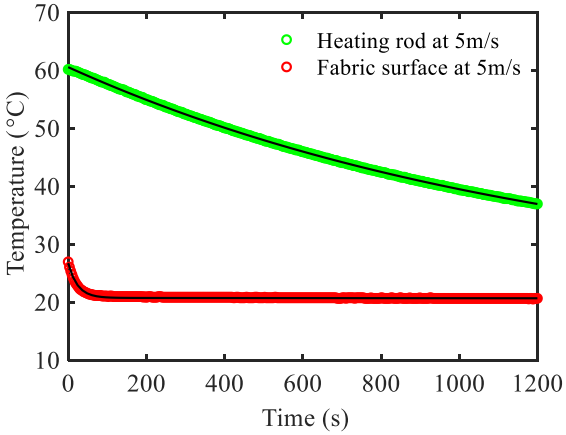		
Exponential model Exp2: f(x) = a*exp(b*x) + c*exp(d*x)		
Airflow velocity 5m/s	Goodness of fit:	Coefficients (with 95% confidence bounds):
Heating rod	SSE: 3.735 R-square: 1 Adjusted R-square: 1 RMSE: 0.05041	a = 37.93 (37.86, 37.99) b = -0.0007999 (-0.0008017, -0.000798) c = 21.66 (21.59, 21.73) d = -7.836e-06 (-8.517e-06, -7.155e-06)
Fabric	SSE: 8.459 R-square: 0.9527 Adj. R-square: 0.9526 RMSE: 0.07586	a = 5.999 (5.903, 6.095) b = -0.04177 (-0.0428, -0.04075) c = 20.78 (20.77, 20.78) d = -2.475e-06 (-2.617e-06, -2.333e-06)
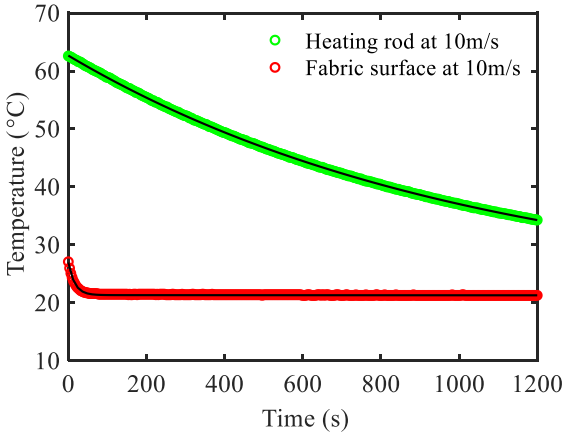		
Exponential model Exp2: f(x) = a*exp(b*x) + c*exp(d*x)		
Airflow velocity 10m/s	Goodness of fit:	Coefficients (with 95% confidence bounds):
Heating rod	SSE: 3.969	a = 41.16 (41.14, 41.18)

	R-square: 1 Adjusted R-square: 1 RMSE: 0.04676	b = -0.000969 (-0.00097, -0.0009679) c = 21.5 (21.47, 21.53) d = -3.335e-06 (-3.576e-06, -3.094e-06)
Fabric	SSE: 7.104 R-square: 0.9373 Adj. R-square: 0.9372 RMSE: 0.06256	a = 5.631 (5.541, 5.721) b = -0.06102 (-0.06256, -0.05948) c = 21.34 (21.33, 21.34) d = -1.257e-06 (-1.339e-06, -1.175e-06)
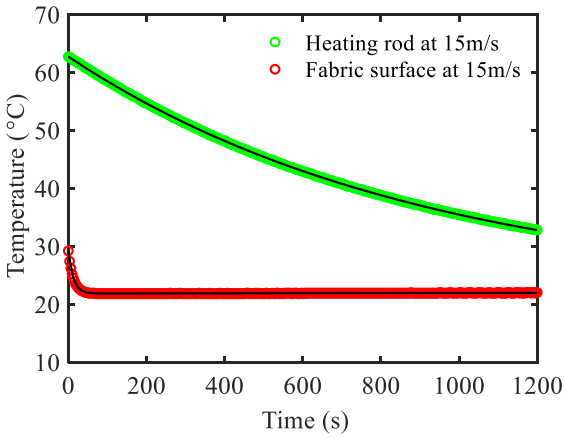		
Exponential model Exp2: f(x) = a*exp(b*x) + c*exp(d*x)		
Airflow velocity 15m/s	Goodness of fit:	Coefficients (with 95% confidence bounds):
Heating rod	SSE: 3.372 R-square: 1 Adjusted R-square: 1 RMSE: 0.04432	a = 40.84 (40.82, 40.86) b = -0.001102 (-0.001103, -0.001101) c = 21.97 (21.95, 21.99) d = 4.911e-07 (2.755e-07, 7.068e-07)
Fabric	SSE: 2.679 R-square: 0.9834 Adj. R-square: 0.9834 RMSE: 0.0395	a = 7.303 (7.241, 7.365) b = -0.07965 (-0.08074, -0.07856) c = 21.93 (21.93, 21.93) d = 4.489e-06 (4.436e-06, 4.543e-06)

Figure 4. 22 Real-time temperature curves of the heating rod and aerogel-encapsulated fabric Q3

It is seen that a low airflow velocity gives a gentle downslope of the heating rod and fabric temperatures, a high velocity leads to rapid temperature declines and higher heat loss rates of the system. Under different airflow velocities, the aerogel-encapsulated fabric has different initial temperatures ranging from 32.5℃to 26.4℃. The reason could be that the airflow requires a few seconds to reach a selected velocity and during this period the heat dissipation, which relies on airflow velocity and the duration, varies and causes different initial temperatures. By comparison with the naked heating rod, it is found that the heating rod has much lower heat loss rate when using the aerogel-encapsulated fibrous material as

insulator, indicating good insulating ability of the material. Meanwhile, very small temperature drop is observed for the fibrous material. The real-time temperatures of the heating rod and fibrous insulator are both exponentially related with cooling time. The same trend is observed for all the multilayered materials as well as aerogel-treated nonwovens, as shown in Appendix.

Figure 4. 23 illustrates the real-time temperature curves from different fabrics. The fabric temperature depends on not only thermal characteristics of the fabric, but also external factors such as airflow temperature, airflow velocity, heating rod temperature and so on.

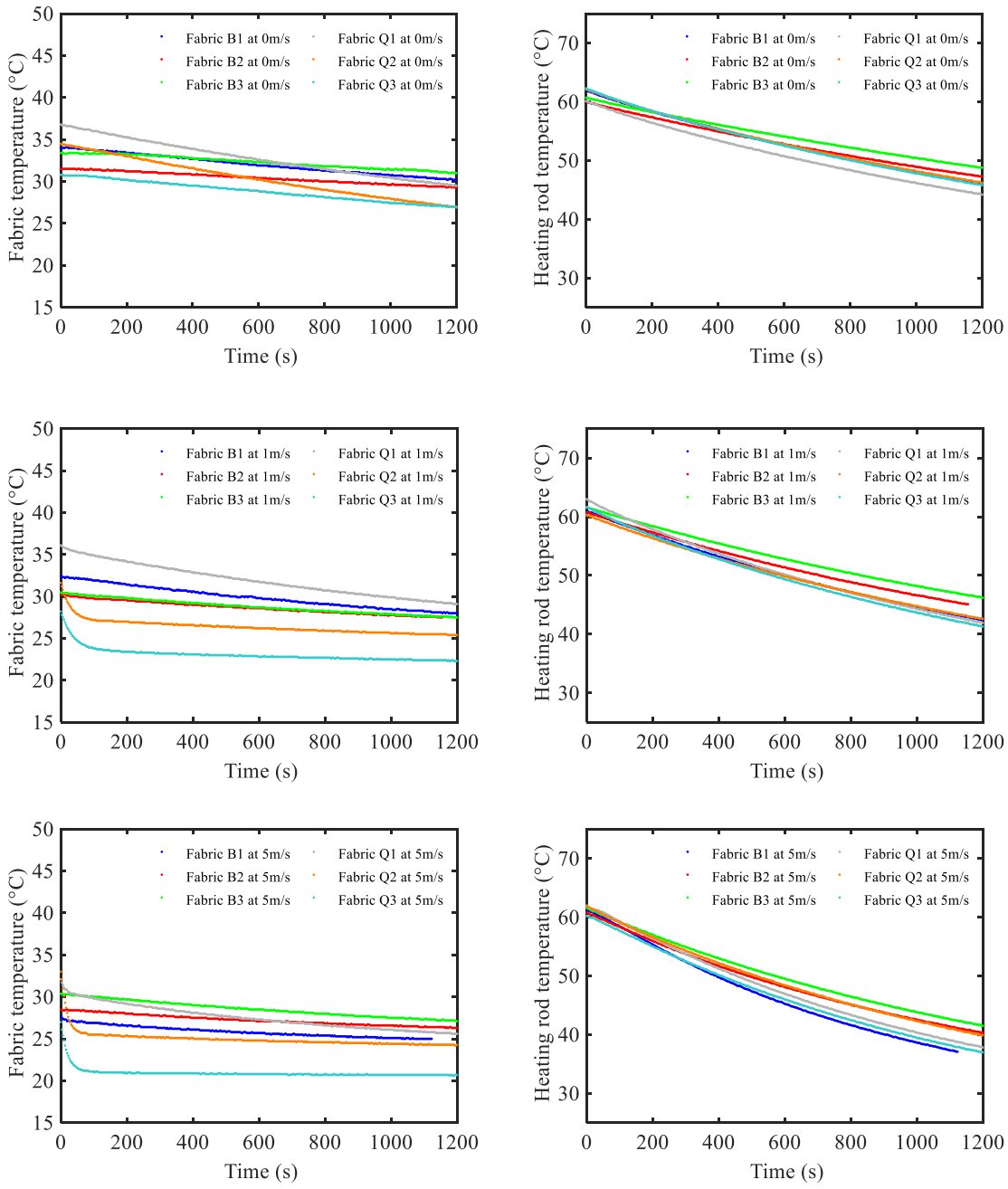

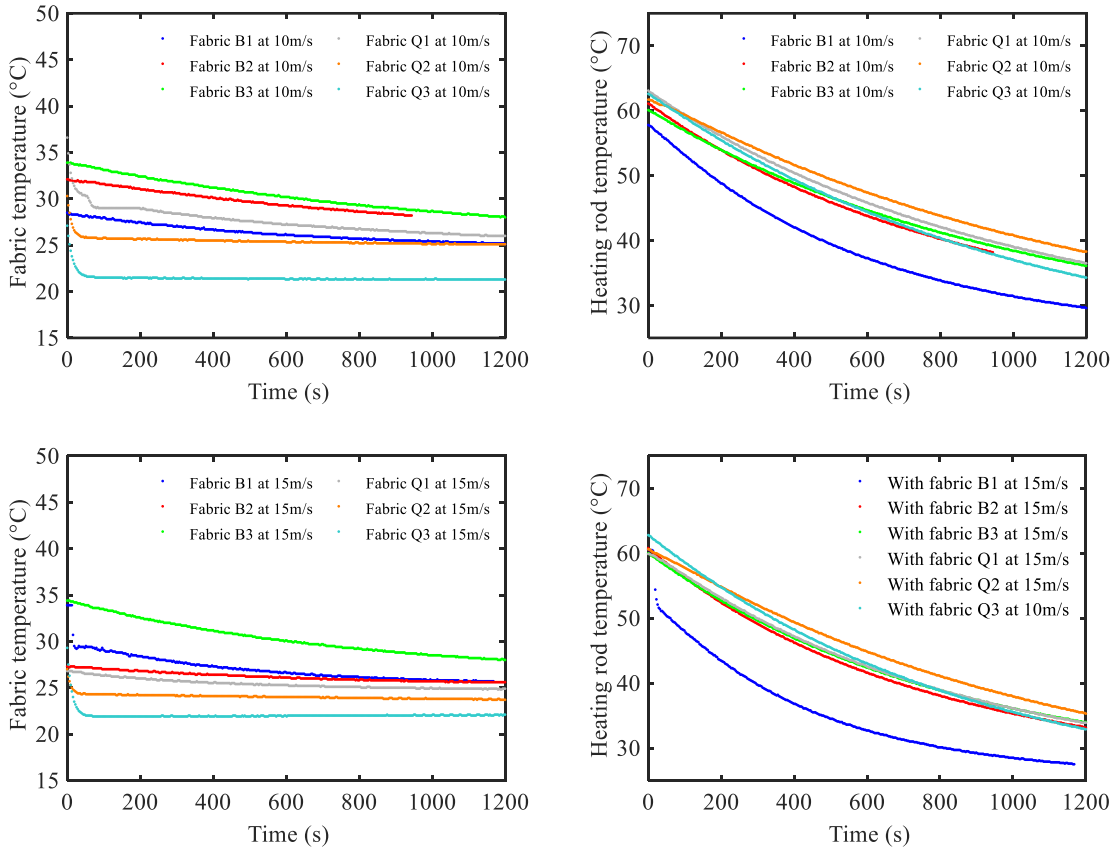

Figure 4. 23 Comparison of real-time temperature curves under preheated condition

Multi-layered samples demonstrate rapid decreases in fabric temperature in the very beginning of the cooling curve while very small temperature drops are observed for aerogel-treated samples. This could be explained by that the multilayered samples exhibit lower density and their heat loss rate is more influenced by airflow, leading to obvious fabric temperature drop at airflow velocity over 1m/s. It is also noted that sample Q2 and Q3 have significantly lower initial temperature, implying that these two types of structures are less conductive and thus less prone to be heated up. However, since the heating rod temperature and the initial fabric temperature varies for each case, the effect of different fabrics still remains unclear.

With respect to the heating rod temperatures, it is clear that the heating rod temperature curves shift to the lower part with the increasing of airflow velocity, showing obvious temperature decrease trend. Generally, the heating rod with aerogel-treated nonwoven B2 and B3 give higher temperature in comparison with sample B1, and the temperature gradient is more significant at high airflow velocities. This could be explained by the difference of fabric structural parameters and aerogel content. Nonwoven fabrics have very

close porosity values over 90%, with pore size ranging from 2 and 4.5 microns which allows bulk of air molecules to flow through.[109] However, the aerogel particles, with an average pore size around 20nm, could prevent airflow stream. As a result, more aerogel content will give less permeability to airflow and thus lower heat transfer rate. Meanwhile, thinner fabrics are easier to be penetrated by air stream, causing more heat loss from the heating rod. As a result, aerogel-treated nonwovens with higher aerogel content and fabric thickness demonstrate better ability to prevent against heat loss under airflow-induced convection. As for the multilayered fibrous materials, since the samples have very similar characteristics of permeability and fabric density, the temperature curves of the heating rod under the same airflow velocity are quite close.

4.3.4.3 Thermal behavior under continuous heating condition

In continuous heating condition, a specific electric power is supplied to the heating rod. For the system composed by the heating rod and the fabric, the heat flow generated by the heating rod was partly converted into its heat capacity, the rest was conducted to the fabric and finally turned into heat capacity of the fabric or dissipated by air-induced convection. The whole dynamic process is influenced by power supply, airflow nature, physical parameters of the heating rod as well as physical and structural parameters of the fabric.

The real-time temperature curves of the heating rod and different fabrics under continuous heating are presented in Figure 4. 24. In comparison with the heating rod, all the fabrics maintain relatively stable temperature values under continuous heating condition. Similar to the results from preheated conditions, sample Q3 shows the lowest temperature under continuous heating, which is benefited from the aerogel-encapsulated structure. Sample Q2 exhibits lower temperature due to the structure with laser-engraved air pockets. Among the aerogel-treated nonwoven fabrics, samples B2 and B3, with higher fabric thickness and aerogel content, demonstrate better ability to prevent against heat loss from the heating rod. Especially at high airflow speed (10 m/s and 15 m/s) the heating rod is able to achieve quite high temperature values, meaning better thermal protection given by these fabrics.

With respect to the heating rod temperatures, slight fluctuations are observed for the temperature curves at low airflow speed (1 m/s and 5 m/s). These fluctuations are well consistent with the current switch. The heating rod with multilayered samples generally demonstrates lower temperature value. This may be attributed to the air permeable

characteristics of the multilayered materials which enables considerable heat loss from the heating rod. A gentle increasing of the heating rod temperature is observed for aerogel-treated nonwoven fabrics when the airflow speed is 10 m/s and 15m/s. Meanwhile, it is notable that the heating rod with aerogel-treated nonwoven B1, has rapid temperature drop from 58℃ to 48.8 ℃ when the airflow with velocity of 15m/s is induced. This implies that aerogel content and fabric thickness are very important factors in protecting against heat loss at high airflow velocity.

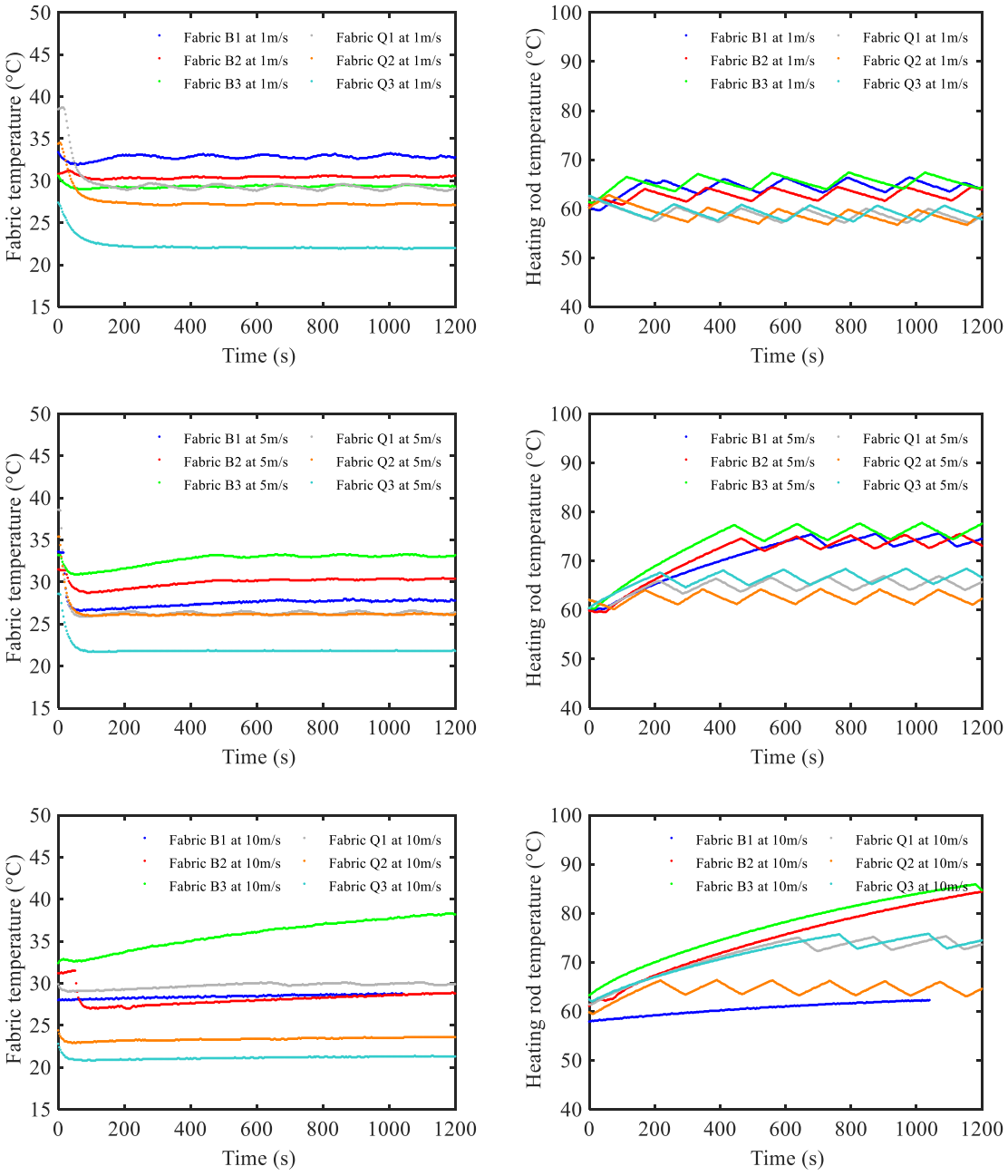

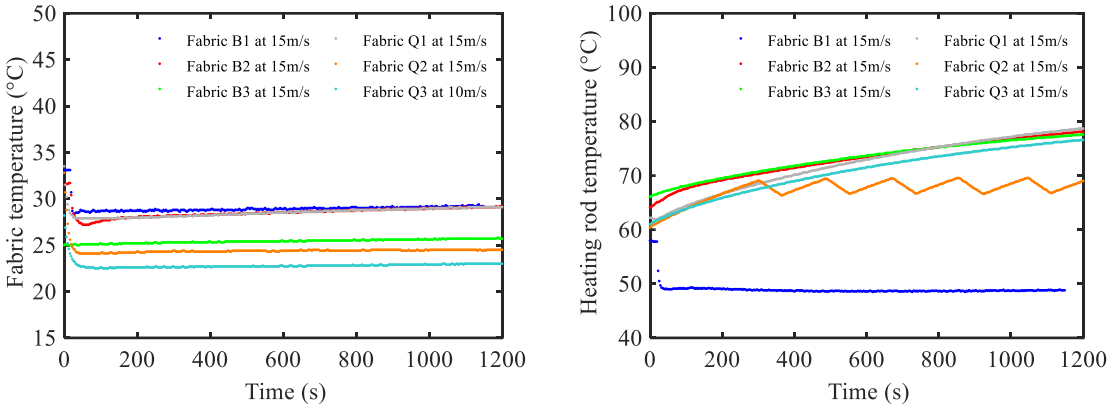

Figure 4. 24 Comparison of real-time temperature curves under continuous heating

4.3.4.4 Comparison of thermal performance under continuous heating condition

The continuous heating of the system under airflow-induced convection is a dynamic process involving complex flow patterns around solid particles or fibers. Due to the random orientations of the solid phase, exact solutions to the detailed local flow field are impossible. In order to compare thermal performance of different fibrous materials, the system can be approximately assumed to reach steady state if the temperature of the heating rod and fabric are fluctuating within a narrow range or showing a very gentle upslope. In this case, the heat flow inlet to the system is roughly equal to the heat loss from the fibrous material by convection as shown in Figure 4. 25.

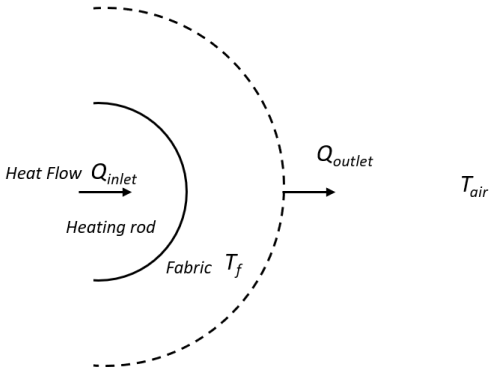

Figure 4. 25 Heat transfer through the system in steady state

Heat flow was measured by noting the current and voltage inputted to the heating rod. The heat transfer coefficient h_c is determined by

$$h_c = \frac{Q_{inlet}}{S(T_f - T_{air})} \tag{4.8}$$

where T_f is the temperature of fabric surface [K], T_{air} is the temperature of ambient air [K], Q_{inlet} is the heat flow inlet to the heating rod [W], S is the surface area of the fibrous material exposed to the airflow [m^2].

Figure 4. 26 illustrates the heating rod to air temperature difference under steady state. Apparently, the temperature difference tends to dramatically decrease with the increase in airflow velocity, while this trend is reversed when a fibrous material is used as insulator. This could be attributed to the decrease of net flux from the boundary while the porous material behaves as a barrier to prevent against airflow and thus the heat loss is reduced. For all the samples, the temperature gradient increases as the airflow velocity increases. Among different materials, aerogel-treated nonwovens with higher aerogel content, and multilayered materials with higher fabric density, demonstrated higher temperature gradient.

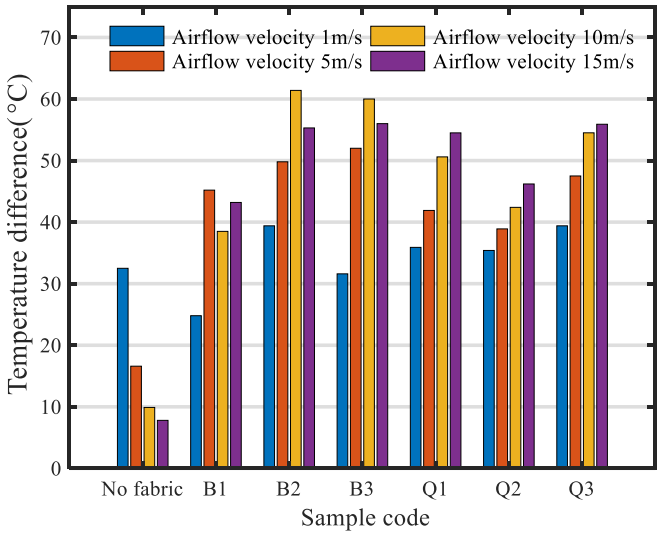

Figure 4. 26 Heating rod to air temperature difference based on insulating material

The Reynolds number is important in predicting flow patterns in different fluid flow situations for convective heat transfer problems. At low Reynolds numbers (Re < 2300), the airflow is laminar flow which is dominated by viscous forces and is characterized by parallel streams of fluid motion. The heat transferred to and through the fluid is essentially by conduction. At high Reynolds numbers (Re > 4000), the airflow is turbulent which is characterized by velocity fluctuations and highly disordered motion. This high velocity fluctuations and disorderliness will case high heat transfer rate. The heating rod to airflow temperature difference is plotted for different Reynolds number as seen in Figure 4. 27.

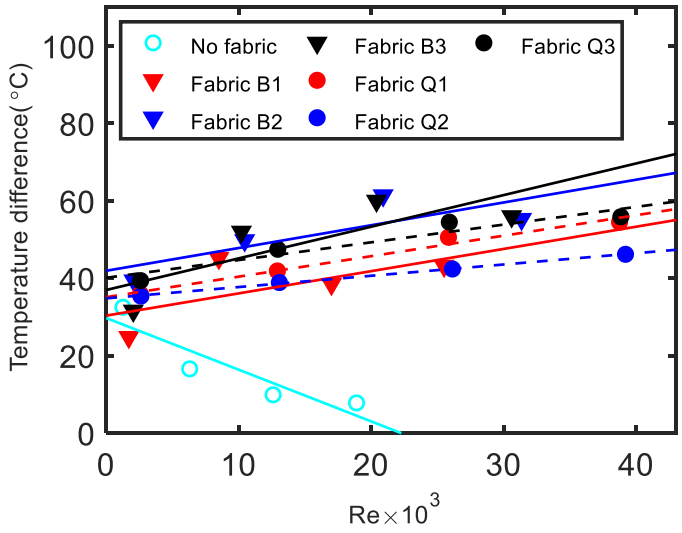

Fabric No.	Equation y = a + b*x	Value	t-test Significance "Yes" or "No"	Adj. R-Square	F-test Significance "Yes" or "No"
Without fabric	**Intercept**	29.73	Yes	0.7519	Yes
	Slope	-1.336	Yes		
B1	**Intercept**	30.36	Yes	0.1250	Yes
	Slope	0.5746	Yes		
B2	**Intercept**	41.95	Yes	0.6397	Yes
	Slope	0.5886	Yes		
B3	**Intercept**	36.98	Yes	0.6437	Yes
	Slope	0.8179	Yes		
Q1	**Intercept**	35.13	Yes	0.9654	Yes
	Slope	0.5296	Yes		
Q2	**Intercept**	34.82	Yes	0.9074	Yes
	Slope	0.2919	Yes		
Q3	**Intercept**	40.14	Yes	0.8589	Yes
	Slope	0.4582	Yes		

Figure 4. 27 Heating rod to air temperature difference vs Reynolds number

For the heating rod without fabric, temperature difference lies in the range of 32℃-8℃,

showing obvious increase in heat transfer rate and considerable decrease in the heating rod to air temperature difference with the increasing of Reynolds number. The heating rod to air temperature difference increases with the Reynolds number when applying a fibrous insulator. It is also observed that the temperature differences from aerogel-treated fabric B2 and B3 are very close, which may be attributed to their close proximity of fabric thickness.

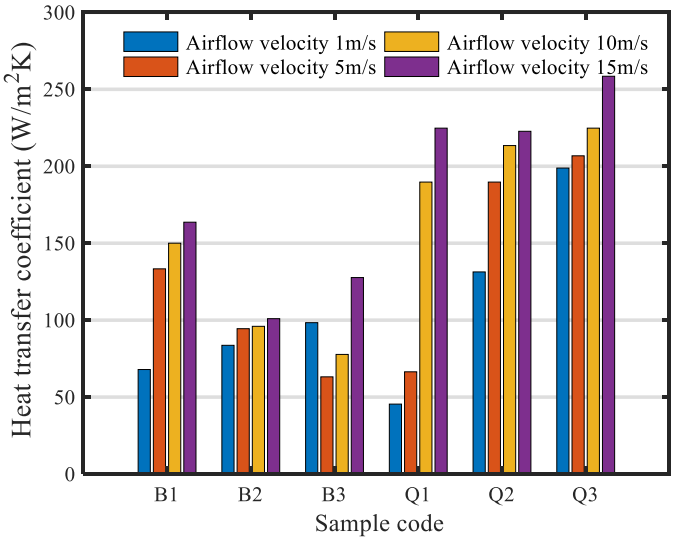

Figure 4. 28 Heat transfer coefficients of different samples

Figure 4. 28 shows the heat transfer coefficient of different samples. The coefficient value tends to increase with the increase in airflow velocity. Multilayered fibrous materials demonstrate higher heat transfer rate in comparison with aerogel treated nonwoven fabrics. This could be explained by that the multilayered samples exbibit lower density and thus higher porosity, leading to higher heat transfer rate under convection. Aerogel-treated nonwovens B2 is observed to have relatively stable heat transfer coefficients, this could be attributed to the present aerogel particles in the low-density fibrous structure.

The heat transfer coefficient increases with Reynolds number as seen in Figure 4. 29. The data fall in distinct groups depending on the fabric density and permeability of the material. For lower-density materials, dispersion dominates any molecular conduction, resulting in heat transfer independent of solid conductivity but more affected by the airflow. The convective heat transfer coefficient of each material shows an increasing trend with the increasing of Reynolds number. A flat upstream trend is observed for aerogel-treated nonwoven B2 and B3. For multilayered materials and aerogel-treated nonwoven B1, the

coefficients significantly increase with the increase in airflow velocity and Reynolds number.

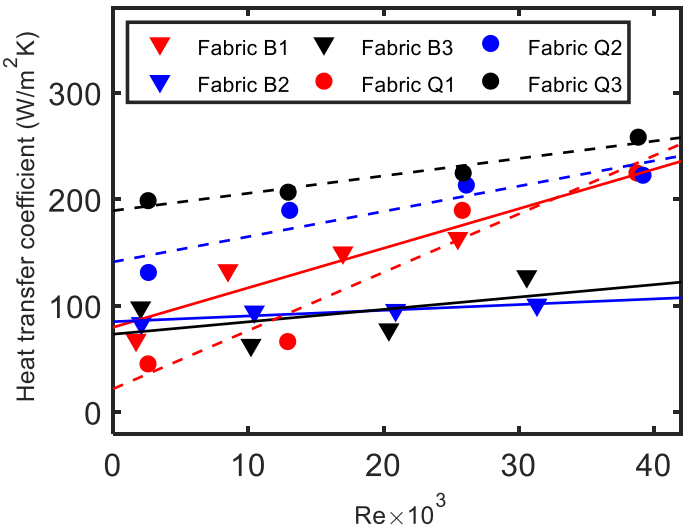

Fabric No.	Equation y = a + b*x	Value	t-test Significance "Yes" or "No"	Adj. R-Square	F-test Significance "Yes" or "No"
B1	**Intercept**	79.84	Yes	0.7269	Yes
	Slope	3.714	Yes		
B2	**Intercept**	85.13	Yes	0.7965	Yes
	Slope	0.5341	Yes		
B3	**Intercept**	73.34	Yes	-0.1014	Yes
	Slope	1.164	Yes		
Q1	**Intercept**	21.95	Yes	0.9016	Yes
	Slope	5.48	Yes		
Q2	**Intercept**	141.3	Yes	0.7622	Yes
	Slope	2.374	Yes		
Q3	**Intercept**	189.4	Yes	0.9138	Yes
	Slope	1.636	Yes		

Figure 4. 29 Heat transfer coefficient vs Reynolds number

4.4 Thermal properties of PUR and PVDF electrospun nanofibrous layer embedded with silica aerogel

Thermal conductivity as a function of areal density for PUR and PVDF electrospun nanofibrous layer embedded with silica aerogel is shown in Figure 4. 30 and Figure 4. 31. The results showed that thermal conductivity of the electrospun nanofibrous layer decreased with increase in density. This can be explained by the fact that as the density increases the fibrous structure becomes more packed. When the density reaches a critical point, the increase in conduction through solid phase and decrease in radiation conductivity results in an increase in total thermal conductivity.[110-111] The superfine fibers in the web have better radiation absorption and extinction due to their higher surface-area-to-volume ratio. Thus, decrease in the average nanofiber diameter leads to lower thermal conductivity. Moreover, smaller pore size between nanofibers decreases the mean free path for photon movement resulting in lower radiative energy transfer. This improvement becomes more significant when the bulk density is increased.

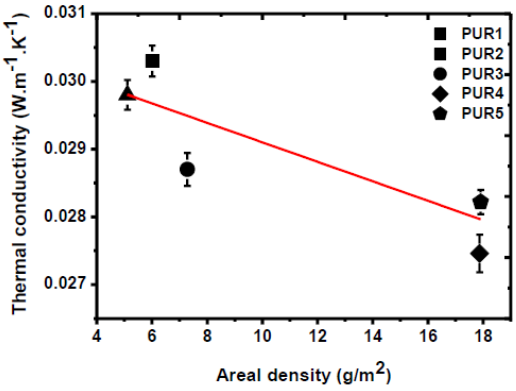

Equation y = a + b*x	Value	t-test Significance "Yes" or "No"	Adj. R-Square	F-test Significance "Yes" or "No"
Intercept	0.03054	Yes	0.67506	Yes
Slope	-0.0001438	Yes		

Figure 4. 30 Thermal conductivity vs areal density of electrospun PUR nanofibrous membranes embedded with silica aerogel

Furthermore, higher porosity of the web with a nanofiber diameter around 250 nm could be the other reason for their lower thermal conductivity. Thus, using thinner nanofibers leads to noticeable performance and helps in achieving very low limit of thermal

conductivity. Of particular interest are the results for the electrospun PUR and PVDF nanofibrous layer. Both materials showed excellent reduction in overall heat transfer compared to standard low-density fibrous insulating materials (at areal densities above 40 g/m^2).

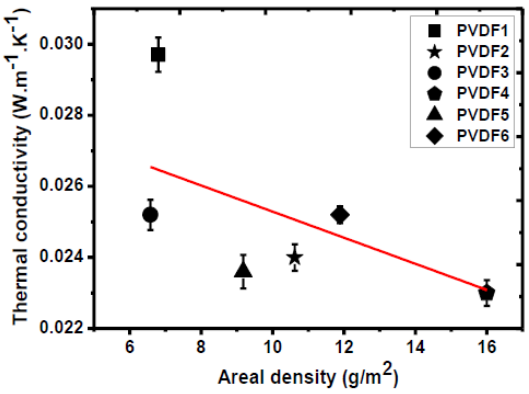

Equation y = a + b*x	Value	t-test Significance "Yes" or "No"	Adj. R-Square	F-test Significance "Yes" or "No"
Intercept	0.02896	Yes	0.2315	Yes
Slope	-0.0003672	Yes		

Figure 4. 31 Thermal conductivity vs areal density of electrospun PVDF nanofibrous membranes embedded with silica aerogel

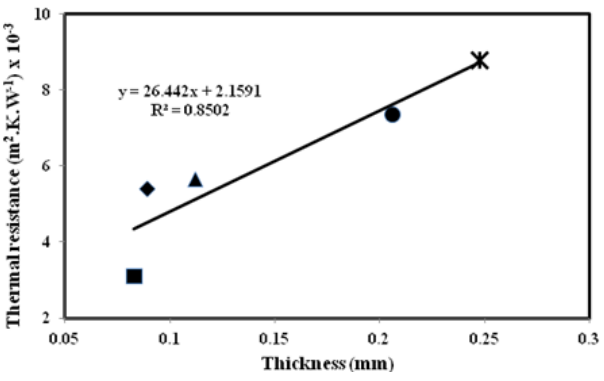

Equation y = a + b*x	Value	t-test Significance "Yes" or "No"	Adj. R-Square	F-test Significance "Yes" or "No"
Intercept	2.1591	Yes	0.8502	Yes
Slope	26.442	Yes		

Figure 4. 32 Correlation of thermal resistance and thickness of electrospun PUR nanofibrous membranes embedded with silica aerogel

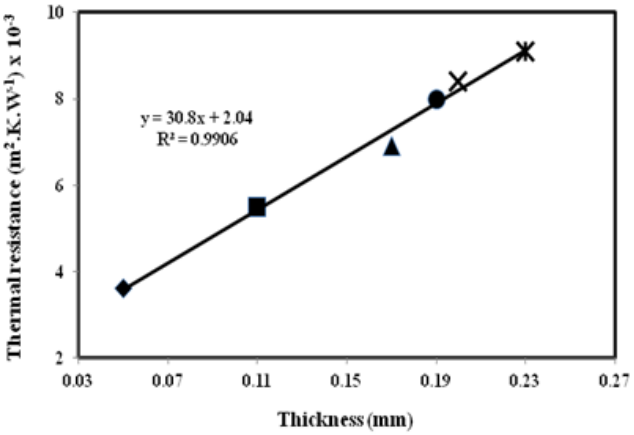

Equation y = a + b*x	Value	t-test Significance "Yes" or "No"	Adj. R-Square	F-test Significance "Yes" or "No"
Intercept	2.04	Yes	0.9906	Yes
Slope	30.8	Yes		

Figure 4. 33 Correlation of thermal resistance and thickness of electrospun PVDF nanofibrous membranes embedded with silica aerogel

The PVDF nanofibrous layer showed superior insulation at higher areal density values. Thermal conductivity testing confirmed that lower fiber diameter tends to increase the thermal resistance of fibrous insulation materials. However, the nanofiber/aerogel becomes an effective insulator since the aerogel structure suppresses conduction and convection, and the fibers reduce radiation heat transfer while increasing the strength of the brittle and weak aerogel structure. The combination of nanofiber and aerogel has demonstrated superior insulation properties for applications where thickness is of concern. With respect to high porosity fibrous insulation materials, the combination of aerogel and nanofiber demonstrated excellent insulation per unit thickness properties. The thermal resistance of electrospun PVDF nanofibrous layer embedded with silica aerogel is higher than electrospun PUR nanofibrous layer embedded with silica aerogel.

4.5 Thermal stability of nanofibrous membranes

The nanofibrous membranes were analyzed using Differential Scanning Calorimetry (DSC) as shown in Figure 4. 34. Large differences were observed in the melting endotherm values. A strong endothermic peak was observed at around 240ºC and 170ºC for PUR and PVDF nanofibrous membranes, which corresponded to oxidation of the surface hydroxyl groups

and evaporation of trapped water and alcohol. PURs can demonstrate different degrees of crystallinity according to the processing conditions.[112] Furthermore, parametric variations in the electrospinning process can also alter the melting temperatures of fibers prepared from the solution.[113] The level of crystallinity is increased when using the electrospinning process, going from film to fiber morphology, resulting in an increase in the melting temperature.[114]

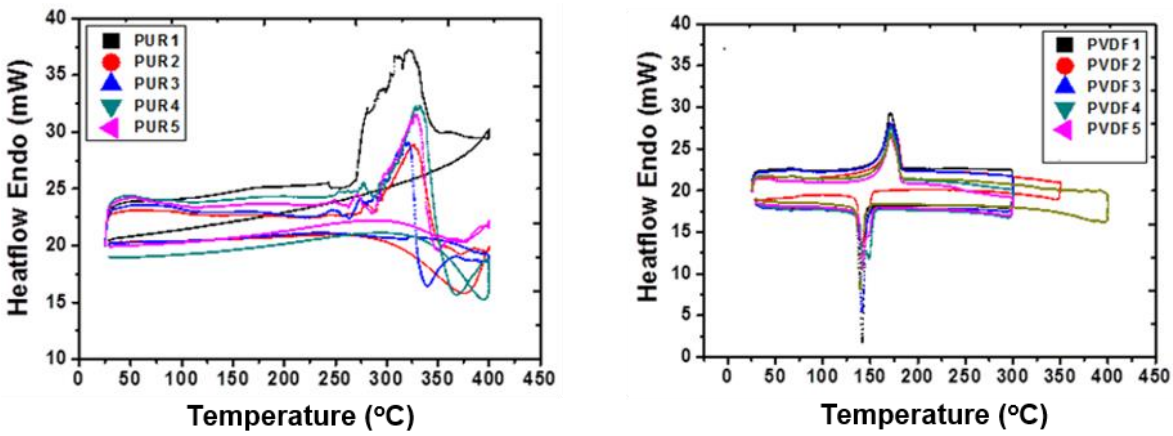

Figure 4. 34 DSC curves of PUR and PVDF nanofibrous membranes embedded with and without aerogel

Figure 4. 35 shows the TGA curves of electrospun PUR and PVDF nanofibrous membranes with and without SiO_2 aerogel. The PUR nanofibrous membranes demonstrated considerable weight loss above 300°C, the electrospun PVDF layers showed significant weight loss in the temperature range of 400-450°C. The weight loss was associated with the degradation of the polymer chain structure, in agreement with previous literature.[115] The weight loss of the PUR nanofibrous membranes embedded with and without aerogel was between 90% to 95% at around 290°C and PVDF nanofibrous membranes embedded with and without aerogel were between 5% and 17% at around 430°C, respectively. Therefore, the PVDF nanofibrous membranes showed better stability than PUR nanofibrous membranes. However, it should be noted that the PVDF nanofibrous membranes may melt at 172°C although no noticeable weight loss exists. Therefore, the PVDF nanofibrous membranes are suitable for the application in thermal insulation below 172°C.

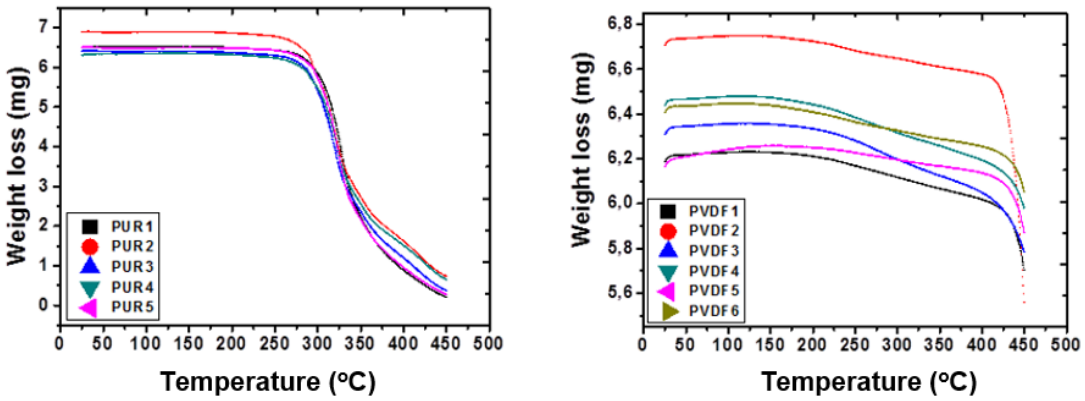

Figure 4. 35 TGA curves of PUR and PVDF nanofibrous membranes embedded with and without aerogel

4.6 Air permeability analysis

4.6.1 Air permeability of layered nanofibrous web/silica aerogel/ nonwoven

The results of air permeability of different fabric systems are given in Table 4. 5. Air permeability of nonwoven substrate was found to sharply decrease when a nanofiber web was laminated onto its surface. This is mainly because the nanofiber web has a large number of smaller pores and relatively lower porosity, which covers the open pores of nonwoven substrate and prevents the air flow go through. Moreover, the thermal adhesive would reduce the pores of nonwoven substrate in some degree, this may also account for the decrease in air permeability. Aerogel showed limited influence on the air permeability of these layered fabrics. For a specified fabric, air permeability had a strong correlation with air pressure gradient. This indicated that the rate of air flow was directly proportional to the pressure gradient, which consisted well with Darcy's law.

Air permeability directly depends on pore size and porosity, since the aerogel granule can be approximately considered as air-proof material due to its nano scale pores, the air permeability of layered fabrics tended to decrease as the increase in aerogel content. From Table 4. 5, It was also observed that there appeared a critical value in aerogel content, above which the air permeability showed an increasing trend with the increasing of aerogel. The reason could be that there may appear more air gap between nanofiber web and nonwoven substrate due to the much bigger size of aerogel granules compared to the thickness of nanofiber web, the enlarged air gap in this layered system will allow more air to flow through. This was also indicated by the significant increase in fabric thickness.

Table 4. 5 Air permeability of samples under different pressure gradients

Sample No.	Air permeability at 100 Pa		Air permeability at 200 Pa	
	Average value [mm/s]	95% confidence level	Average value [mm/s]	95% confidence level
S	2160	2160 ± 33.88	3743	3743 ± 117.23
N	32.22	32.22 ± 0.55	73.48	73.48 ± 0.68
A0	32.59	32.59 ± 1.87	61.01	61.01 ± 3.15
A1	39.55	39.55 ± 1.25	84.52	84.52 ± 2.01
A2	33.08	33.08 ± 1.69	67.28	67.28 ± 2.93
A3	30.58	30.58 ± 1.30	54.97	54.97 ± 3.17
A4	36.71	36.71 ± 1.53	74.77	74.77 ± 2.31
A5	41.28	41.28 ± 0.70	84.21	84.21 ± 1.18

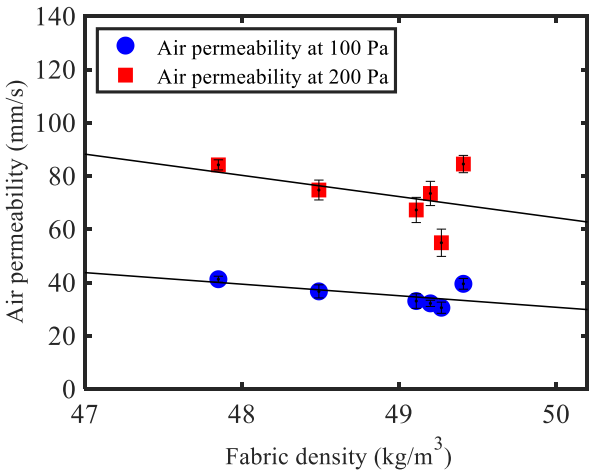

Pressure Pa	Equation y = a + b*x	Value	t-test Significance "Yes" or "No"	Adj. R-Square	F-test Significance "Yes" or "No"
100	**Intercept**	247.5	Yes	0.4676	Yes
	Slope	-4.335	Yes		
200	**Intercept**	462.4	Yes	0.2843	Yes
	Slope	-7.96	Yes		

Figure 4. 36 Correlation of air permeability with fabric density

The correlation of air permeability with fabric density is presented in Figure 4. 36. Air

permeability is an expression describing the properties of a fabric that permit the passage of air through the fabric's interstices. The air permeability is extremely important as it will directly affect the thermal properties to some degree. Fabrics with higher density usually possess lower porosity and thus demonstrate lower air permeability.

4.6.2 Air permeability of multilayered fibrous materials

The air permeability of multilayer fabrics is influenced not only by the porosity, but also by other parameters relating the number of layers, the structural parameters of a single fabric and the multilayer structure of the system. In a multilayer fibrous system, under the same pressure difference, the air permeability decreases with the increasing of the number of layers due to the increase in the resistance to flow of air through the pores of the fibrous material. The resistance to flow depends upon the alignment of pores in one layer with that of another layer, the gap between individual layers of the fabric, and the distortion of the fibers caused by the airflow.[116]

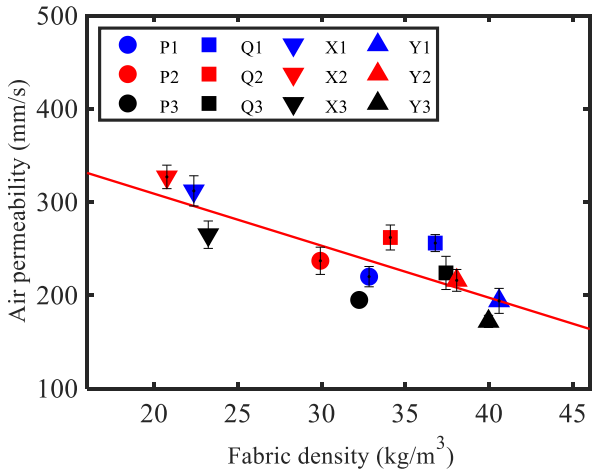

Equation y = a + b*x	Value	t-test Significance "Yes" or "No"	Adj. R-Square	F-test Significance "Yes" or "No"
Intercept	420.5	Yes	0.6525	Yes
Slope	-5.58	Yes		

Figure 4. 37 Air permeability of multilayered fibrous materials

As shown in Figure 4. 37, the multilayered samples with air pockets had slightly higher air permeability, it is attributed to the lower resistance to airflow through the pores in the middle layer and hence the loss in the airflow velocity will be lower. The aerogel particles

present in the multilayered fibrous materials led to small decrease in air permeability because the large voids in the fibrous structure were divided into many smaller pores and partly replaced by mesopores in the aerogels. However, aerogels had negligible effect on the porosity of fibrous material since the dominant component of aerogel particles is air.

4.6.3 Air permeability of PUR and PVDF electrospun nanofibrous layer embedded with silica aerogel

The air permeability of nanofibrous membranes is presented in Figure 4. 38 and Figure 4. 39. Apparently, samples containing PUR nanofiber with double layer (0.16 and 0.24 mm) showed lower air permeability. This behavior may be attributed to the finer diameter of PUR nanofiber compared to PVDF nanofiber. Lower air permeability was achieved by increasing the number of nanofibrous membranes. It confirmed the relationship of the important parameter to thermal insulation. The increased weight as well as thickness of electrospun nanofiber web reduced air permeability. The PUR samples had low air permeability as compared to PVDF samples. This may be attributed to fiber diameter and web porosity of the samples.

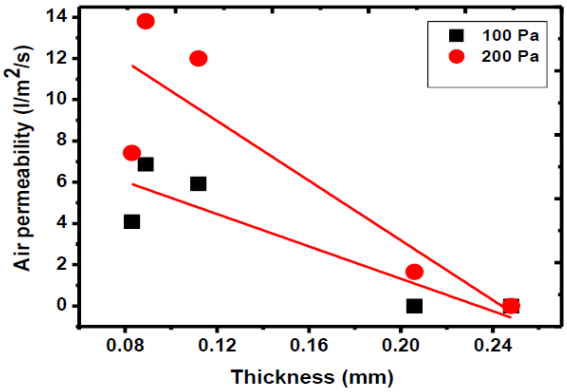

Pressure Pa	Equation y = a + b*x	Value	t-test Significance "Yes" or "No"	Adj. R-Square	F-test Significance "Yes" or "No"
100	**Intercept**	9.1614	Yes	0.7612	Yes
	Slope	-39.211	Yes		
200	**Intercept**	17.658	Yes	0.7158	Yes
	Slope	-72.383	Yes		

Figure 4. 38 Air permeability of PUR nanofibrous layer embedded with silica aerogel

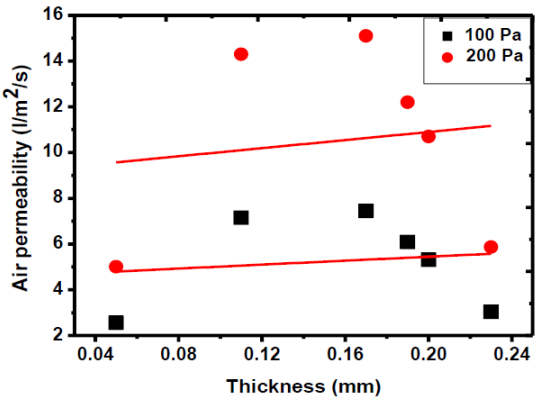

Pressure Pa	Equation y = a + b*x	Value	t-test Significance "Yes" or "No"	Adj. R-Square	F-test Significance "Yes" or "No"
100	**Intercept**	4.5821	Yes	-0.2259	Yes
	Slope	4.3132	Yes		
200	**Intercept**	9.1312	Yes	-0.2261	Yes
	Slope	8.8347	Yes		

Figure 4. 39 Air permeability of PVDF nanofibrous layer embedded with silica aerogel

4.7 Compression properties of multilayered fibrous materials

The compression resistance of multilayered fabrics under 560 gf/cm^2 pressure in terms of the percentage change in thickness, is shown in Figure 4. 40. Nonwoven-based materials with air pockets or aerogel generally have slightly lower compression resistance than regular samples. During the process of fabric compression, the inter-fiber spaces decrease continuously, the resistance force necessary to compress a fabric has to overcome the internal stresses of the fibers and the inter-fiber frictional force.[117] Thus, the compression resistance is closely related to fiber quantity, materials with less fibers have a lower compression resistance if the fiber arrangement of the fabrics are assumed to be the same. However, it is found that for foam-based materials the air pockets have insignificant effect on compression resistance while the encapsulated aerogel gives slightly increase to compression resistance. The reason could be that the deformed networks are easy to return back to their earlier position because of no fiber-to-fiber slippage and fiber entanglement happening during the process of compression.

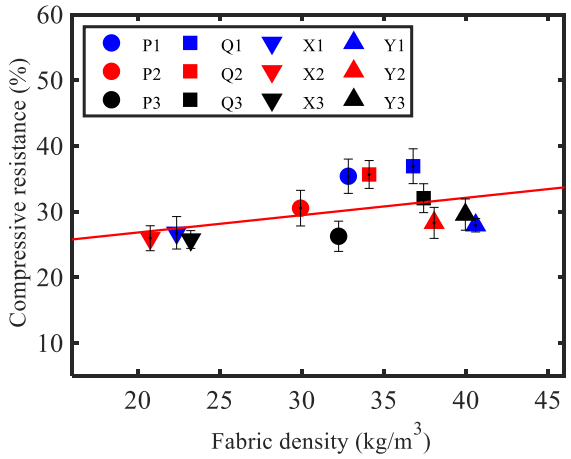

Equation y = a + b*x	Value	t-test Significance "Yes" or "No"	Adj. R-Square	F-test Significance "Yes" or "No"
Intercept	21.55	Yes	0.2063	Yes
Slope	0.2642	Yes		

Figure 4. 40 Compression resistance of multi-layered fibrous materials

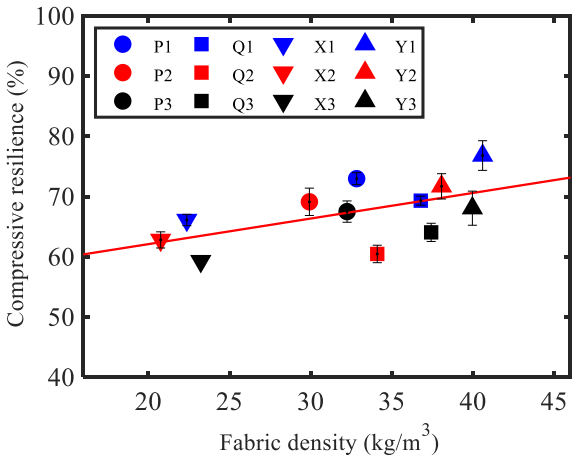

Equation y = a + b*x	Value	t-test Significance "Yes" or "No"	Adj. R-Square	F-test Significance "Yes" or "No"
Intercept	53.6	Yes	0.3267	Yes
Slope	0.425	Yes		

Figure 4. 41 Compressive resilience of different materials

The compression resilience values of regular materials, as shown in Figure 4. 41, are found to lie in the range of 66.11% -76.82%, samples with air pockets and encapsulated aerogel are observed to recover slightly less than regular structures. This may be attributed to the

fact that the amount of fibers per unit area of laser-engraved nonwovens is much lower, the compressive load will be shared by a fewer number of fibers, resulting in a stronger fiber-to-fiber slippage, fiber bending and fiber entanglement during the compression phase, this may lead to higher energy loss and reduced percentage compression resilience.[118] Results also indicates that the decrease in compression resilience induced by air pockets and aerogel-encapsulated structure are very small.

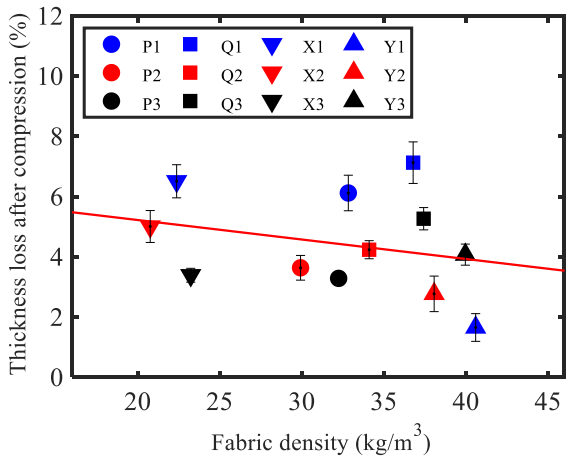

Equation y = a + b*x	Value	t-test Significance "Yes" or "No"	Adj. R-Square	F-test Significance "Yes" or "No"
Intercept	6.517	Yes	-0.01621	Yes
Slope	-0.06471	Yes		

Figure 4. 42 Thickness loss after compression test

Nonwoven materials with air pockets and encapsulated aerogel exhibit lower thickness loss in comparison with regular samples (as shown in Figure 4. 42), indicating these two kinds of nonwoven-based structures are able to maintain relatively higher thermal insulating ability after exposed to external forces. This is because during compression process all the fibers get compressed and trapped to each other, which will restrict the thickness recovery when the load is released. Thus, the percentage thickness loss is much higher in the case of regular structures. The sponge foam is in a reasonably consolidated state, with compression the material gets denser, resulting in better recovery after the compression pressure is released. However, this consolidated state may be partly destroyed by laser engraving treatment, which will reduce its ability to recover back to initial thickness. This is also reflected by the trend with compression resilience percentage.

Chapter 5 Summary and Conclusions

5.1 Summary

This research was an endeavor to study the thermal insulation behavior of fibrous materials embedded with silica aerogel. Based on the objectives set for this research, a detailed review was conducted on existing literature. The literature review provided necessary theoretical background, baseline data and insights into similar research conducted in the past. It assisted in understanding the gaps and limitations of the past research. The objectives were crystallized to add to this knowledgebase and also address a few of the identified gaps and limitations. The broad objectives of this research were to investigate the effect of aerogel and thermal adhesive on transport properties especially thermal properties of porous textile materials; to explore new techniques to develop aerogel-encapsulated fibrous structures; to conduct a comparative analysis of thermal and non-thermal properties of novel developed insulating materials; to study and analyze convective heat transfer through aerogel-embedded fibrous materials; to study transport behavior of electrospun PUR and PVDF nanofibrous layers embedded with silica aerogel.

Layered nanofibrous web/silica aerogel/ nonwoven materials were fabricated via laminating technique by using low-melting powder as thermal binding material. Aerogel-encapsulated fibrous materials were developed based on laser engraving and laminating technique to evaluate the effect of novel structures on thermal and compression performance. Moreover, electrospun nanofibrous layers embedded with silica aerogel was produced via electrospinning process. Thermal properties of these materials were characterized by means of different evaluation techniques. Air permeability and compressibility of selected samples were investigated as well. The data generated from the experiments were statistically analyzed and various conclusions were drawn based on the results.

5.2 Conclusions from the research

Thermal resistance of the layered fibrous material is directly proportional to aerogel content. Remarkably, the thermal adhesive powder used for combining aerogel particles with fibrous structure could cause considerable reduction in total thermal resistance. This indicated that novel techniques to combine silica aerogel with high porous textiles with

less use of binding materials should be considered. Meanwhile, the thermal resistance predicted by a series model showed a good agreement with the measured thermal resistance of the layered fibrous materials.

Results of the novel developed multilayered fibrous materials revealed that the aerogel-encapsulated samples demonstrated reduced thermal conductivity, significantly increased thermal resistance and coefficient of heat retention ability. The silica aerogel present in the fibrous structure plays an important role in contributing to the thermal performance of multilayered fibrous materials. The air pockets created by laser engraving could marginally improve the thermal performance as well. Meanwhile, thermal resistance and coefficient of heat retention ability were both strongly related to fabric thickness of the multilayered materials. Thermal properties measured by Alambeta device and KES-FT-II Thermolabo were well correlated, proving the accuracy of the measured data. Infrared thermography results showed that under infrared radiation the aerogel-encapsulated structure demonstrated lowest temperature, with 1- 1.5°C lower than regular samples when the temperature difference between hot plate and environment is 10 °C. Besides, Struto nonwoven based multilayered materials were observed to have lower temperature values in comparison with PU foam-based samples, which could be attributed to the lower fabric density and higher fabric thickness. Study of the compression properties of multilayered materials revealed that nonwoven materials with air pockets and aerogel-encapsulated structure exhibited slightly lower compression resistance and thickness loss after compression test. These materials could recover to a smaller extent than regular samples. However, air pockets and the aerogel present in PU foam-based multilayered materials showed insignificant effect on compression resistance.

Measurement of thermal behavior of selected aerogel-embedded fibrous materials by convection were performed on a laboratory-made device. In preheated conditions, it was found that a low airflow velocity gave a gentle temperature drop of the heating rod and fibrous insulator while a high velocity led to a rapid temperature decline and fairly high heat transfer rate. The multilayered fibrous materials with air pockets and aerogel-encapsulated structures exhibited significantly lower initial temperature. Aerogel-treated nonwoven fabrics with higher aerogel content and higher fabric thickness demonstrated better ability to prevent against heat loss from the preheated heating rod. The real-time temperature values of the heating rod and all the selected fibrous insulator were

exponentially related to the cooling time. In continuous heating conditions, the content of aerogel present in the fibrous structure and fabric thickness are very important factors in protecting against heat loss at high airflow velocity. The heating rod to air temperature difference and heat transfer coefficient were observed to increase with the increase in airflow velocity and Reynolds number. Aerogel-treated nonwoven fabrics with lower fabric thickness and aerogel content demonstrated lower temperature difference under convection. However, all the multilayered fabrics showed higher heat transfer rate in comparison with aerogel treated nonwoven fabrics. This could be attributed to the lower fabric density and permeable characteristic of the multilayered fibrous materials.

Study of nanofibrous membranes embedded with aerogel showed that the PVDF nanofibrous membranes had better thermal stability than PUR nanofibrous membranes. The glass transition and melting point was not affected by the aerogel content in the fibrous layers. The increase in duration of electrospinning leads to higher web thickness which results in considerable decrease in air permeability. Considerable improvement of thermal insulation was observed by increasing the number and the weight per unit area of nanofibrous membranes. The results confirmed the increase in thermal insulation by embedding silica aerogel in nanofibrous membranes.

5.3 Scope for future work

The ideas, experiments and data generated as part of this research, have added to the knowledgebase that could be useful to define the future direction and provide insightful references to researchers. The potential of this research can be realized by pursuing further studies into areas given below:

- Study convective heat transfer through aerogel-encapsulated fibrous materials by using Particle Image Velocimetry
- Use empirical models to evaluate effective thermal conductivity and overall thermal resistance of aerogel-encapsulated fibrous materials and compare with measured data
- Develop a numerical model for predicting the effective thermal conductivity of the aerogel-encapsulated fibrous materials
- Modeling and simulation of convective heat transfer phenomena in aerogel-embedded fibrous materials

Appendix

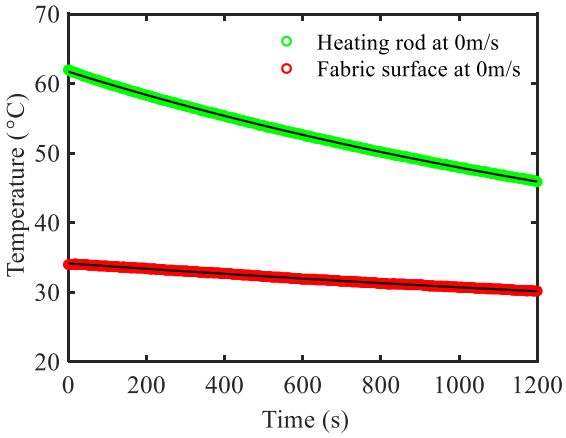

Exponential model Exp2: f(x) = a*exp(b*x) + c*exp(d*x)		
Airflow velocity 0m/s	Goodness of fit:	Coefficients (with 95% confidence bounds):
Heating rod	SSE: 2.278 R-square: 1 Adj. R-square: 1 RMSE: 0.04715	a = 28.98 (28.38, 29.57) b = -0.0005575 (-0.0005656, -0.0005494) c = 32.76 (32.16, 33.36) d = -4.367e-05 (-4.698e-05, -4.036e-05)
Fabric	SSE: 1.769 R-square: 0.9997 Adj. R-square: 0.9997 RMSE: 0.04155	a = 28.76 (27.87, 29.64) b = -0.0001736 (-0.0001814, -0.0001657) c = 5.41 (4.521, 6.298) d = 0.000192 (0.0001692, 0.0002148)

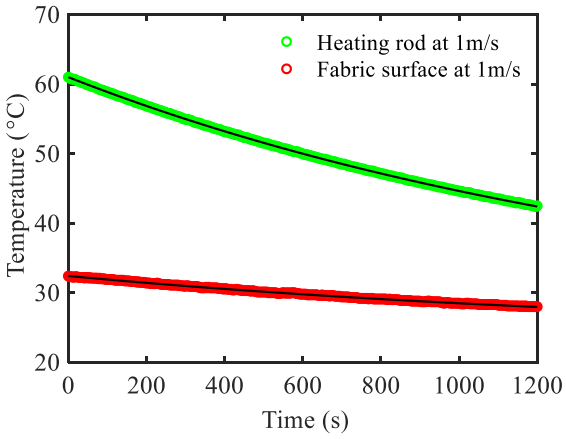

Exponential model Exp2: f(x) = a*exp(b*x) + c*exp(d*x)		
Airflow velocity 1m/s	Goodness of fit:	Coefficients (with 95% confidence bounds):
Heating rod	SSE: 0.8357 R-square: 1 Adjusted R-square: 1	a = 30.33 (28.93, 31.73) b = -0.0006776 (-0.0006976, -0.0006577) c = 30.67 (29.26, 32.07)

	RMSE: 0.03714	d = -4.803e-05 (-5.911e-05, -3.695e-05)
Fabric	SSE: 1.221 R-square: 0.9993 Adj. R-square: 0.9993 RMSE: 0.04488	a = 9.232 (7.366, 11.1) b = -0.0005879 (-0.0006693, -0.0005066) c = 23.18 (21.31, 25.06) d = 7.763e-06 (-1.089e-05, 2.642e-05)

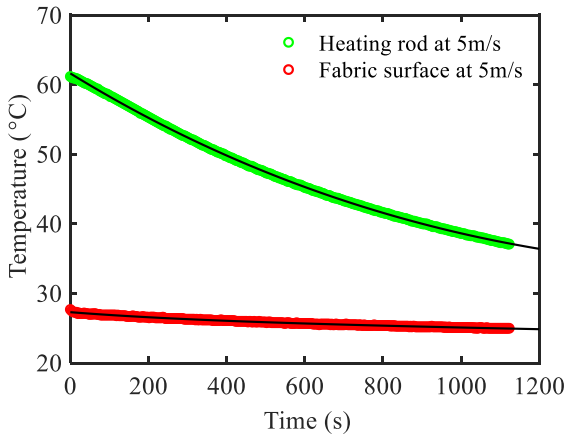

Exponential model Exp2: f(x) = a*exp(b*x) + c*exp(d*x)		
Airflow velocity 5m/s	Goodness of fit:	Coefficients (with 95% confidence bounds):
Heating rod	SSE: 2.63 R-square: 0.9999 Adj. R-square: 0.9999 RMSE: 0.08694	a = 57.71 (56.46, 58.96) b = -0.0006516 (-0.0006763, -0.0006268) c = 3.927 (2.652, 5.202) d = 0.0007799 (0.0006178, 0.0009419)
Fabric	SSE: 0.8072 R-square: 0.9946 Adj. R-square: 0.9945 RMSE: 0.04816	a = 1.211 (0.9935, 1.429) b = -0.00273 (-0.003267, -0.002193) c = 26.1 (25.87, 26.33) d = -4.194e-05 (-4.869e-05, -3.519e-05)

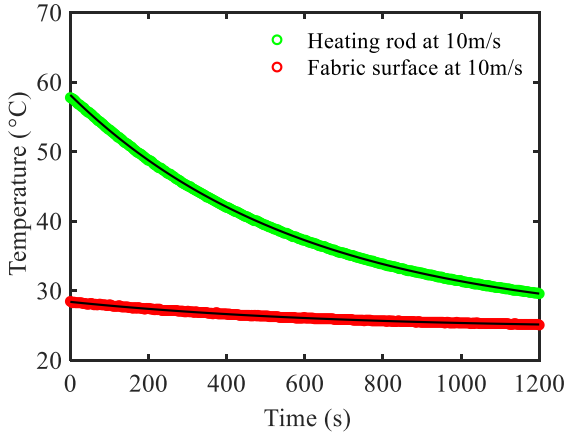

Exponential model Exp2: f(x) = a*exp(b*x) + c*exp(d*x)		
Airflow velocity 10m/s	Goodness of fit:	Coefficients (with 95% confidence bounds):
Heating rod	SSE: 1.713 R-square: 1	a = 32.21 (32, 32.43) b = -0.001705 (-0.001717, -0.001692)

	Adjusted R-square: 1 RMSE: 0.05611	c = 25.96 (25.74, 26.19) d = -1.658e-05 (-2.077e-05, -1.238e-05)
Fabric	SSE: 0.8502 R-square: 0.9984 Adj. R-square: 0.9984 RMSE: 0.03953	a = 4.574 (4.317, 4.832) b = -0.001335 (-0.001407, -0.001264) c = 23.86 (23.59, 24.12) d = 1.393e-05 (9.212e-06, 1.865e-05)
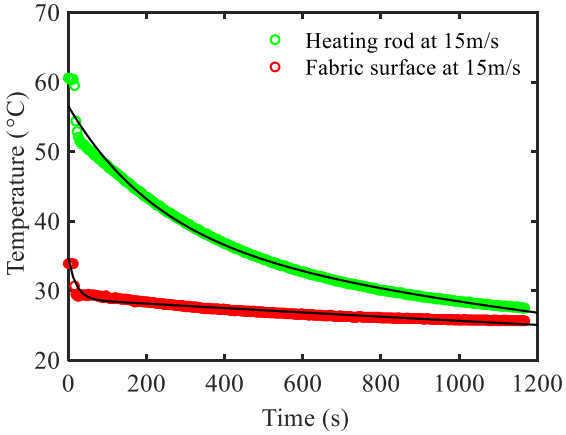		
Exponential model Exp2: f(x) = a*exp(b*x) + c*exp(d*x)		
Airflow velocity 15m/s	Goodness of fit:	Coefficients (with 95% confidence bounds):
Heating rod	SSE: 205.7 R-square: 0.9901 Adj. R-square: 0.99 RMSE: 0.7538	a = 19.73 (18.38, 21.08) b = -0.004336 (-0.004783, -0.00389) c = 36.82 (35.32, 38.33) d = -0.0002662 (-0.0003046, -0.0002279)
Fabric	SSE: 40.56 R-square: 0.9426 Adj. R-square: 0.9421 RMSE: 0.3347	a = 5.945 (5.489, 6.4) b = -0.05046 (-0.05683, -0.0441) c = 28.81 (28.73, 28.9) d = -0.000115 (-0.0001192, -0.0001108)

Figure I. Real-time temperature curves of the heating rod and aerogel-treated nonwoven fabric B1

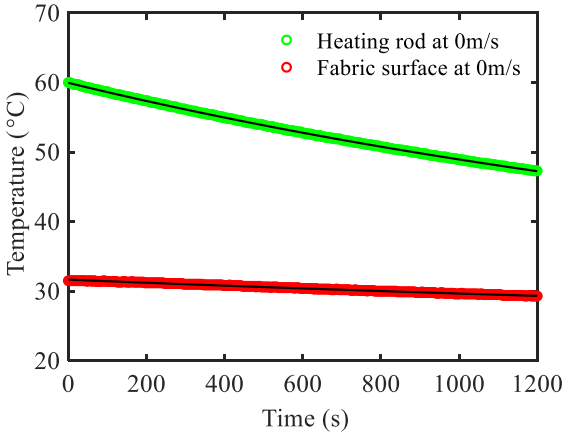

Exponential model Exp2: f(x) = a*exp(b*x) + c*exp(d*x)		
Airflow velocity 0m/s	Goodness of fit:	Coefficients (with 95% confidence bounds):
Heating rod	SSE: 1.505 R-square: 1 Adjusted R-square: 1 RMSE: 0.03741	a = 21.69 (21.17, 22.2) b = -0.0005298 (-0.0005383, -0.0005212) c = 38.26 (37.74, 38.78) d = -5.632e-05 (-5.862e-05, -5.403e-05)
Fabric	SSE: 1.97 R-square: 0.9991 Adj. R-square: 0.9991 RMSE: 0.04281	a = 14.65 (11.26, 18.04) b = -0.000199 (-0.0002328, -0.0001652) c = 17.01 (13.61, 20.41) d = 3.726e-05 (1.768e-05, 5.684e-05)

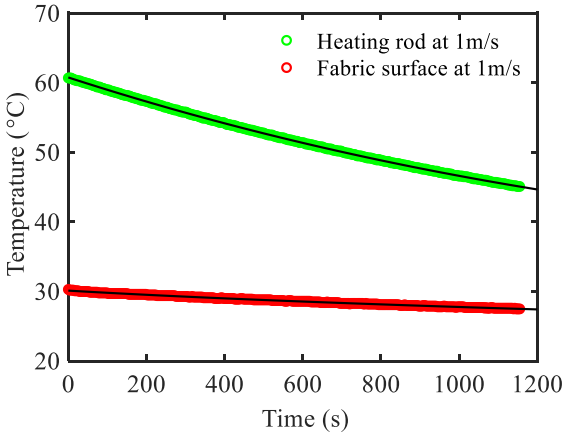

Exponential model Exp2: f(x) = a*exp(b*x) + c*exp(d*x)		
Airflow velocity 1m/s	Goodness of fit:	Coefficients (with 95% confidence bounds):
Heating rod	SSE: 0.526 R-square: 0.9999 Adj. R-square: 0.9999 RMSE: 0.03833	a = 53.66 (49.77, 57.54) b = -0.0003868 (-0.0004207, -0.0003528) c = 7.116 (3.221, 11.01) d = 0.0003582 (0.0001916, 0.0005249)
Fabric	SSE: 0.6085	a = 1.056 (0.3537, 1.759)

	R-square: 0.997 Adj. R-square: 0.997 RMSE: 0.04123	b = -0.001612 (-0.002442, -0.0007824) c = 29.07 (28.36, 29.78) d = -5.317e-05 (-6.637e-05, -3.996e-05)
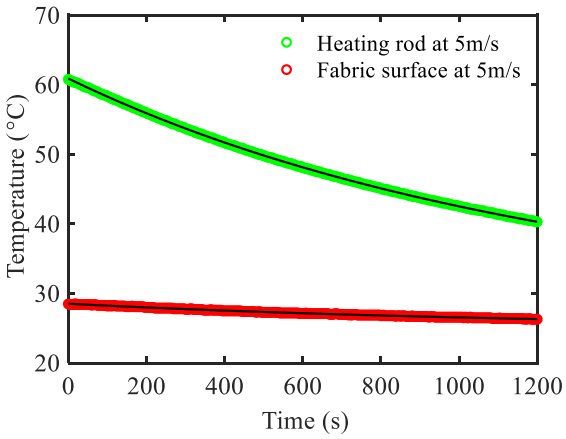		
Exponential model Exp2: f(x) = a*exp(b*x) + c*exp(d*x)		
Airflow velocity 5m/s	Goodness of fit:	Coefficients (with 95% confidence bounds):
Heating rod	SSE: 0.9474 R-square: 1 Adjusted R-square: 1 RMSE: 0.04331	a = 24.76 (23.58, 25.94) b = -0.000973 (-0.001004, -0.0009424) c = 36.15 (34.96, 37.34) d = -8.609e-05 (-9.683e-05, -7.535e-05)
Fabric	SSE: 0.7264 R-square: 0.9974 Adj. R-square: 0.9974 RMSE: 0.03793	a = 2.847 (1.998, 3.695) b = -0.0009403 (-0.001146, -0.0007343) c = 25.68 (24.83, 26.54) d = -9.18e-06 (-2.045e-05, 2.087e-06)
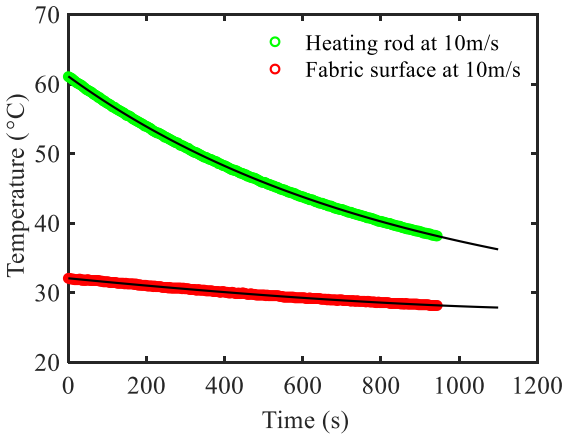		
Exponential model Exp2: f(x) = a*exp(b*x) + c*exp(d*x)		
Airflow velocity 10m/s	Goodness of fit:	Coefficients (with 95% confidence bounds):
Heating rod	SSE: 0.4331 R-square: 1 Adjusted R-square: 1 RMSE: 0.03851	a = 28.48 (26.16, 30.8) b = -0.001333 (-0.001402, -0.001265) c = 32.66 (30.33, 34.99) d = -8.66e-05 (-0.000121, -5.221e-05)

Fabric	SSE: 0.5659 R-square: 0.9985 Adj. R-square: 0.9985 RMSE: 0.04402	a = 31.34 (30.31, 32.36) b = -0.0002044 (-0.0002384, -0.0001705) c = 0.7655 (-0.2709, 1.802) d = 0.001201 (0.000504, 0.001898)
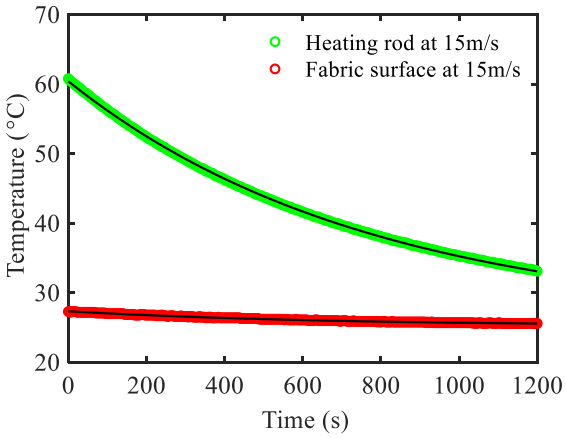		
Exponential model Exp2: f(x) = a*exp(b*x) + c*exp(d*x)		
Airflow velocity 15m/s	Goodness of fit:	Coefficients (with 95% confidence bounds):
Heating rod	SSE: 8.851 R-square: 0.9999 Adj. R-square: 0.9999 RMSE: 0.08277	a = 34.21 (34.15, 34.26) b = -0.001311 (-0.001314, -0.001307) c = 26.22 (26.16, 26.27) d = -6.981e-06 (-7.601e-06, -6.362e-06)
Fabric	SSE: 1.33 R-square: 0.9947 Adj. R-square: 0.9947 RMSE: 0.03208	a = 2.389 (2.371, 2.406) b = -0.00138 (-0.001401, -0.001359) c = 24.96 (24.94, 24.98) d = 5.65e-06 (5.426e-06, 5.874e-06)

Figure II. Real-time temperature curves of the heating rod and aerogel-treated nonwoven fabric B2

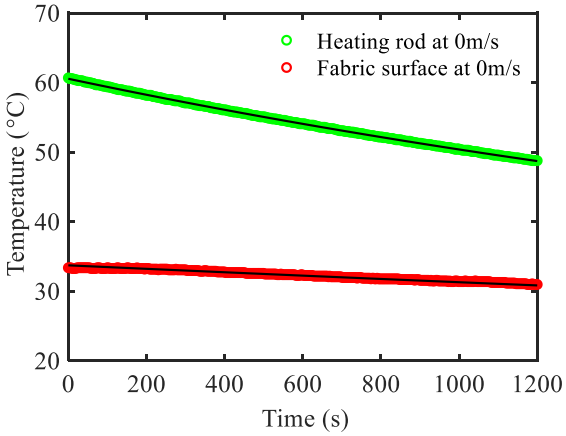
Exponential model Exp2: f(x) = a*exp(b*x) + c*exp(d*x)

Airflow velocity 0m/s	Goodness of fit:	Coefficients (with 95% confidence bounds):
Heating rod	SSE: 1.567 R-square: 1 Adjusted R-square: 1 RMSE: 0.04083	a = 37.82 (35.57, 40.06) b = -0.000317 (-0.0003292, -0.0003047) c = 22.76 (20.5, 25.01) d = 4.692e-06 (-8.107e-06, 1.749e-05)
Fabric	SSE: 12.62 R-square: 0.9959 Adj. R-square: 0.9958 RMSE: 0.1159	a = 33.75 (33.73, 33.77) b = -7.497e-05 (-7.579e-05, -7.414e-05) c = 0.001245 (0.0002144, 0.002276) d = 0.002233 (0.001966, 0.002501)

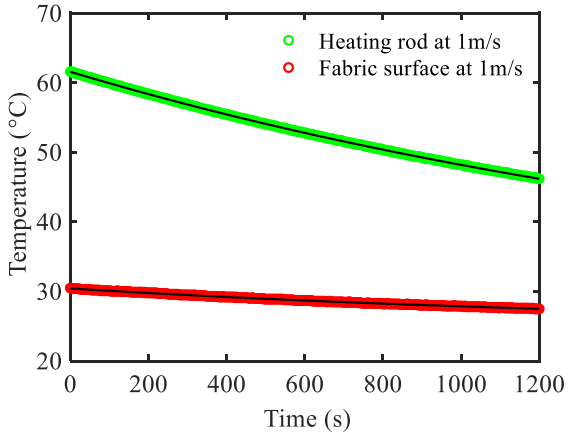

Exponential model Exp2: f(x) = a*exp(b*x) + c*exp(d*x)

Airflow velocity 1m/s	Goodness of fit:	Coefficients (with 95% confidence bounds):
Heating rod	SSE: 1.45 R-square: 1 Adjusted R-square: 1 RMSE: 0.03797	a = 28.89 (28.31, 29.48) b = -0.0005323 (-0.0005397, -0.0005249) c = 32.69 (32.1, 33.28) d = -4.568e-05 (-4.885e-05, -4.252e-05)
Fabric	SSE: 1.307 R-square: 0.9993 Adj. R-square: 0.9993 RMSE: 0.03604	a = 3.93 (3.759, 4.101) b = -0.0007662 (-0.0007969, -0.0007354) c = 26.51 (26.33, 26.68) d = -1.79e-05 (-1.945e-05, -1.634e-05)

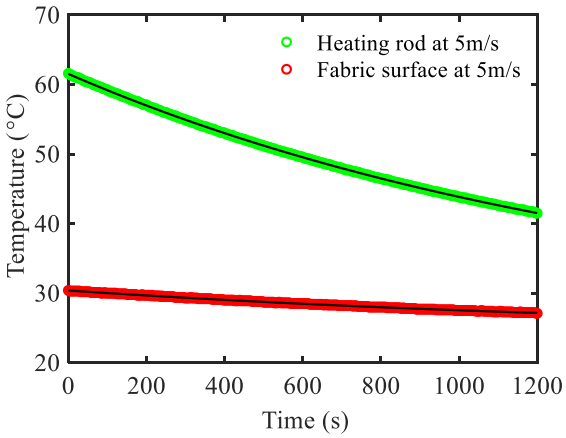

Exponential model Exp2: f(x) = a*exp(b*x) + c*exp(d*x)		
Airflow velocity 5m/s	Goodness of fit:	Coefficients (with 95% confidence bounds):
Heating rod	SSE: 1.939 R-square: 1 Adjusted R-square: 1 RMSE: 0.03898	a = 34.58 (34.46, 34.69) b = -0.0006893 (-0.0006917, -0.0006869) c = 26.95 (26.82, 27.07) d = -1.734e-05 (-1.826e-05, -1.642e-05)
Fabric	SSE: 1.573 R-square: 0.9995 Adj. R-square: 0.9995 RMSE: 0.03511	a = 6.525 (6.39, 6.659) b = -0.0005991 (-0.0006111, -0.0005871) c = 23.86 (23.72, 24) d = 3.983e-06 (2.896e-06, 5.069e-06)

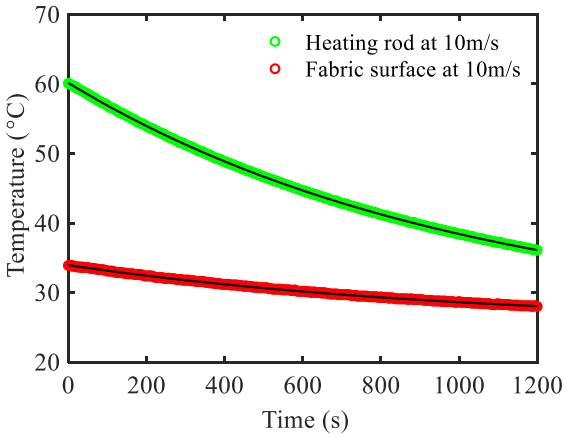

Exponential model Exp2: f(x) = a*exp(b*x) + c*exp(d*x)		
Airflow velocity 10m/s	Goodness of fit:	Coefficients (with 95% confidence bounds):
Heating rod	SSE: 1.873 R-square: 1 Adjusted R-square: 1 RMSE: 0.03793	a = 34.81 (34.77, 34.85) b = -0.0009812 (-0.000983, -0.0009795) c = 25.34 (25.29, 25.38) d = 1.739e-06 (1.303e-06, 2.175e-06)
Fabric	SSE: 1.804 R-square: 0.9997 Adj. R-square: 0.9997	a = 8.83 (8.787, 8.873) b = -0.0009516 (-0.0009583, -0.0009449) c = 25.12 (25.07, 25.17)

	RMSE: 0.03722	d = 3.839e-06 (3.389e-06, 4.29e-06)
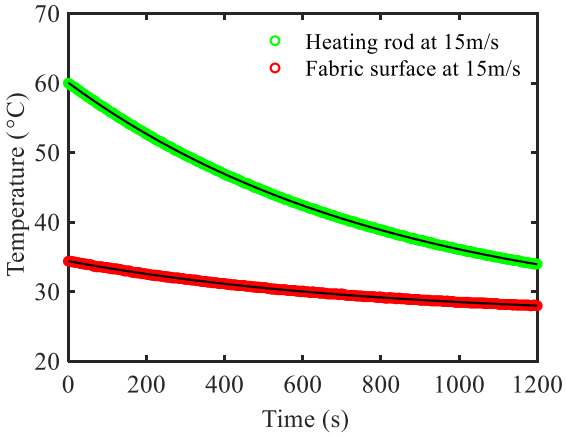		
Exponential model Exp2: f(x) = a*exp(b*x) + c*exp(d*x)		
Airflow velocity 15m/s	Goodness of fit:	Coefficients (with 95% confidence bounds):
Heating rod	SSE: 1.368 R-square: 1 Adj. R-square: 1 RMSE: 0.0396	a = 33.98 (33.9, 34.06) b = -0.001224 (-0.001227, -0.00122) c = 26.09 (26, 26.18) d = 1.155e-06 (5.777e-08, 2.252e-06)
Fabric	SSE: 1.161 R-square: 0.9997 Adj. R-square: 0.9997 RMSE: 0.03649	a = 8.247 (8.178, 8.316) b = -0.001265 (-0.001278, -0.001251) c = 26.16 (26.09, 26.24) d = 1.305e-06 (3.541e-07, 2.256e-06)

Figure 1. Real-time temperature curves of the heating rod and aerogel-treated nonwoven fabric B3

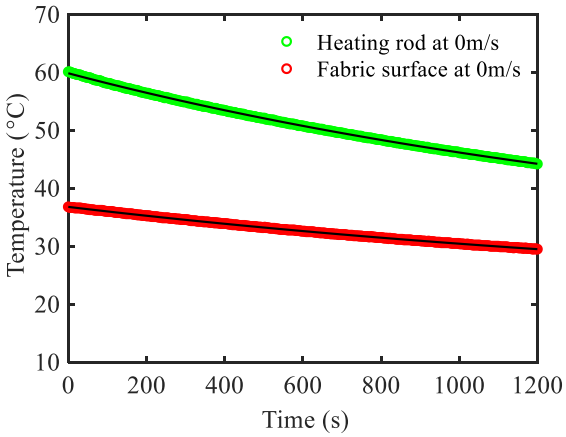		
Exponential model Exp2: f(x) = a*exp(b*x) + c*exp(d*x)		
Airflow velocity 0m/s	Goodness of fit:	Coefficients (with 95% confidence bounds):

Heating rod	SSE: 3.789 R-square: 1 Adjusted R-square: 1 RMSE: 0.05013	a = 29.46 (29.31, 29.62) b= -0.0005782(-0.0005811, -0.0005753) c = 28.38 (28.21, 28.54) d = -2.608e-05 (-2.703e-05, -2.513e-05)
Fabric	SSE: 1.955 R-square: 0.9999 Adj. R-square: 0.9999 RMSE: 0.03601	a = 15.65 (15.51, 15.8) b = -0.0004989 (-0.0005031, -0.0004946) c = 24.63 (24.48, 24.78) d = -8.207e-06 (-9.14e-06, -7.273e-06)

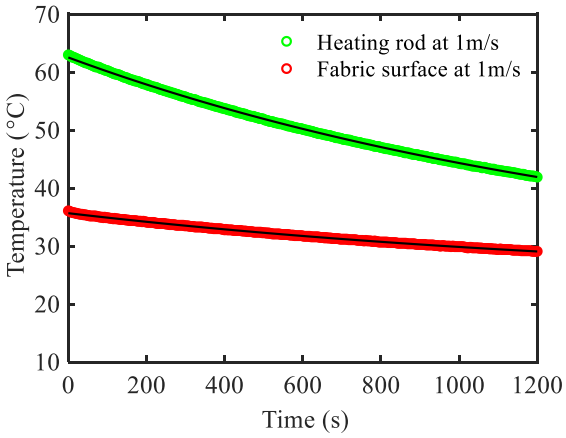

Exponential model Exp2: f(x) = a*exp(b*x) + c*exp(d*x)		
Airflow velocity 1m/s	Goodness of fit:	Coefficients (with 95% confidence bounds):
Heating rod	SSE: 7.212 R-square: 1 Adjusted R-square: 1 RMSE: 0.06548	a = 35.98 (35.89, 36.07) b = -0.0006773 (-0.0006795, -0.0006751) c = 26.56 (26.46, 26.67) d = -1.914e-05 (-1.981e-05, -1.847e-05)
Fabric	SSE: 2.739 R-square: 0.9998 Adj. R-square: 0.9998 RMSE: 0.04035	a = 12.09 (12.03, 12.15) b = -0.0006491 (-0.000653, -0.0006452) c = 23.59 (23.53, 23.65) d = -2.093e-06 (-2.546e-06, -1.64e-06)

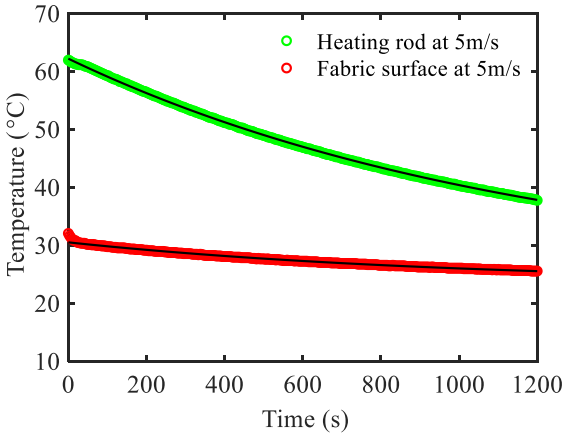

Exponential model Exp2: f(x) = a*exp(b*x) + c*exp(d*x)		
Airflow velocity	Goodness of fit:	Coefficients (with 95% confidence bounds):

5m/s		
Heating rod	SSE: 9.001 R-square: 0.9999 Adj. R-square: 0.9999 RMSE: 0.06829	a = 38 (37.97, 38.04) b = -0.0008471 (-0.0008486, -0.0008455) c = 24.24 (24.19, 24.28) d = -3.845e-06 (-4.163e-06, -3.526e-06)
Fabric	SSE: 9.252 R-square: 0.9982 Adj. R-square: 0.9982 RMSE: 0.06924	a = 7.152 (7.124, 7.18) b = -0.001002 (-0.00101, -0.0009938) c = 23.4 (23.37, 23.43) d = 1.338e-06 (1.082e-06, 1.595e-06)
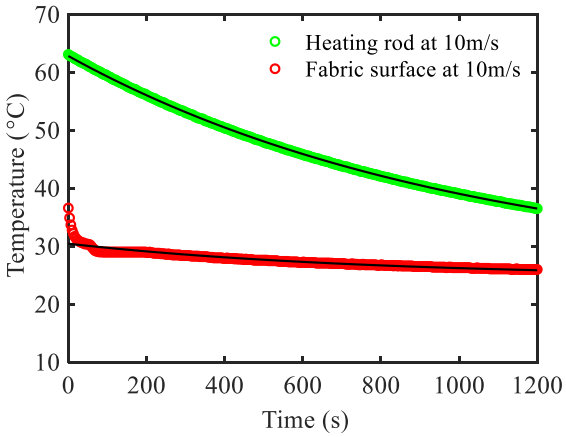		
Exponential model Exp2: f(x) = a*exp(b*x) + c*exp(d*x)		
Airflow velocity 10m/s	Goodness of fit:	Coefficients (with 95% confidence bounds):
Heating rod	SSE: 7.259 R-square: 1 Adjusted R-square: 1 RMSE: 0.05933	a = 37.92 (37.9, 37.94) b = -0.0009802 (-0.0009815, -0.000979) c = 24.9 (24.88, 24.93) d = -2.936e-06 (-3.116e-06, -2.755e-06)
Fabric	SSE: 107.1 R-square: 0.9694 Adj. R-square: 0.9693 RMSE: 0.228	a = 5.653 (5.584, 5.722) b = -0.001325 (-0.001362, -0.001288) c = 24.79 (24.73, 24.85) d = -2.604e-06 (-3.098e-06, -2.11e-06)
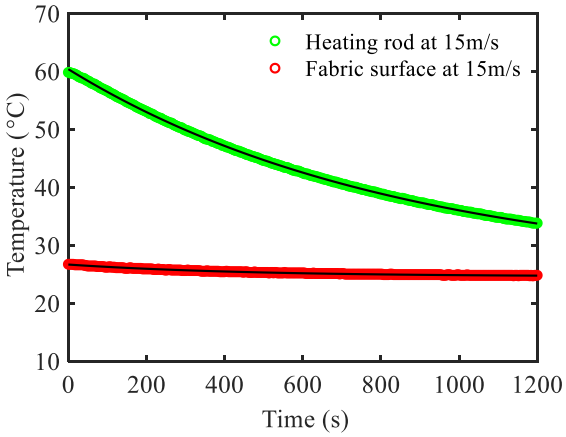		
Exponential model Exp2: f(x) = a*exp(b*x) + c*exp(d*x)		

Airflow velocity 15m/s	Goodness of fit:	Coefficients (with 95% confidence bounds):
Heating rod	SSE: 205.7 R-square: 0.9901 Adj. R-square: 0.99 RMSE: 0.7538	a = 19.73 (18.38, 21.08) b = -0.004336 (-0.004783, -0.00389) c = 36.82 (35.32, 38.33) d = -0.0002662 (-0.0003046, -0.0002279)
Fabric	SSE: 0.9868 R-square: 0.995 Adj. R-square: 0.9949 RMSE: 0.03608	a = 2.05 (2.02, 2.08) b = -0.002179 (-0.002239, -0.002119) c = 24.7 (24.66, 24.73) d = -4.265e-07 (-1.068e-06, 2.153e-07)

Figure IV. Real-time temperature curves of the heating rod and multilayered fibrous material Q1

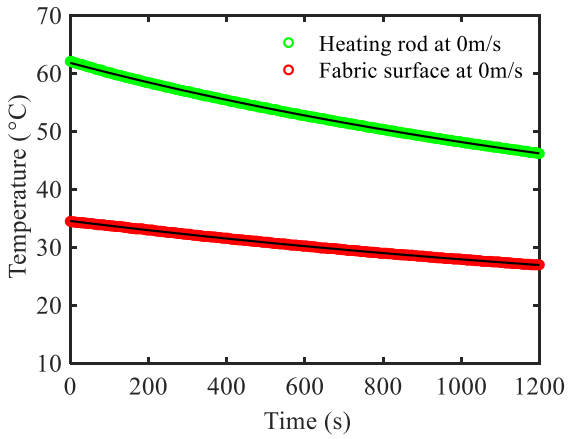

Exponential model Exp2: f(x) = a*exp(b*x) + c*exp(d*x)		
Airflow velocity 0m/s	Goodness of fit:	Coefficients (with 95% confidence bounds):
Heating rod	SSE: 3.886 R-square: 1 Adjusted R-square: 1 RMSE: 0.05021	a = 7.142 (7.058, 7.227) b = -0.8214 (-0.8254, -0.8174) c = 26.54 (26.45, 26.63) d = -0.03604 (-0.03732, -0.03476)
Fabric	SSE: 2.157 R-square: 0.9999 Adj. R-square: 0.9999 RMSE: 0.03744	a = 5.005 (4.912, 5.097) b = -0.6974 (-0.7031, -0.6918) c = 23.96 (23.86, 24.05) d = -0.009041 (-0.01038, -0.007699)

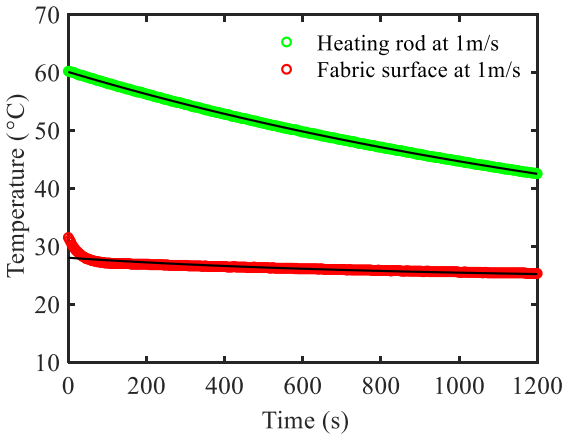

Exponential model Exp2: f(x) = a*exp(b*x) + c*exp(d*x)		
Airflow velocity 1m/s	Goodness of fit:	Coefficients (with 95% confidence bounds):
Heating rod	SSE: 2.672 R-square: 1 Adjusted R-square: 1 RMSE: 0.04366	a = 9.089 (8.997, 9.181) b = -0.7599 (-0.7631, -0.7566) c = 25.37 (25.28, 25.47) d = -0.02103 (-0.02239, -0.01967)
Fabric	SSE: 65.27 R-square: 0.9602 Adj. R-square: 0.9601 RMSE: 0.2158	a = 0.1157 (0.08569, 0.1458) b = -1.867 (-2.005, -1.729) c = 24.42 (24.38, 24.47) d = -0.01769 (-0.01925, -0.01613)

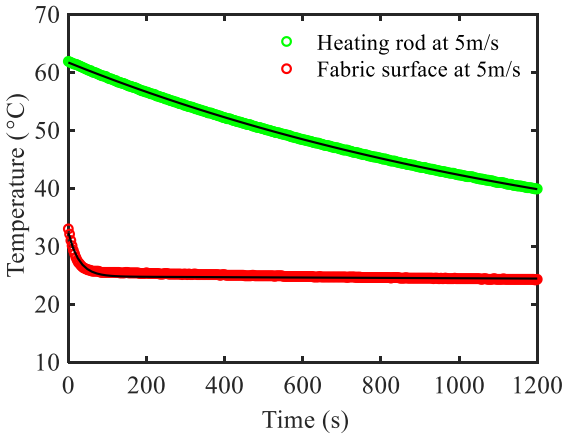

Exponential model Exp2: f(x) = a*exp(b*x) + c*exp(d*x)		
Airflow velocity 5m/s	Goodness of fit:	Coefficients (with 95% confidence bounds):
Heating rod	SSE: 2.764 R-square: 1 Adjusted R-square: 1 RMSE: 0.04435	a = 7.39 (7.343, 7.437) b = -0.9403 (-0.9427, -0.9378) c = 23.99 (23.94, 24.03) d = -0.00272 (-0.003663, -0.001777)
Fabric	SSE: 106.7 R-square: 0.8383 Adj. R-square: 0.838	a = 1.412e-13 (-1.609e-13, 4.434e-13) b = -18.01 (-19.27, -16.76) c = 24.08 (24.06, 24.09)

	RMSE: 0.2756	d = -0.01394 (-0.0146, -0.01328)
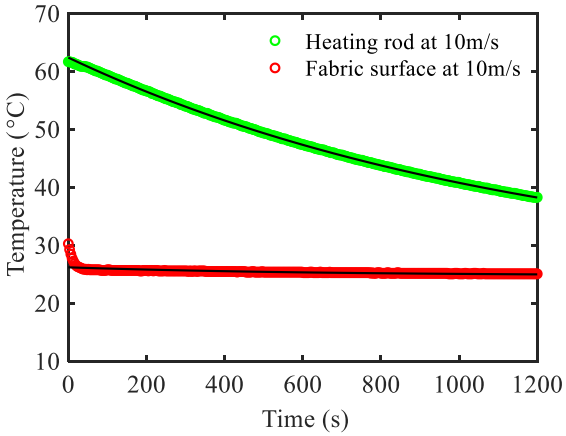		
Exponential model Exp2: f(x) = a*exp(b*x) + c*exp(d*x)		
Airflow velocity 10m/s	Goodness of fit:	Coefficients (with 95% confidence bounds):
Heating rod	SSE: 8.415 R-square: 0.9999 Adj. R-square: 0.9999 RMSE: 0.06826	a = 3.376 (3.356, 3.395) b = -1.401 (-1.404, -1.399) c = 24.4 (24.37, 24.42) d = 0.003664 (0.003025, 0.004303)
Fabric	SSE: 43.62 R-square: 0.8191 Adj. R-square: 0.8188 RMSE: 0.1554	a = 0.01309 (0.008036, 0.01814) b = -2.687 (-2.909, -2.466) c = 24.75 (24.73, 24.76) d = -0.002574 (-0.003217, -0.001931)
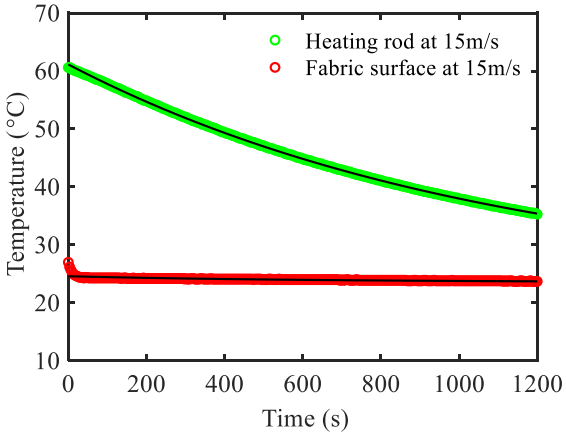		
Exponential model Exp2: f(x) = a*exp(b*x) + c*exp(d*x)		
Airflow velocity 15m/s	Goodness of fit:	Coefficients (with 95% confidence bounds):
Heating rod	SSE: 6.251 R-square: 0.9999 Adj. R-square: 0.9999 RMSE: 0.07275	a = 7.205 (7.135, 7.276) b = -0.9831 (-0.987, -0.9791) c = 22.13 (22.05, 22.2) d = 0.01217 (0.01053, 0.01381)
Fabric	SSE: 13.42 R-square: 0.8993	a = 0.01861 (0.008758, 0.02847) b = -2.154 (-2.447, -1.862)

	Adj. R-square: 0.8991 RMSE: 0.1066	c = 23.53 (23.51, 23.55) d = -0.007066 (-0.007789, -0.006342)

Figure V. Real-time temperature curves of the heating rod and multilayered fibrous material Q2

References

1. Rosace, G., Guido, E., Colleoni, C. and Barigozzi, G. (2016). Influence of textile structure and silica-based finishing on thermal insulation properties of cotton fabrics. International Journal of Polymer Science.
2. Shaid, A., Fergusson, M. and Wang, L. (2014). Thermo-physiological comfort analysis of aerogel nanoparticle incorporated fabric for fire fighter's protective clothing. Chemical and Materials Engineering, 2(2), 37-43.
3. Ziaei, M., & Ghane, M. (2013). Thermal insulation property of spacer fabrics integrated by ceramic powder impregnated fabrics. Journal of Industrial Textiles, 43(1), 20-33.
4. Venkataraman, M., Mishra, R., Militky, J. and Behera, B. K. (2017). Modelling and simulation of heat transfer by convection in aerogel treated nonwovens. The Journal of The Textile Institute, 108(8), 1442-1453.
5. Venkataraman, M., Mishra, R. and Militky, J. (2018). Unconventional measurement methods and simulation of aerogel assisted thermoregulation. Journal of Mechanical Engineering, 5(5), 62-96.
6. Hager, N. E., and Steere. R. C. (1967). Radiant heat transfer in fibrous thermal insulation. Journal of Applied Physics, 38, 4663- 4668.
7. Strong, H. M., Bundy, F. P., and Bovenkerk, H. P. (1960). Flat panel vacuum thermal insulation. Journal of Applied Physics, 31, 39-50.
8. Daryabeigi, K. (2002). Thermal analysis and design optimization of multilayer insulation for reentry aerodynamic heating. Journal of Spacecraft and Rockets, 39(4), 509-513.
9. Daryabeigi, K. (2003). Heat transfer in high-temperature fibrous insulation. Journal of Thermophysics and Heat Transfer, 17(1), 10-19.
10. Doggett, M. S. and Brunjes R. F. (2016). Simulation of convective heat loss through mineral wool in a rainscreen façade, 1-20.
11. Powell, F., Krarti, M. and Tuluca, A. (1989). Air movement influence on the effective thermal resistance of porous insulations: a literature survey. Journal of Thermal Insulation, 12(3), 239-251.
12. Martin, J. R. (1987). Measurement of thermal conductivity of nonwovens using a dynamic method. Textile Research Journal, 57(12), 721-727.

13. Tien, C.L. and Cunnington, G.R. (1973). Cryogenic insulation heat transfer. Advances in Heat Transfer, 9, 349-417.
14. Lu, X., Caps, R., Fricke, J., Alviso, C. T., & Pekala, R. W. (1995). Correlation between structure and thermal conductivity of organic aerogels. Journal of Non-Crystalline Solids, 188(3), 226-234.
15. Simmler, H., Brunner, S. and Heinemann, U. et al. (2005). Study on VIP components and panels for service life prediction of VIP in building applications (Subtask A). Technical Report, IEA/ECBCS Annex 39 HiPTI-project (High Performance Thermal Insulation for Buildings and Building Systems).
16. Arenas, J. P., Crocker, M.J. (2010). Recent trends in porous sound-absorbing materials. Sound & Vibration, 12-17.
17. Venkataraman, M., Mishra, R., Jasikova, D., Kotresh, T. and Militky, J. (2015). Thermodynamics of aerogel-treated nonwoven fabrics at subzero temperatures. Journal of Industrial Textiles, 45(3), 387-404.
18. Jirsak, O., Sadikoglu, T. G., Ozipek, B. and Pan, N. (2000). Thermo-insulating properties of perpendicular-laid versus cross-laid lofty nonwoven fabrics. Textile Research Journal, 70(2), 121-128.
19. Reneker, D. H. and Yarin, A. L. (2008). Electrospinning jets and polymer nanofibers. Polymer, 49(10), 2387-2425.
20. Li, D., McCann, J. T., Xia, Y. and Marquez, M. (2006). Electrospinning: a simple and versatile technique for producing ceramic nanofibers and nanotubes. Journal of the American Ceramic Society, 89(6), 1861-1869.
21. Greiner, A. and Wendorff, J. H. (2007). Electrospinning: a fascinating method for the preparation of ultrathin fibers. Angewandte Chemie, 46(30), 5670-5703.
22. Wang, C., Yan, E., Huang, Z., Zhao, Q., and Xin, Y. (2007). Fabrication of Highly Photoluminescent TiO2/PPV Hybrid Nanoparticle-Polymer Fibers by Electrospinning. Macromolecular Rapid Communications, 28(2), 205-209.
23. Faccini, M., Vaquero, C., and Amantia, D. (2012). Development of protective clothing against nanoparticle based on electrospun nanofibers. Journal of Nanomaterials, 9 pages, doi:10.1155/2012/892894.
24. Gibson, P. and Lee, C. (2007). Application of nanofiber technology to nonwoven thermal insulation. Journal of Engineered Fibers and Fabrics, 2(2), 32-39.

25. Nasouri, K., Shoushtari, A. M. and Haji, A. The Role of Nanofibers Diameter in the enhanced thermal conductivity of electrospun nanofibers. The 6th Texteh International Conference, Bucharest, Romania, Oct 17-18, 2013.
26. Wu, H., Chen, Y., Chen, Q., Ding, Y., Zhou, X. and Gao, H. (2013). Synthesis of flexible aerogel composites reinforced with electrospun nanofibers and microparticles for thermal insulation. Journal of Nanomaterials, Article ID 375093, 8 pages.
27. Ller, R.K. (1980). The Chemistry of Silica-solubility, polymerization, colloid and surface properties, and biochemistry. Angewandte Chemie, 92(4), 328.
28. Valdes-Solis, T. and Fuertes, A. B. (2006). High-surface area inorganic compounds prepared by nanocasting techniques. Materials Research Bulletin, 41(12), 2187-2197.
29. Maleki, H., Durães, L., Portugal, A. (2014). An overview on silica aerogels synthesis and different mechanical reinforcing strategies. Journal of Non-Crystalline Solids, 385, 55-74.
30. Pierre, A. C. and Pajonk, G. M. (2002). Chemistry of aerogels and their applications, 102(11), 243-4265.
31. Mulder, C. A. M. and Lierop, J. G. (1986). Preparation, densification and characterization of autoclave dried SiO2 gels, Berlin, Germany, pp. 68-75.
32. Hrubesh, L. W. (1990). Aerogels: the world's lightest solids. Chemistry and Industry, 24, 824-827.
33. Woignier, T., Reynes, J., Hafidi Alaoui, A., Beurroies, I. and Phalippou, J. (1998). Different kinds of structure in aerogels: relationships with the mechanical properties. Journal of Non-Crystalline Solids, 241(1), 45-52.
34. Lu, H., Luo, H. and Leventis, N. (2011). Mechanical characterization of aerogels, Aerogel Handbook, pp. 499-535, Springer, New York, NY, USA.
35. Mazraehshahi, Z. T. and Shoushtari A.M. (2014). Synthesis, structure and thermal protective behavior of silica aerogel/PET nonwoven Fiber composite. Journal of Fibers and Polymers, 15, 2154-2159.
36. Zhang, Z. and Shen, J. (2006). Hydrophobic silica aerogels strengthened with nonwoven fibers. Journal of Macromolecular Science, Part A, 43, 1663-1670.
37. Stepanian, C. (2007). Highly flexible Aerogel Insulated Textile-like Blankets. US Patent 20070154698 A1.

38. Oh, K.W., Kim, D.K. and Kim, S.H. (2009). Ultra-porous flexible PET/Aerogel blanket for sound absorption and thermal insulation. Journal of Fibers & Polymers, 10, 731-737.
39. Prevolnik,V. , Zrim, P. K, Rijavec, T. (2014). Textile technological properties of laminated silica aerogel blanket. Contemporary Materials, V-1, 117-123.
40. Nocentini, K., Achard, P., Biwole, P., & Stipetic, M. (2018). Hygro-thermal properties of silica aerogel blankets dried using microwave heating for building thermal insulation. Energy and Buildings, 158, 14-22.
41. Hoseini, A., McCague, C., Andisheh-Tadbir, M., & Bahrami, M. (2016). Aerogel blankets: From mathematical modeling to material characterization and experimental analysis. International Journal of Heat and Mass Transfer, 93, 1124-1131.
42. Hsu, M. W., Chen, Y. S., Horng, R. S. S., Wu, C. M., and Lee, S. K. (2017). To Improve the Thermal Properties of Mineral Wool by Adding Aerogel. Sensors and Materials, 29 (4), 445-452.
43. Hoseini, A., Malekian, A., & Bahrami, M. (2016). Deformation and thermal resistance study of aerogel blanket insulation material under uniaxial compression. Energy and Buildings, 130, 228-237.
44. Sanz-Pont, D., Sanz-Arauz, D., Bedoya-Frutos, C., Flatt, R. J. and López-Andrés, S. (2016). Anhydrite/aerogel composites for thermal insulation. Materials and Structures, 49(9), 3647-3661.
45. Shaid, A., Fergusson, M. and Wang, L. (2014). Thermo-physiological comfort analysis of aerogel nanoparticle incorporated fabric for fire fighter's protective clothing. Chemical and Materials Engineering, 2, 37-43.
46. Rosace, G., Guido, E., Colleoni, C., and Barigozzi, G. (2016). Influence of textile structure and silica-based finishing on thermal insulation properties of cotton fabrics. International Journal of Polymer Science, Article ID 1726475, 10 pages.
47. Venkataraman, M., Mishra, R., Militky, J. and Hes, L. (2014). Aerogel based nanoporous fibrous materials for thermal insulation. Fibers and Ploymers, 15(7), 1444-1449.
48. Venkataraman, M., Mishra, R., Kotresh, T. M., Sakoi, T. and Militky, J. (2015). Effect of compressibility on heat transport phenomena in aerogel-treated nonwoven fabrics. The Journal of The Textile Institute, 107(9), 1150-1158.

49. Venkataraman, M., Mishra, R. Militky, J. and Behera, B. K. (2016). Modelling and simulation of heat transfer by convection in aerogel treated nonwovens. The Journal of The Textile Institute, 108 (8), 1442-1453.
50. Sachithanadam, M. and Joshi, S.C. (2016). Silica Aerogel Composites: Novel Fabrication Methods. DOI: 10.1007/978-981-10-0440-7
51. http://www.nonwovens-innovation.com/ip-library/hydrospace/
52. Höffele, S., Russell, S. J., and Brook, D. B. (2005). Light-weight nonwoven thermal protection fabrics containing nanostructured materials. International Nonwovens Journal, 14(4), 10-16.
53. Li, L., Yalcin, B., Nguyen, B. N. et al. (2009). Flexible nanofiber-reinforced aerogel (xerogel) synthesis, manufacture, and characterization. ACS Applied Materials & Interfaces, 1 (11), 2491-2501.
54. Si, Y., Mao, X., Zheng, H., Yu, J., & Ding, B. (2015). Silica nanofibrous membranes with ultra-softness and enhanced tensile strength for thermal insulation. RSC Advances, 5(8), 6027-6032.
55. Al-Homoud, D. M. S. (2005). Performance characteristics and practical applications of common building thermal insulation materials. Building and Environment, 40(3), 353-366.
56. Bhatia, A. (2013). Overview of Insulation Materials. Continuing Education and Development Inc. New York. Retrieved April, 12.
57. Mao, N. and Russell, S.J. (2015). Chapter 13 - Fiber to Fabric: Nonwoven Fabrics. Textiles and Fashion Materials, Design and Technology, Woodhead Publishing Series in Textiles, pages 307-335.
58. Sinclair, R. (2015). Chapter 1 - Understanding Textile Fibers and Their Properties: What is a Textile Fiber. Textiles and Fashion Materials, Design and Technology, Woodhead Publishing Series in Textiles, pages 3-27.
59. Ukponmwan, J. O. (1993). Thermal-Insulation Properties of Fabrics, Textile Progress, 24 (4), 1-54.
60. Strong, H. M., Bundy, F. P., & Bovenkerk, H. P. (1960). Flat panel vacuum thermal insulation. Journal of Applied Physics, 31(1), 39-50.
61. Holcombe, B. (1984). Thermal insulation performance of textile fabrics. Wool Science Review, 60, 12-22.

62. Wang, M., He, J., Yu, J., & Pan, N. (2007). Lattice Boltzmann modeling of the effective thermal conductivity for fibrous materials. International Journal of Thermal Sciences, 46(9), 848-855.
63. Vallabh, R., Lee, P. B., & Mohammadi, M. (2008). Determination of radiative thermal conductivity in needle-punched nonwovens. Journal of Engineered Fibers and Fabrics, 3(4), 46-52.
64. Kong, L. X., Li, Y., She, F. H. et. al. (2001). Effect of fiber geometry and porosity on heat and moisture transfer in textiles. Proceedings of the Textile Institute 81st World Conference, Melbourne, Australia.
65. Farnworth, B. (1983). Mechanisms of Heat Flow Through Clothing Insulation. Textile Research Journal, 53(12), 717-725.
66. Wu, H., Fan, J. and Du, N. (2007). Thermal energy transport within porous polymer materials: Effects of fiber characteristics. Journal of Applied Polymer, 106(1), 576-583.
67. Cheng, X. and Fan, J. (2004). Simulation of heat and moisture transfer with phase change and mobile condensates in fibrous insulation. International Journal of Thermal Sciences, 43(7), 665-676.
68. Sun, J., Hu, Z., Li, J., Zhang, H., Sun, C. (2014). Thermal and mechanical properties of fibrous zirconia ceramics with high porosity. Ceramics International, 40(8), Part A, 11787-11793.
69. Li, Y. and Ren, S. Buiding Decorative Materials. 1st Edition, Woodhead Publishing, 2011.
70. Slater, K. (1977). Comfort properties of textiles. The Textile Institute, Manchester, England, pp.1-11.
71. Mohammadi, M., Lee-Banks, P. (2003). Determining effective thermal conductivity of multilayered nonwovens fabrics. Textile Research Journal, 73(9), 802.
72. Stark, C., & Fricke, J. (1993). Improved heat-transfer models for fibrous insulations. International Journal of Heat and Mass Transfer, 36(3), 617-625.
73. Obendorf, S. K., & Smith, J. P. (1986). Heat Transfer Characteristics of Nonwoven Insulating Materials. Textile Research Journal, 56(11), 691-696.
74. Ozturk, M. K., Venkataraman, M. and Mishra, R. (2018). Influence of structural parameters on thermal performance of polypropylene nonwovens. Polymers Advanced Technologies, https://doi.org/10.1002/pat.4423.

75. Mao, N., & Russell, S. J. (2007). The Thermal Insulation Properties of Spacer Fabrics with a Mechanically Integrated Wool Fiber Surface. Textile Research Journal, 77(12), 914-922.
76. Arambakam, R., Vahedi Tafreshi, H., & Pourdeyhimi, B. (2013). A simple simulation method for designing fibrous insulation materials. Materials & Design, 44, 99-106.
77. Caps, R., Umbach K. (1990). Optimizing polyester nonwoven fabric thermal insulation. Melliand English, pp. E201.
78. American Society of Heating, Refrigerating and Air-Conditioning Engineers Inc., ASHRAE Handbook, Fundamentals 1993, I-P edn, Atlanta.
79. Paul, H. L., & Diller, K. R. (2003). Comparison of thermal insulation performance of fibrous materials for the advanced space suit. Journal of Biomechanical Engineering, 125(5), 639-647.
80. Piekaar, H.W. and Clarenburg, L.A. (1967). Aerosol filters - the tortuosity factor in fibrous filters. Chem Eng Sci, 22(12): 1817-1827.
81. Xiao, X., Zeng, X., Bandara, P. and Long, A. (2012). Experimental study of dynamic air permeability for woven fabrics. Textile Research Journal, 82(9): 920-930.
82. Pradhan, A. K., Das, D., Chattopadhyay, R. & Singh, S. N. (2017). Studies on air permeability of multi-constituent nonwovens. The Journal of the Textile Institute, 108(5), doi: 10.1080/00405000.2016.1191720.
83. Gervais, P.C., Monnier, N.B. and Thomas, D. (2012). Permeability modeling of fibrous media with bimodal fiber size distribution. Chemical Engineering Science, 73, 239-248.
84. Zhu, G, Kremenakova, D., Wang, Y. and Militky, J. (2015). Air permeability of polyester nonwoven fabrics. Autex Research Journal, 15(1), 8-12.
85. Kosiński, P. and Wójcik, R. (2016). An Impact of Air Permeability on Heat Transfer through Partitions insulated with fibrous materials. Applied Mechanics and Materials, 861, 190-197.
86. Zhu, G, Kremenakova, D., Wang, Y., Militky, J. and Mishra, R. (2015). Study on air permeability and thermal resistance of textiles under heat convection. Textile Research Journal, https://doi.org/10.1177/0040517515573407.
87. Banks-Lee, P., Mohammadi, M. and Ghadimi, P. (2004). Utilization of air permeability in predicting the thermal conductivity. Int. Nonwovens J., 13(2), 28-33.

88. Jaganathana, S., Tafreshi, H.V., Shim, E. and Pourdeyhimi, B. (2009). A study on compression-induced morphological changes of nonwoven fibrous materials. Colloids and Surfaces A: Physicochemical and Engineering Aspects, 337, 173-179.
89. Stankovic, S. B. (2008). Compression hysteresis of fibrous systems. Polymer Engineering and Science, 676-682.
90. Akimov, Y. K. (2003). Fields of application of aerogels (Review). Instruments and Experimental Techniques, 46(3), 287-299.
91. Alzoubi, M. F., Tanbour, E. Y., & Al-Waked, R. (2011). Compression and hysteresis curves of nonlinear polyurethane foams under different densities, strain rates and different environmental conditions. ASME 2011 International Mechanical Engineering Congress and Exposition, 101-109.
92. Parikh, D.V., Calamari, T.A., Goynes, W.R., et al. (2004). Compressibility of cotton blend perpendicularly-laid nonwovens. Textile Research Journal, 74, 7-12.
93. Parikh, D.V., Calamari, T.A., Sawhney, A.P.S., et al. (2002). Compressional behavior of perpendicularly-laid nonwovens containing cotton. Textile Research Journal, 72, 550-554.
94. Jaganathana, S., Tafreshi, H.V., Shim, E. and Pourdeyhimi, B. (2009). A study on compression-induced morphological changes of nonwoven fibrous materials. Colloids and Surfaces A: Physicochemical and Engineering Aspects, 337, 173-179.
95. Somerton, W. H. (1992). Thermal properties and temperature-related behavior of rock/fluid systems. Elsevier in Amsterdam, New York, 77.
96. Yang, T., Xiong, X., Mishra, R., Novák, J., & Militký, J. (2016). Acoustic evaluation of Struto nonwovens and their relationship with thermal properties. Textile Research Journal, doi: 4051751668195.
97. Ghorannevissa, M., Shahidia, S., Moazzenchia, B. et al. (2007). Comparison between decolorization of denim fabrics with oxygen and argon glow discharge. Surface & Coatings Technology, 201, 4926-4930.
98. Yuan, G., Jiang, S., Newton, E., Fan, J., & Au, W. (2012). Application of laser treatment for fashion design. The Journal of Textile Institute, 103(1), 48-54.
99. Dembickỳ, J. (2010). Impact of laser thermal stress on cotton fabric. Fibers & Textiles in Eastern Europe, 18(3), 80.
100. Singha, K. (2012). A Review on Coating, Lamination in Textiles: Processes and Applications. American Journal of Polymer Science, 2(3), 39-49.

101. Rozek, Z., Kaczorowski, W., Luk, D. et al. (2008). Potential applications of nanofiber textile covered by carbon coatings. Journal of Achievements in Materials and Manufacturing Engineering, 27(1), 35-38.
102. Newehy, M. H. E., Deyab, S. S. A., Kenawy, E. R, and Megeed, A. A. (2011). Nanospider technology for the production of nylon-6 nanofibers for biomedical applications. Journal of Nanomaterials, 8, 1-8.
103. Ramakrishnan, R., Gimbun, J., Samsuri, F. et al. (2016). Needleless electrospinning technology-An entrepreneurial perspective. Indian Journal of Science and Technology, 9(15), 1-11.
104. Stančić, M., Grujić, D., Novaković, D., Kašiković, N., Ružičić, B., Geršak, J. (2014). Dependence of warm or cold feeling and heat retention ability of knitwear from digital print parameters. Journal of Graphic Engineering and Design, 5 (1), 25-32.
105. Bergman, T. L., & Incropera, F. P. (Eds.). (2011). Fundamentals of heat and mass transfer (7th ed). Hoboken, NJ: Wiley. pp: 455-458.
106. Ziaei, M., & Ghane, M. (2013). Thermal insulation property of spacer fabrics integrated by ceramic powder impregnated fabrics. Journal of Industrial Textiles, 43(1), 20-33.
107. Bhattacharyya, R. K. (1980). Heat-transfer model for fibrous insulations, thermal insulation performance, edited by D. L. McElroy and R. P. Tye, ASTM Special Technical Publication 718, American Society for Testing and Materials, Philadelphia, 272-286.
108. Akimov, Y. K. (2003). Fields of application of aerogels (Review). Instruments and Experimental Techniques, 46(3), 287-299.
109. Burleigh Jr, E. G., Wakeham, H., Honold, E., & Skau, E. L. (1949). Pore-size distribution in textiles. Textile Research Journal, 19(9), 547-555.
110. Fohr, JP., Couton, D. and Treguier, G. (2002). Dynamic heat and water transfer through layered fabrics. Textile Research Journal, 72(1), 1-12.
111. Sukigara, S., Yokura, H. and Fujimoto, T. (2003). Compression and thermal properties of recycled fiber assemblies made from industrial waste of sweater products. Textile Research Journal, 3(4), 310-315.
112. Pompe, G., Pohlers, A., Potschke, P. and Pionteck, J. (1998). Influence of processing conditions on the multiphase structure of segmented polyurethane. Polymer, 39(21), 5147-5153.

113. Zhuo, H., Hu, J., Chen, S. and Yeung, L. (2008). Preparation of polyurethane nanofibers by electrospinning. Journal of Applied Polymer Science, 109, 406-411.
114. Kaursoin, J and Agrawal, A. (2007). Melt spun thermo-responsive shape memory fibers based on polyurethanes: Effect of drawing and heat-setting on fiber morphology and properties. Journal of Applied Polymer Science, 103(4), 2172-2182.
115. Li, W. and Wan, M. (1999). Stability of polyaniline synthesized by a doping-dedoping-redoping method. Journal of Applied Polymer Science, 71(4), 615-621.
116. Sundaramoorthy, S., Nallampalayam, P. K. and Jayaraman, S. (2011). Air permeability of multilayer woven fabric systems. The Journal of the Textile Institute, 102(3), 189-202.
117. Huang, W. and Ghosh, T. K. (1999). Online measurement of fabric mechanical properties: compressional behavior. Textile, Fiber and Film Industry Technical Conference, 1.
118. Debnath, S. and Madhusoothanan, M. (2009). Compression properties of polyester needle punched fabric. Journal of Engineered Fibers and Fabrics, 4, 14-19.

Research Outputs

Journal publications

[1] **Xiaoman Xiong**, Tao Yang, Rajesh Mishra, Hiroyuki Kanai, Jiri Militky, Thermal and Compression Characteristics of Aerogel-encapsulated Textiles, *Journal of Industrial Textiles*, Vol.47, 1998-2013, 2017.

[2] **Xiaoman Xiong**, Tao Yang, Rajesh Mishra, Jiri Militky and Jakub Wiener, Investigation on Laser Engraving based Application of Silica Aerogel into Nonwovens, *Fibers and Polymers*, Vol.18, No. 12, 2469-2475, 2017.

[3] **Xiaoman Xiong**, Tao Yang, Rajesh Mishra, Jiri Militky, Transport Properties of Aerogel-based Nanofibrous Nonwoven Fabric, *Fibers and Polymers*, Vol.17, No.10, 1709-1714, 2016.

[4] Mohanapriya Venkataraman, **Xiaoman Xiong**, Rajesh Mishra, Jiri Militky, Jaromir Marek, Juming Yao, Guocheng Zhu, Electrospun nanofibrous membranes embedded with aerogel for advanced thermal and transport properties, *Polymers and Advanced Technologies*, Vol. 29, Issue-10, 2583-2592, 2018.

[5] **Xiaoman Xiong**, Mohanapriya Venkataraman, Darina Jašíková, Tao Yang, Rajesh Mishra and Jiří Militký, Experimental investigation of convective heat transfer in aerogel-embedded nonwovens, *Journal of Materials Science*, under review.

[6] **Xiaoman Xiong**, Mohanapriya Venkataraman, Darina Jašíková, Tao Yang, Rajesh Mishra and Jiří Militký, Thermal performance of aerogel-encapsulated fibrous materials by convection, under submission.

[7] Tao Yang, **Xiaoman Xiong**, Rajesh Mishra, Jan Novak and Jiri Militky, Sound Absorption and Compression Properties of Perpendicular-laid Nonwovens, *Textile Research Journal*, doi: 10.1177/0040517517753634, First Published January 18, 2018.

[8] Tao Yang, **Xiaoman Xiong**, Rajesh Mishra, Jan Novak and Jiri Militky, Acoustic Evaluation of Struto Nonwovens and Their Relationship with Thermal Properties, *Textile Research Journal*, doi: 10.1177/0040517516681958, First Published December 06, 2016.

[9] Tao Yang, **Xiaoman Xiong**, Rajesh Mishra, Jiri Militky, Investigation on Acoustic Behavior and Air Permeability of Struto Nonwovens, *Fibers and Polymers*, Vol.17, No.12, 2078-2084, 2016.

[10] Tao Yang, **Xiaoman Xiong**, Mohanapriya Venkataraman, Rajesh Mishra, Jan Novák and Jiří Militký, Investigation on sound absorption properties of aerogel nonwoven blankets, *The Journal of the Textile Institute*, Accepted.

[11] Tao Yang, **Xiaoman Xiong**, Ferina Saati, Kai Yang, Rajesh Mishra, Kirill V Horoshenkov, Rajesh Mishra, Steffen Marburg and Jiří Militký, Study on sound absorption behavior of multi-component polyester nonwovens: Practical and numerical methods, *Textile Research Journal*, Accepted.

Book chapters

[1] **Xiaoman Xiong**, Tao Yang, Rajesh Mishra, Juan Huang and Jiří Militký, A Review on Nanofibrous Membranes and Their Applications, Advances in fibrous material science, ISBN 978-80-87269-48-0, 2016.

[2] **Xiaoman Xiong**, Tao Yang, Rajesh Mishra, Juan Huang, T M Kotresh and Jiří Militký, Heat Transfer through Thermal Insulation Materials Part I – Nonwoven Fabrics, Recent developments in fibrous material science, ISBN 978-80-87269-45-9, 2015.

[3] **Xiaoman Xiong**, Tao Yang, Rajesh Mishra, Juan Huang, T M Kotresh and Jiří Militký, Heat Transfer through Thermal Insulation Materials Part II – Nano-porous Aerogel, Recent developments in fibrous material science, ISBN 978-80-87269-45-9, 2015.

[4] Tao Yang, **Xiaoman Xiong**, Rajesh Mishra, Jan Novak and Jiří Militký, Comparative Analysis on Acoustic Properties of Different Struto-type Nonwovens, Advances in fibrous material science, ISBN 978-80-87269-48-0, 2016.

[5] Tao Yang, **Xiaoman Xiong**, Rajesh Mishra, Jan Novák, Filip Sanetrník and Jiří Militký, A Review of Acoustic Properties Measurements and Wave Propagation Models of Porous Materials, Recent developments in fibrous material science, ISBN 978-80-87269-45-9, 2015.

Conference publications

[1] **Xiaoman Xiong**, Mohanapriya Venkataraman, Rajesh Mishra and Jiří Militký, Experimental Study on Convective Heat Transfer Through Fibrous Insulators, 46th Textile Research Symposium, Teijin Academy Fuji, Susono City, Japan, September 3-5, 2018.

[2] **Xiaoman Xiong**, Tao Yang, Rajesh Mishra, Jiri Militky, Transport Properties of Nonwovens with Aerogel, CLOTECH 2017, Lodz, Poland, October 11-14, 2017.

[3] **Xiaoman Xiong**, Tao Yang, Rajesh Mishra, Jiri Militky, Laser Engraving based Application of Silica Aerogel into Nonwovens for Thermal Insulation, 45th Textile Research Symposium, KIT Kyoto, September 14-16, 2017.

[4] **Xiaoman Xiong**, Tao Yang, Rajesh Mishra, Jiri Militky, Investigation on Thermal and Compression Performance of Aerogel Incorporated Textiles, Textile Bioengineering and Informatics Symposium, TBIS-2017, Wuhan, China, May 18-20, 2017.

[5] **Xiaoman Xiong**, Tao Yang, Rajesh Mishra, and Jiri Militky, Thermophysiological Performance of Aerogel Embedded Electrospun Nonwoven Layers, 44th Textile Research Symposium, IIT Delhi, December 14-16, 2016.

[6] **Xiaoman Xiong**, Aerogel-based Nanofibrous Nonwoven Fabrics for Thermal Insulation, Workshop Bílá voda 2016, Harrachov, Liberec, September 20-23, 2016.

[7] **Xiaoman Xiong**, Tao Yang, Rajesh Mishra, Effect of weaving friction on yarn hairiness and mechanical properties, 8th TBIS-APCC International conference, Zadar, June 14-17, 2015.